

In-situ benchmarking of fault-tolerant quantum circuits. I. Clifford circuits

Xiao Xiao,^{1,*} Dominik Hangleiter,^{2,3} Dolev Bluvstein,⁴ Mikhail D. Lukin,⁴ and Michael J. Gullans^{1,5,†}

¹*Joint Center for Quantum Information and Computer Science,
NIST/University of Maryland, College Park, Maryland 20742, USA.*

²*Simons Institute for the Theory of Computing, University of California at Berkeley, Berkeley, California 94270, USA.*

³*Institute for Theoretical Physics, ETH Zürich, 8093 Zürich, Switzerland.*

⁴*Department of Physics, Harvard University, Cambridge, Massachusetts 02138, USA.*

⁵*National Institute of Standards and Technology, Gaithersburg, MD 20899, USA.*

(Dated: February 5, 2026)

Benchmarking physical devices and verifying logical algorithms are important tasks for scalable fault-tolerant quantum computing. Numerous protocols exist for benchmarking devices before running actual algorithms. In this work, we show that both physical and logical errors of fault-tolerant circuits can even be characterized in-situ using syndrome data. To achieve this, we map general fault-tolerant Clifford circuits to subsystem codes using the spacetime code formalism and develop a scheme for estimating Pauli noise in Clifford circuits using syndrome data. We give necessary and sufficient conditions for the learnability of physical and logical noise from given syndrome data, and show that we can accurately predict logical fidelities from the same data. Importantly, our approach requires only a polynomial sample size, even when the logical error rate is exponentially suppressed by the code distance, and thus gives an exponential advantage against methods that use only logical data such as direct fidelity estimation. We demonstrate the practical applicability of our methods in various scenarios using synthetic data as well as the experimental data from a recent demonstration of fault-tolerant circuits by Bluvstein *et al.* [Nature 626, 7997 (2024)]. Our methods provide an efficient, in-situ way of characterizing a fault-tolerant quantum computer to help gate calibration, improve decoding accuracy, and verify logical circuits.

I. INTRODUCTION

Quantum error correction (QEC) is crucial for preserving quantum information in a noisy environment using redundant encodings. Recent experiments have demonstrated promising results [1–6] that realize error-corrected quantum memory and computations. In these experiments, information is encoded in stabilizer codes. In such codes, certain Pauli operators are measured and the resulting bits of information known as the *syndrome* are decoded to infer the (Pauli) errors that occurred. These errors can then be corrected.

When designing fault-tolerant circuits and developing decoders, the precise physical error model can have a significant impact on the performance of the fault-tolerant computation. Typically, the model is assumed to be simple, single-qubit depolarizing noise [7–10]. However, this is an idealized model that does not adequately capture the scenarios present in different physical platforms. Understanding and learning error mechanisms and error rates occurring in a physical system is therefore critical in optimizing the performance of FTCs, specifically, for gate tune-up, code and circuit design, and improving decoders. A second, closely related challenge is to assess the quality of the outcome of an FTC in the presence of said physical noise channels. This is particularly important in the near term, when the accessible code distances limit the suppression of the logical error rate.

In this work, we present a practical and scalable method for learning physical and logical Pauli error rates of fault-tolerant computations that only uses the naturally available syndrome data. We show that the logical error rate of fault-tolerant computations can be learned using a number of samples that scales polynomially in the distance of the code. In contrast, direct methods that only use logical data require an exponential number of samples. We demonstrate the practicality of our methods by applying them to experimental data from the recent demonstration of fault-tolerant computation [1].

To achieve this, we develop a new systematic framework for learning physically motivated Pauli errors in general subsystem codes, by further developing the ideas of Wagner *et al.* [11, 12] which lay the groundwork for our method. We then apply this framework to general, non-adaptive fault-tolerant Clifford circuits using the circuit-to-code mapping [13–15]. This mapping converts the problem of correcting errors in Clifford circuits into correcting errors in subsystem codes.

Our work provides a general framework for in-situ characterization of both physical and logical noise in fault-tolerant quantum computations, using syndrome data. These problems include fault-tolerant quantum memory experiments as studied in this work, but also magic-state distillation, and classically hard logical circuits such as Clifford operations augmented with magic-state inputs which we study in Part II [16]. Thus, it enables benchmarking and verifying circuits and algorithms using the natively available syndrome data.

* xiaoxiao@umd.edu

† mgullans@umd.edu

A. Contributions

Our concrete contributions are as follows. For the noise model, we give a necessary and sufficient condition regarding the learnability of the total Pauli channel as well as individual Pauli channels. We prove for general stabilizer code/Clifford circuits that after grouping errors into syndrome classes, the total error rate of each class can be accurately learned with negligible second-order correction. Moreover, we show that under circuit-level Pauli noise, if the circuit is fault-tolerant with respect to the assumed noise model, then the logical error rates are learnable solely from the circuit's syndrome data, enabling efficient estimation of the circuit's logical fidelity.

We also analyze the sample complexity, under the local sparse noise model assumption, for learning both physical- and logical-level noise from syndrome data as a function of the circuit's spacetime volume. For logical circuits corresponding to quantum low-density parity-check (qLDPC) codes, we prove that in the low physical-error-rate regime, the required sample complexity for physical error rate learning becomes constant. Finally, we show that in the below-threshold regime, learning the logical error rate from syndrome data achieves an exponential sample-complexity advantage over direct logical-level measurements.

We first demonstrate the efficacy and scalability of our noise-learning algorithm using numerical benchmarks on simulated data. We then demonstrate its practicality by applying it to the experimental data of Ref. [1] where a fault-tolerant protocol for logical GHZ state preparation was demonstrated. In particular, we show that the estimated logical error rates are consistent with independently obtained experimental results.

B. Significance

Our work studies and verifies the effectiveness of the physically motivated Pauli error model in the context of fault-tolerant logical circuits; taking advantage of readily available data from near-term experiments on fault-tolerance. Within this error model, we prove an exponential sampling advantage for learning the logical error rate from syndrome data in a regime of low error rates. Finally, our work solves an important practical problem by providing a systematic framework for estimating logical and physical noise rates with improved accuracy using small amounts of syndrome data, without the need for independent logical measurements. In part II of this work, we show that these ideas can be extended to efficiently verifying and benchmarking classically hard circuits from syndrome data [16].

C. Related work

Earlier works attempted to solve the physical noise learning task from syndrome for specific codes and error detection/correction circuits [17–19], benchmarking circuits with a single parameter using detector data [20], or for general Pauli noise but in a heuristic way [21]. More recently, a series of works [22–24] generalized the formalism of Ref. [18] to other codes, e.g., when the decoding graph can be a hypergraph. However, these works focused on a restricted Pauli error model commonly used in decoding graphs, often referred to as the detector error model. The model typically assumes that each error occurs independently, also known as the inclusive error model (see the discussion in Appendix E of [25]). However, a more natural and general model is to assign each noisy operation a local Pauli channel, where Pauli errors occur exclusively. Moreover, [23, 24] provide analytical solutions to the general detector-error-model learning problem, but they do not address the balance between model complexity and shot noise. In practice, purely analytical solutions can overfit when syndrome data are limited, leading to degraded learning precision.

In a parallel series of works, Wagner *et al.* [11, 12, 26] rigorously investigated the sufficient conditions under which physical and logical error rates can be extracted from the syndrome of general stabilizer codes in the channel coding setting under a more general and natural Pauli noise model. However, the identifying conditions are not satisfied in many cases, and no efficient algorithms for estimating noise based on this framework have been developed for the general case. Our work builds upon the formalism developed in those works.

Finally, the above works focus on learning error rates from the syndromes produced during rounds of error correction. None of the prior literature focuses on the problem of learning physical- or logical-level Pauli noise in general fault-tolerant circuits encountered in an algorithm using syndrome data. As a result, a systematic, broadly applicable framework for exploiting syndrome information throughout a logical circuit or algorithm has been lacking prior to our work.

D. Overview

This paper is structured as follows. In Section II, we introduce the Pauli noise model. In Section III, we apply the formalism to the static-code setting, where a single round of syndrome information is extracted. In this section, we present necessary and sufficient conditions for the learnability of physical Pauli noise and the sample complexity to achieve the learning task to a desired accuracy. In Section IV, we apply these results to the problem of learning the noise in fault-tolerant circuits by using the mapping of those circuits to the spacetime code. We demonstrate the effectiveness of our method using synthetic and experimental data. Finally, in Sec-

tion V, we consider the problem of learning logical error rates in static codes and fault-tolerant computations. We give learnability conditions, demonstrate the method, and show analytically and numerically that a polynomial number of samples is sufficient to learn the logical error rates in circuits that correspond to qLDPC spacetime codes under the local sparse Pauli error model. We conclude with a discussion. All proofs and details are deferred to the appendices.

CONTENTS

I. Introduction	1	E. Proof of syndrome class error rate learnability condition	33
A. Contributions	2	F. Existence of a family of logically equivalent physical error rates	35
B. Significance	2	G. Spacetime code	38
C. Related work	2	H. Logical error rate learnability	43
D. Overview	2	I. Sample complexity	45
II. Model	3	1. Sample complexity for learning physical error rates	45
III. Efficient Pauli Noise Learning on Static Code	4	2. Sample complexity for learning logical error rates	47
A. Basic formalism	4	J. Intraclass uniformity constraints	49
B. Learning syndrome class total error rate for generic static codes	5	K. Extra plots	49
C. Physical error rate estimation	7		
D. Simulation on static code	8		
E. Sample complexity for physical error rate learning	9		
IV. Circuit-level noise learning	10		
A. Mapping to the spacetime code	10		
B. Simulation on circuit-level noise learning	13		
C. Learning from experimental data	16		
V. Learning logical error rates and logical fidelity from syndrome data	16		
A. Logical error rate learnability	16		
B. Benchmarks	18		
C. Logical error rates in experiments	19		
D. Exponential sample complexity advantage at very low logical error rates	19		
VI. Discussion	21		
Acknowledgments	22		
References	22		
A. Overview	25		
B. The transformed eigenvalue basis	26		
1. $\log F$: Basis of the canonical factor [12]	27		
2. $\log U$: Basis of the transformed eigenvalues	28		
C. Rank of matrix A and D	29		
D. Minimal number of equations for the syndrome data	31		

II. MODEL

We denote the Pauli group without phases over n qubits as $\mathcal{P}_n = \{I, X, Y, Z\}^{\otimes n}$ and focus on learning a Pauli error channel

$$\mathcal{N}(\rho) = \sum_{e \in \mathcal{P}_n} P(e) e \rho e^\dagger, \quad (1)$$

acting on an n -qubit state ρ . Here, $P(e)$ are the error rates of the Pauli errors $e \in \mathcal{P}_n$. In the most generic case, learning cannot be efficiently possible as there are $4^n - 1$ independent parameters that need to be specified. This is why in practice we focus on a *local* error model in which high-weight errors are given by products of individual low-weight errors.

To be more precise, we define Γ as a set of supports such that each $\gamma \in \Gamma$ is a subset of qubits on which a Pauli channel \mathcal{N}_γ acts non-trivially, i.e.,

$$\mathcal{N}_\gamma(\rho) = \sum_{e \in \mathcal{P}_n \mid \text{supp}(e) \subset \gamma} P_\gamma(e) e \rho e^\dagger. \quad (2)$$

Here, $P_\gamma(e)$ are the error rates of the individual channels satisfying the local condition $P_\gamma(e) = 0$ if $\text{supp}(e) \not\subset \gamma$. The total Pauli noise channel, now denoted as \mathcal{N}_Γ , is the composition of these individual Pauli error channels and acts as

$$\mathcal{N}_\Gamma(\rho) = \circ_{\gamma \in \Gamma} \mathcal{N}_\gamma(\rho). \quad (3)$$

Since all Pauli channels commute with each other, the order of the composition does not matter here. An example of this Pauli noise model is illustrated in Fig. 1a. Since in general Γ could contain overlapping supports, the resulting probability distribution

$$P(e) = \ast_{\gamma \in \Gamma} P_\gamma(e), \quad (4)$$

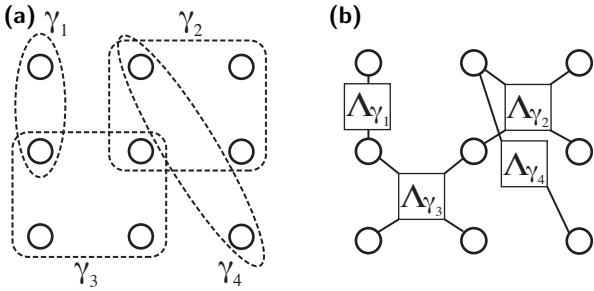


FIG. 1: An example of the total Pauli error channel \mathcal{N}_Γ as the composition of local Pauli channels \mathcal{N}_γ (enclosed in dotted lines) acting on subsets $\gamma \in \Gamma$ of qubits (circles), where $\Gamma = \{\gamma_1, \gamma_2, \gamma_3, \gamma_4\}$. (a) The error rate P is the convolution of the error rates P_γ of all local error channels. (b) The factor graph of Pauli eigenvalues of the total channel \mathcal{N}_Γ can be written as the product of eigenvalues Λ_γ of the local channels after performing Walsh-Hadamard transformation of the error rates in (a).

of the total Pauli channel \mathcal{N}_Γ is the convolution over all individual error distributions $P_\gamma(e)$, denoted by $*$. The convolution over the Pauli group is defined by $P_{\gamma_1} * P_{\gamma_2}(e) = \sum_{e' \in \mathcal{P}_n} P_{\gamma_1}(e')P_{\gamma_2}(e'e)$. The structure of the error rate is sometimes referred to as a "convolutional factor graph" [11, 27]. For analytical convenience, we make the following assumption about each individual channel.

Assumption 1. *Let a total Pauli error channel \mathcal{N}_Γ be a composition of Pauli channels \mathcal{N}_γ with support $\gamma \in \Gamma$. We assume for any individual channel \mathcal{N}_γ , we have $P_\gamma(I) > 1/2$, and for any non-identity error e in \mathcal{N}_γ with $\text{supp}(e) \subseteq \gamma$, $P_\gamma(e) > 0$.*

When considering sample complexity and classical computational cost, we focus on the case when individual channels are local. We emphasize that 'local' here refers to the concept of k -locality rather than geometric locality. To be quantitative, we say that a Pauli channel \mathcal{N}_Γ is a (r_Γ, c_Γ) -Pauli channel if each local channel $\mathcal{N}_\gamma, \forall \gamma \in \Gamma$, acts on at most r_Γ qubits and each qubit is only involved in c_Γ channels. Moreover, we call \mathcal{N}_Γ a *local sparse* Pauli channel if both r_Γ and c_Γ are $\mathcal{O}(1)$. In this setting, the noise channel \mathcal{N}_Γ is fully described by at most $c_\Gamma 4^{r_\Gamma} n = \mathcal{O}(n)$ parameters. In general, there are gauge degrees of freedom in the choice of local Pauli channels that give rise to a given total Pauli channel. We use two sets $\bar{\mu}$ and μ of irredundant quantities that parametrize the total channel \mathcal{N}_Γ and the collection of local channels respectively, and show the gauge freedom of μ with respect to $\bar{\mu}$ in Section B.

We use this model to describe circuit-level noise by using a formalism [13–15] that maps a Clifford circuit to a subsystem stabilizer code referred to as the spacetime code, see Section IV A. Qubits at each circuit layer are mapped to an additional layer of qubits in the space-

time code, and therefore each individual Pauli channel defined here should be thought of as acting on a region of the circuits in space and time. In the main text, we focus on the parametrization of the collection of local channels and the learnable quantities therein, instead of studying the total channel \mathcal{N}_Γ (see Section III B). This is because benchmarking is most naturally framed in terms of local noise processes. In the numerical part of this work, we only considered non-overlapping local channels when implementing the learning algorithm, in line with the standard local stochastic Pauli error model typically being used in the error correction and fault-tolerant literature [7, 10, 28].

III. EFFICIENT PAULI NOISE LEARNING ON STATIC CODE

Our learning algorithm takes the framework of Wagner *et al.* [11] as a starting point. They considered subsystem codes in the channel coding setting, where a single round of Pauli errors is applied to the error-correcting code followed by perfect syndrome measurement. Their work [11] establishes sufficient conditions on the noise channels and code properties that guarantee the learnability of the total channel \mathcal{N}_Γ from syndrome data. In the following subsection (Section III A), we introduce this basic framework for learning Pauli noise. We then adapt this formalism and introduce our algorithm to estimate physical error rates of arbitrary stabilizer subsystem codes from syndrome data in the subsequent subsections. We refer to the noise learning problem in this channel coding setting as the *static code* problem. We then show in Sections IV and V how to learn *circuit-level* Pauli noise in Clifford circuits by reducing it to a static code problem using the circuit-to-spacetime-code mapping.

A. Basic formalism

We consider a system of n qubits encoded in a subsystem code, which is a generalization of a stabilizer code. It is defined by the gauge group \mathcal{G} , a non-abelian subgroup of the Pauli group \mathcal{P}_n . The gauge group is the group of operators that preserve the code space and the encoded logical information. Considering general subsystem codes will be important when applying our formalism to circuit-level noise when using the spacetime code mapping in Section IV A, since in that case there are logically trivial errors in the circuit outside of the stabilizer group of the spacetime code.

For the purpose of learning physical error rates, it suffices to consider the stabilizer group

$$\mathcal{S} = Z(\mathcal{G}) = \{S \in \mathcal{G} | SG = GS, \forall G \in \mathcal{G}\}, \quad (5)$$

which is the center $Z(\mathcal{G})$ of the gauge group \mathcal{G} and coincides with \mathcal{G} for stabilizer codes. An encoded state in

the code, referred to as a codeword, is stabilized by the stabilizer group, i.e.,

$$S|\psi\rangle = |\psi\rangle, \forall S \in \mathcal{S}. \quad (6)$$

We say a stabilizer subsystem code is a (r_s, c_s) -quantum low-density parity-check code (qLDPC) when there exists a set of stabilizer group generators such that each generator acts on at most r_s qubits, and there are at most c_s generators acting on each qubit.

The measurement outcomes of stabilizer operators $S \in \mathcal{S}$, known as the *syndrome*, provide the information needed for decoding and error correction. To obtain a complete syndrome, that is, measurement outcomes for all $S \in \mathcal{S}$, a generating set of stabilizer operators needs to be measured. Here, we consider the generic case in which only a subset of generators $\{M_1, M_2, \dots\}$ is measured. We denote the resulting measured subgroup as $\mathcal{M} = \langle M_1, M_2, \dots \rangle \leq \mathcal{S}$. A Pauli error $e \in \mathcal{P}_n$ is detectable if there exists $M \in \mathcal{M}$ that anticommutes with e .

The learning algorithm makes use of the fact that the Pauli eigenvalue, defined as

$$\Lambda(O) = \sum_{e \in \mathcal{P}_n} [[e, O]] P(e), \quad (7)$$

of the channel for all Pauli operators $O \in \mathcal{P}_n$ is a Fourier transform (Walsh-Hadamard transform) of the probability distribution $P(e)$ over the Pauli group \mathcal{P}_n . Here we denote $[[A, B]] = 2^{-n} \text{Tr}[ABA^{-1}B^{-1}]$ as the scalar commutator of two Pauli operators A and B , which takes the value 1 if A and B commute and -1 if they anticommute. Based on the local structure of the total error rate shown in Eq. (4) and the convolution theorem, the Pauli eigenvalue $\Lambda(O)$ of the total channel \mathcal{N}_Γ has a structure of a factor graph (see Fig. 1b)

$$\Lambda(O) = \hat{P}(O) = \prod_{\gamma \in \Gamma} \hat{P}_\gamma(O) = \prod_{\gamma \in \Gamma} \Lambda_\gamma(O_\gamma). \quad (8)$$

Here, O_γ is the tensor product of components of $O \in \mathcal{P}_n$ restricted to the support γ , and identity operators on all qubits outside of γ .

All the factors on the right-hand side of Eq. (8) are contained within the set of all local Pauli eigenvalues, which provides a complete description of the unknown channel \mathcal{N}_Γ . Conversely, for any $M \in \mathcal{M}$, the left-hand side can be estimated from repeated error-correction experiments (comprising noise state preparation and syndrome measurement), under the assumption that the same error channel \mathcal{N}_Γ is applied each time the codeword is reinitialized. To see this, given the initial state ρ as a codeword stabilized by \mathcal{S} , we have

$$\langle M \rangle_{\mathcal{N}(\rho)} = \text{Tr}\{M\mathcal{N}(\rho)\} \quad (9)$$

$$= \sum_e P(e) \text{Tr}\{M e \rho e^\dagger\} \quad (10)$$

$$= \Lambda(M) \langle M \rangle_\rho \quad (11)$$

$$= \Lambda(M), \quad (12)$$

for any $M \in \mathcal{M} \leq \mathcal{S}$. In other words, the Pauli eigenvalue $\Lambda(M)$ is the expectation value of the syndrome measurement outcomes obtained from repeated measurements followed by reinitialization.

Given the estimated Pauli eigenvalues of all $M \in \mathcal{M}$ from the syndrome measurement data, one can attempt to recover the local Pauli eigenvalues $\Lambda_\gamma(M_\gamma)$ by solving for the factors on the right-hand side in Eq. (8), in order to reconstruct the overall Pauli channel \mathcal{N}_Γ . Wagner *et al.* [11] rigorously prove conditions of learnability of \mathcal{N}_Γ from syndrome data, and we state their main result (adapted to our model in Section II) here.

Theorem 2 (Wagner *et al.* [11]). *Let a Pauli error channel \mathcal{N}_Γ be a composition of local Pauli channels with support $\gamma \in \Gamma$ as defined in Eq. (3). Furthermore, assume $P_\gamma(I) > \frac{1}{2}$ for all γ . Then \mathcal{N}_Γ is learnable from the syndrome statistics if any union $\gamma_1 \cup \gamma_2$ of $\gamma_1, \gamma_2 \in \Gamma$ only supports detectable errors.*

Another way to phrase this condition is that the collection of local errors $\bar{\mathcal{E}}_\Gamma$ must have nontrivial and distinct syndromes. Since the product of two errors with the same syndrome must have a trivial syndrome, it suffices to check the product of pairwise local errors, thus the condition in Theorem 2. The notion of pure distance [11] is central to understanding the sufficient condition of learnability. It is defined to be the minimum weight of *any* undetectable error

$$d_{\text{pure}} = \min_{e \in N(\mathcal{S}) \setminus I} \text{weight}(e), \quad (13)$$

where $N(\mathcal{S})$ is the normalizer of the stabilizer group. Recall that, in contrast, the distance is the minimum weight of an undetectable error which *also* alters the logical information. If the weight of the product of any two errors e_1, e_2 from the local channels is less than the pure distance, then $e_1 e_2$ is detectable. Therefore, we see from Theorem 2 that error channels with maximum support size up to $\lfloor \frac{d_{\text{pure}}-1}{2} \rfloor$ are learnable from the syndrome expectations of a pure-distance d_{pure} code.

B. Learning syndrome class total error rate for generic static codes

In this section, we consider the general case when the learnability condition in Theorem 2 may fail. We provide concrete, efficient algorithms that learn the sum of error rates for errors with the same syndrome and estimate physical error rates for any subsystem code, under extra constraints when necessary.

We first establish the notation used throughout this work. For each local Pauli channel defined in Section II with support $\gamma \in \Gamma$, we denote the set of all non-identity Pauli errors of \mathcal{N}_γ as \mathcal{E}_γ (e.g. $\mathcal{E}_{\{2\}} = \{X_2, Y_2, Z_2\}$ for a single-qubit error channel on qubit 2 and $X_2 = I \otimes X \otimes I \otimes \dots$) and the set of all local errors of the total channel

\mathcal{N}_Γ as

$$\mathcal{E}_\Gamma = \bigcup_{\gamma \in \Gamma} \mathcal{E}_\gamma. \quad (14)$$

When local channels overlap, there can be distinct local channels containing the same Pauli error. We distinguish elements that correspond to the same operator but from different channels, i.e., each element $e \in \mathcal{E}_\Gamma$ is also implicitly labeled by its associated local channel, denoted γ_e . We denote as $\bar{\mathcal{E}}_\Gamma$ the set that does not distinguish the same Pauli errors from different local channels. $\bar{\mathcal{E}}_\Gamma = \mathcal{E}_\Gamma$ if and only if the supports in Γ do not overlap.

We define the vector of both individual and aggregated local error rates as $\vec{p}_\gamma = (P_\gamma(e)|e \in \mathcal{E}_\gamma)$ and $\vec{p} = (P_{\gamma_e}(e)|e \in \mathcal{E}_\Gamma)$. Similarly, we define the vector of individual and aggregated local Pauli eigenvalues as $\vec{\lambda}_\gamma = (\Lambda_\gamma(e)|e \in \mathcal{E}_\gamma)$ and $\vec{\lambda} = (\Lambda_{\gamma_e}(e)|e \in \mathcal{E}_\Gamma)$ respectively. We adopt a convention in which the entries of these vectors follow the tensor-product ordering of Pauli operators:

$$(I, X, Y, Z)^{\otimes n}. \quad (15)$$

For example, the vector $\vec{\lambda}_{\{2,5\}}$ has the following order: $\vec{\lambda}_{\{2,5\}} = (\Lambda(I_2 X_5), \dots, \Lambda(Z_2 Y_5), \Lambda(Z_2 Z_5))$.

The collection of either local error rates or local Pauli eigenvalues over all local channels is a succinct description of \mathcal{N}_Γ . The two are related by the (inverse) Fourier transformation

$$\vec{p}_\gamma = (W_{4^{|\gamma|}}^{-1})' (\vec{1}_\gamma - \vec{\lambda}_\gamma). \quad (16)$$

Here, W_{4^k} is the Walsh-Hadamard matrix defined recursively as $W_{4^k} = W_4 \otimes W_{4^{k-1}}$ where

$$W_4 = \begin{pmatrix} 1 & 1 & 1 & 1 \\ 1 & 1 & -1 & -1 \\ 1 & -1 & 1 & -1 \\ 1 & -1 & -1 & 1 \end{pmatrix}. \quad (17)$$

$(W_{4^{|\gamma|}}^{-1})'$ refers to the submatrix of $W_{4^{|\gamma|}}^{-1}$ after eliminating the first row and the first column. Assuming $P_\gamma(I) > \frac{1}{2}$ for all local support γ , we arrive at the matrix equation between expectation values of elements in the measured stabilizer group and the local channel Pauli eigenvalues:

$$\log \vec{\Lambda}^{(\mathcal{M})} = A^{(\mathcal{M})} \log \vec{\lambda}, \quad (18)$$

by taking the logarithm on both sides of Eq. (8). Here, $\vec{\Lambda}^{(\mathcal{M})} = (\Lambda(M))_{M \in \mathcal{M}}$ and the rows and columns of matrix $A^{(\mathcal{M})}$ are labeled by elements $M \in \mathcal{M}$ and $e \in \mathcal{E}_\Gamma$ respectively. The matrix elements indexed by row M and column e , denoted $A^{(\mathcal{M})}[M, e]$, have the values

$$A^{(\mathcal{M})}[M, e] = \begin{cases} 1 & \text{if } M_{\gamma_e} = e, \\ 0 & \text{else.} \end{cases} \quad (19)$$

$A^{(\mathcal{M})}$ is not invertible when the learnability condition in Theorem 2 fails. For example, this happens when error-correcting codes contain weight-two stabilizer elements or

logical operators, such as in the rotated surface code [29]. Spacetime codes constructed from most Clifford circuits typically contain low-weight gauge operators that also lead to a violation of this condition under simple circuit-level noise models, as will be discussed in Section IV.

To understand what can be learned when the learnability condition in Theorem 3 fails, we transform the set of local eigenvalues λ into another set of parameters μ which we refer to as the transformed local eigenvalues. We show that μ approximates the local error rate, and any transformed local eigenvalue corresponding to a unique column of the resulting matrix equation can be identified.

We consider an inverse Walsh-Hadamard transform of $\log \vec{\lambda}$, where $\vec{\lambda}$ is the collection of all local channel Pauli eigenvalues. This results in an equivalent set (vector) of transformed eigenvalues μ ($\vec{\mu}$) describing all local channels:

$$\log \vec{\mu} = -2 \left(\bigoplus_{\gamma \in \Gamma} (W_{4^{|\gamma|}}^{-1})' \right) \log \vec{\lambda}. \quad (20)$$

Since $\log \vec{\lambda} \approx \vec{\lambda} - \vec{1}$, from Eq. (16) we have the approximation to the local error rates

$$\log \vec{\mu} \approx -2\vec{p}. \quad (21)$$

The deviation is negligible when error rates are low, i.e., at the order of 10^{-2} or below, and remains insignificant compared to the shot noise arising from the finite sample size.

With the parametrization using the transformed Pauli eigenvalues, we arrive at a new matrix equation

$$\log \vec{\Lambda}^{(\mathcal{M})} = D^{(\mathcal{M})} \log \vec{\mu}, \quad (22)$$

where $D^{(\mathcal{M})}$ encodes the commutations between measured stabilizer elements \mathcal{M} and the local errors \mathcal{E}_Γ and is referred to as the syndrome matrix. Specifically, the entry at row $M \in \mathcal{M}$ and column $e \in \mathcal{E}_\Gamma$ is

$$D^{(\mathcal{M})}[M, e] = \langle M, e \rangle, \quad (23)$$

and $\langle e, f \rangle$ equals 0 when e and f commute and 1 otherwise. We systematically derive the syndrome matrix D in Section B and show in Section C that distinct columns of D will be linearly independent. Note that if two errors e and e' are in the same syndrome class, then the columns of e and e' of the matrix D will be identical. Therefore, it is natural to partition the error set \mathcal{E}_Γ into equivalence classes, which we refer to as ‘‘syndrome error classes’’ or simply ‘‘syndrome classes’’ and denote the set of classes as \mathcal{C} . Errors are in the same class $C \in \mathcal{C}$ if and only if they have the same syndrome. Furthermore, we distinguish the class C_0 of trivial syndrome from the set $\mathcal{C}^* = \mathcal{C} \setminus \{C_0\}$ of classes of non-trivial syndromes. As a result, we denote as ν_C the learnable quantity for each syndrome class $C \in \mathcal{C}^*$, and refer to them as learnable

Pauli eigenvalues:

$$\log \nu_C = \sum_{e \in C} \log \mu_e \approx -2 \sum_{e \in C} p_e = -2P_C, \quad (24)$$

where we define $P_C = \sum_{e \in C} p_e$ as the syndrome class error rate for the class C . The learnable Pauli eigenvalues can be obtained by solving the equation

$$\log \vec{\Lambda}^{(\mathcal{M})} = D'^{(\mathcal{M})} \log \vec{\nu}. \quad (25)$$

Here, D' is the full-rank matrix eliminating the redundant columns of D and $\vec{\nu} = (\nu_C)_{C \in \mathcal{C}^*}$. Given a syndrome class C , we denote $\Gamma_C = \{\gamma \in \Gamma | \mathcal{E}_\gamma \cap C \neq \emptyset\}$ as the collection of local channels that contribute to the error class C . We then denote $\vec{p}^{(\Gamma_C)} = (P_{\gamma_e}(e) | e \in \mathcal{E}_{\Gamma_C})$ as their error rates grouped into a vector. We have the following results.

Theorem 3 (Learnability conditions). *Let a total Pauli error channel \mathcal{N}_Γ be a composition of Pauli channels \mathcal{N}_γ with support $\gamma \in \Gamma$. Under Assumption 1, using the syndrome data we have:*

1. *The total channel \mathcal{N}_Γ is learnable if and only if every error $e \in \bar{\mathcal{E}}_\Gamma$ has a unique and nontrivial syndrome.*
2. *Each individual channel \mathcal{N}_γ is learnable if and only if every $e \in \mathcal{E}_\gamma$ produces a syndrome that is nontrivial and unique among the syndromes of all errors in \mathcal{E}_Γ .*
3. *For all non-trivial syndrome error classes $C \in \mathcal{C}^*$, the sum of syndrome error class error rates $P_C = \sum_{e \in C} p_e$ can be learned up to an $\mathcal{O}(\|\vec{p}^{(\Gamma_C)}\|^2)$ deviation.*

See the proof in Section E.

Note that the matrix $A^{(\mathcal{M})}$ and $D^{(\mathcal{M})}$ have exponentially ($|\mathcal{M}| = 2^{\Theta(n)}$) many rows while there are only polynomial many (transformed) local Pauli eigenvalues λ (μ). We prove in Section C that the number of independent equations is exactly the number of nontrivial syndromes $|\mathcal{C}^*|$ and design an efficient algorithm (Algorithm 1) that finds $|\mathcal{C}^*|$ elements in \mathcal{M} from the product of correlated generators of \mathcal{M} . We denote the reduced subset of \mathcal{M} as \mathcal{M}' . The algorithm ensures that \mathcal{M}' will generate $|\mathcal{C}^*|$ independent equations (see Section D):

$$\log \vec{\Lambda}^{(\mathcal{M}')} = A^{(\mathcal{M}')} \log \vec{\lambda}, \quad (26)$$

or

$$\log \vec{\Lambda}^{(\mathcal{M}')} = D'^{(\mathcal{M}')} \log \vec{\nu}. \quad (27)$$

We conclude this subsection by noting a related quantity for each nontrivial syndrome class C , i.e., the detector error rate P_C^{detect} for a syndrome class C defined as the probability of an odd number of errors in C occurring. As a special case, if one assumes every single

Pauli error is independent, then we can exactly learn the detector error rate as (see Section E)

$$P_C^{\text{detect}} = \frac{1 - \nu_C}{2}, \quad (28)$$

where ν_C is the learnable Pauli eigenvalues from Eq. (27).

C. Physical error rate estimation

We can further estimate all individual error rates by incorporating a prior belief of the relative strength $r(e)$ of errors e with a non-unique syndrome. For example, these could be obtained from offline benchmarking before running the logical circuit, or in the absence of any prior information, they could be simply uniform constraints $r(e) = 1, \forall e \in \mathcal{E}_\Gamma$. We express this additional information as linear constraints on the error rates:

$$B\vec{p} = \vec{0}. \quad (29)$$

More specifically, for each non-trivial syndrome error class $C_i \in \mathcal{C}^*$ for $i \in [|\mathcal{C}^*|]$, we pick a representative error $e_{C_i} \in C_i$, and then add pairwise constraints between the error rate $p_{e_{C_i}}$ and all other rates $p_{e'}$ for $e' \in C_i \setminus e_{C_i}$. Each constraint between e_{C_i} and e' thus corresponds to a row of B as

$$B_{ij} = \begin{cases} 1, & \text{if } e_j = e_{C_i}, \\ -\frac{r(e_{C_i})}{r(e_j)}, & \text{if } e_j = e', \\ 0, & \text{else.} \end{cases} \quad (30)$$

We use the abbreviation $e_j := (\bar{\mathcal{E}}_\Gamma)_j$ where $\bar{\mathcal{E}}_\Gamma$ is the tuple of all local errors following the order given in Eq. (15). On the other hand, each error e_{C_0} in the trivial syndrome error class C_0 is independent of the syndrome data and we could declare them as unlearnable. Alternatively, we could estimate its error rates as the weighted average over the error rate of the set of detectable errors $\mathcal{E}_\Gamma^* := \mathcal{E}_\Gamma \setminus C_0$ according to the prior belief $r(e)$:

$$B_{ij} = \begin{cases} 1, & \text{if } e_j = e_{C_0}, \\ \frac{-r(e_{C_0})}{|\mathcal{E}_\Gamma^*| r(e_j)}, & \text{if } e_j \in \mathcal{E}_\Gamma^*, \\ 0, & \text{else.} \end{cases} \quad (31)$$

This adds $|C_0|$ rows to B in addition to the $\sum_{C \in \mathcal{C}^*} (|C| - 1)$ rows from Eq. (30).

For estimating general Pauli channels, we resort to the system of non-linear equations Eq. (26)/Eq. (27) and Eq. (29). In practice, the empirical expectation values $\tilde{\Lambda}(M)$ do not lie in the image of $A^{(\mathcal{M})}$ due to shot noise, and we implement least square optimization to solve the two sets of equations:

$$\begin{aligned} & \underset{\vec{p}}{\text{minimize}} \quad \|\log \vec{\Lambda}^{(\mathcal{M}')} - A^{(\mathcal{M}')} \log \vec{\lambda}\|^2 + \|B\vec{p}\|^2, \\ & \text{subject to} \quad \vec{p} \geq 0. \end{aligned} \quad (32)$$

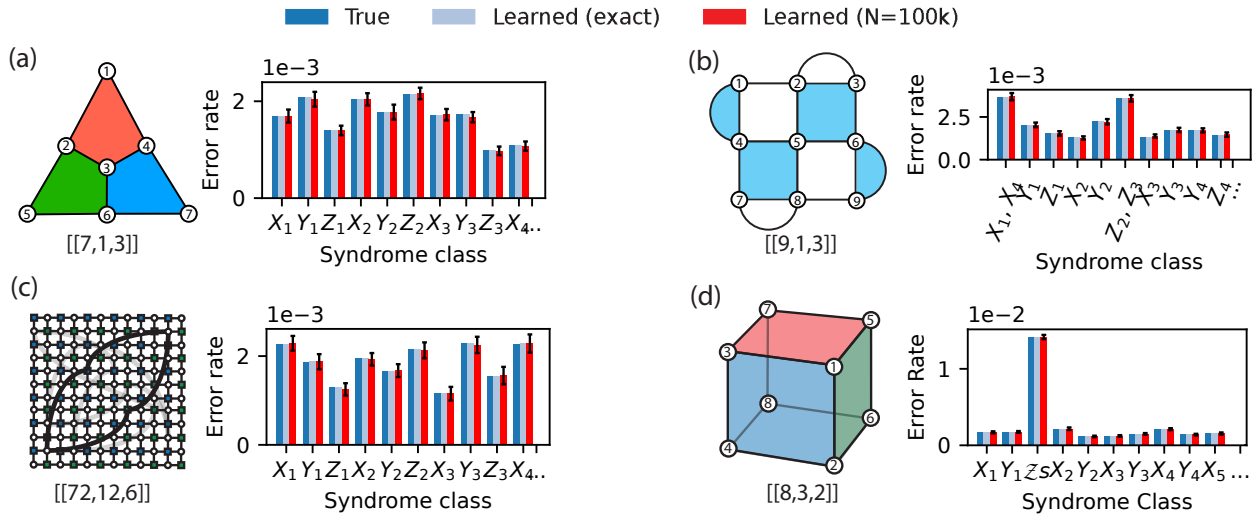


FIG. 2: Simulation result on various codes of learning syndrome class total error rates (true error rates in blue) using exact syndrome expectation values (light blue) and expectation values (red) from 100k samples. Here, single-qubit Pauli error rates are randomly generated around the mean. Codes in (a) seven-qubit Steane code and (c) the $[[72, 12, 6]]$ bivariate bicycle codes with polynomial $A(x, y) = x^3 + y + y^2$, $B(x, y) = y^3 + x + x^2$, have $d_{\text{pure}} \geq 3$, therefore all error rates are learnable. (b) The 3×3 rotated surface code has weight-2 XX (blue) and ZZ (white) generators on the boundary. (d) The $[[8, 3, 2]]$ 3D color code have Z stabilizers on the faces and a single X stabilizer generator $X^{\otimes 8}$. Therefore, all Z errors, denoted as Z_s , are indistinguishable. Both codes in (b) and (d) have $d_{\text{pure}} = 2$, and the sum of error rates in each syndrome error class can be learned.

Alternatively, optimization can be constructed using the transformed eigenvalues $\vec{\mu}$. For low error rates or assuming the independent errors assumption (Eq. (28)), one could reduce the number of variables and solve a simple system of linear equations Eq. (27) to estimate syndrome class error rates, i.e., $|\mathcal{C}^*|$ parameters. Physical error rate can be estimated using Eq. (29) thereafter. For noisy empirical syndrome expectation values, a straightforward pseudoinverse of $D'(\mathcal{M}')$ will give the least-squares estimate of the error rates, but may result in negative error rates for large shot noise. Alternatively, we solve the optimization:

$$\begin{aligned} \underset{\vec{p}}{\text{minimize}} \quad & \|\log \vec{\Lambda}^{(\mathcal{M}')} - D'(\mathcal{M}') \log \vec{\nu}\|^2, \\ \text{subject to} \quad & \log \vec{\nu} \leq 0. \end{aligned} \quad (33)$$

Most numerical results in this work are generated via Eq. (32), but Eq. (33) gives comparable results in the practically relevant error rate regime.

D. Simulation on static code

We simulate single qubit Pauli noise $\Gamma = \{\gamma_1 = \{1\}, \gamma_2 = \{2\}, \dots, \gamma_n = \{n\}\}$ on stabilizer codes of n qubits and solve the optimization problem in Eq. (32). Different codes with various parameters are chosen to show the generality of the algorithm. The simulated error rate of each single Pauli component in \mathcal{E}_Γ follows a

Gaussian distribution with mean 5×10^{-3} and standard deviation 10^{-3} .

We begin by simulating the $[[7, 1, 3]]$ Steane code [30], a CSS code with both X and Z stabilizer generators on every plaquette shown in Fig. 2(a). The code has pure distance $d_{\text{pure}} = 3$ as defined in Eq. (13) since it has stabilizers with minimum weight 4 and distance 3. This implies that all the single-qubit errors are learnable from the syndrome data. Therefore it has an empty trivial syndrome error class C_0 , and all non-trivial classes being singlets: $\mathcal{C}^* = \{\{X_1\}, \dots, \{Z_7\}\}$.

We first test the Pauli noise learning based on the exact syndrome expectation values for $M \in \mathcal{M}'$ from the simulated true noise \vec{p}^{true} :

$$\Lambda(M) = \prod_{i \in \text{supp}(M)} \Lambda_{\{i\}}(M_i) = \prod_{i \in \text{supp}(M)} (W_4 \vec{p}_{\{i\}}^{\text{true}})_{M_i} \quad (34)$$

Next, we benchmark the learning algorithm with empirical syndrome expectation values $\vec{\Lambda}(M)$ obtained from sampling syndromes $N = 100,000$ times and repeat the learning 30 times with resampled noise rates. As shown in Fig. 2(a), there is a perfect agreement between the simulated true error rates and the learned error rates based on exact syndrome expectation values and good agreement with the learned error rate based on sampled expectation values.

We perform a similar test on the rotated surface code [31], a family of topological codes, defined on a $d \times d$

square lattice with parameters $[[d^2, 1, d]]$. Note that its pure distance d_{pure} is always 2 for any distance d due to the stabilizer generators on the weight-2 plaquettes on the boundary. Every single-qubit error is detectable so C_0 is empty, but there are indistinguishable errors in some of the non-trivial syndrome error classes. In Fig. 2(b), we show our learned error rates on the 3×3 rotated surface codes and compare with the actual true error rate we simulated. The classes of indistinguishable errors are $\{X_1, X_4\}, \{Z_2, Z_3\}, \{X_6, X_9\}, \{Z_7, Z_8\}$. Theorem 3 implies that the sum of errors of each syndrome class is learnable. With the exact syndrome expectation value, we observe that all syndrome class error rates are learned accurately. With 100,000 samples, the learned syndrome class error rates closely match the true error rates.

Fig. 2(c) and (d) show the simulation on the $[[72, 12, 6]]$ bivariate bicycle code, where every single qubit Pauli channel is learnable, and on the $[[8, 3, 2]]$ 3D color codes where the sum of all Z errors and every other Pauli errors, is learnable.

E. Sample complexity for physical error rate learning

In this section, we study the number of samples N required to learn the syndrome class error rates P_C , which are related to the learnable Pauli eigenvalues by $P_C \approx -\frac{\log \nu_C}{2}$. We focus on low error rates for which $-\log \nu_C \approx 1 - \nu_C$. The precision in ν depends on the subset of the stabilizer elements chosen as well as how one solves Eq. (27) when we have an overdetermined system of linear equations. A recursive analytic solution is proposed in Ref. [23] for learning the detector error rate P_C^{detect} in Eq. (28) in an error model where every local Pauli error is independent. We show in Section I 1 that this method can be generalized to solve the linear equations Eq. (27) for our more general error model. Furthermore, we show in Theorem 4 that the sample size required to achieve a constant additive precision ϵ of estimating syndrome class error rate can be shown to be independent of the system size for qLDPC codes and local sparse Pauli channel.

Given a set of measured stabilizer generators $\{M_i\}_i^m$ for the measured stabilizer group $\mathcal{M} = \langle M_1, \dots, M_m \rangle$, we denote the indices of the stabilizer generators violated for each syndrome class $C \in \mathcal{C}$ as $J(C) \subseteq [m]$. We define $X_C = \log \nu_C$ and for any $S \subseteq [m]$, let $Y_S = \log \Lambda(\prod_{i \in S} M_i)$. The recursive solution in [23] for any syndrome class $C \in \mathcal{C}$ can be written as

$$X_C = - \sum_{\substack{C' \in \mathcal{C} \\ J(C') \supset J(C)}} X_{C'} + \frac{1}{2^{|J(C)|-1}} \sum_{S \subseteq J(C)} (-1)^{(|S|-1)} Y_S. \quad (35)$$

We show in Section I that this solves Eq. (27) using Gaussian elimination. The subset \mathcal{M}' of stabilizer elements

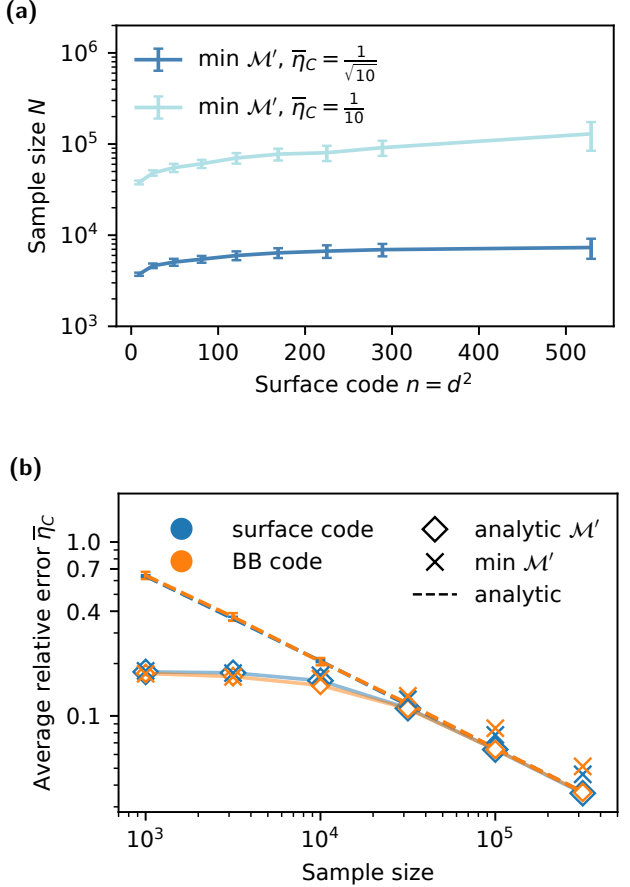


FIG. 3: Numerical results of relative error of learned single-qubit error rates vs sample size. The true error rates are sampled from $p \sim \mathcal{N}(\mu, \sigma^2)$, where $\mu = 5/3 \times 10^{-3}$, $\sigma = 1/3 \times 10^{-3}$. (a) Estimated sample size needed for surface code with various code distances using the optimization Eq. (32) with uniform constraints B within each syndrome class. This does not involve avoiding overfitting, and only the minimal stabilizer subset is used. Sample size is almost constant with respect to code size n . (b) Result of optimization while avoiding overfitting. We test the relative error of learning for surface code $d = 23$ (blue) and the $[[72, 12, 6]]$ bivariate bicycle codes (orange). With the same stabilizer subset \mathcal{M}' , the optimization (diamonds) outperforms the analytical solution (dotted lines) in Eq. (35) at low sample sizes ($N \leq 30k$) and is comparable to it at larger sample sizes. Using only a minimal stabilizer subset gives similar performance (crosses) at low sample size. The result is the average of 20 sets of error rates from the normal distribution \mathcal{N} .

involved here is the union of elements in the local stabilizer group, i.e., $\mathcal{M}' = \bigcup_{C \in \mathcal{C}} \{\prod_{i \in J'} M_i \mid J' \subseteq J(C)\}$. For a (r_s, c_s) -qLDPC code and a local sparse (r_Γ, c_Γ) -total Pauli error channel \mathcal{N}_Γ , we have $|J(C)| \leq r_\Gamma c_s$ and $|\{C' \in \mathcal{C} \mid J(C') \supset J(C)\}| \leq r_s c_\Gamma$ for any syndrome class C . Each variable X_C , therefore, depends on a bounded

number of Y_S 's, and each involved Y_S has a bounded additive error from shot noise due to all elements in \mathcal{M}' being constant-weight. With this observation, we show the sample complexity for learning syndrome class error rates below:

Theorem 4 (Sample complexity for syndrome class learning). *Consider a local sparse Pauli channel \mathcal{N}_Γ on an n -qubit qLDPC code. Given $\epsilon > 0$, there exists a constant $C_c > 0$ such that if $\|\vec{p}\|_\infty^2 < \epsilon/(2C_c)$, the sample size N required to estimate the syndrome error class $P_C, \forall C \in \mathcal{C}^*$ to additive precision ϵ using Eq. (35) is $\tilde{\mathcal{O}}(\epsilon^{-2})$, independent of the system size n .*

See the details of the proof in Section I1 using Hoeffding's inequality. Note that applying Chernoff bound to the Bernoulli distribution (syndrome bit flip) gives a more precise scaling $N = \tilde{\mathcal{O}}(p_{\max}/\epsilon^2)$, where $p_{\max} = \|\vec{p}\|_\infty$.

We test the quality of learning as a function of sample size and system size using both the minimal \mathcal{M}' syndrome data, i.e. the minimal subset \mathcal{M}' with $|\mathcal{M}'| = \text{rank } \mathcal{M}$ from Algorithm 1, and analytical \mathcal{M}' , i.e., the subset \mathcal{M}' involved in the analytical solution Eq. (35). We measure the quality of learning using the average relative error:

$$\bar{\eta}_C = \frac{1}{|\mathcal{C}^*|} \sum_{C \in \mathcal{C}^*} \frac{\epsilon_C}{P_C}, \quad (36)$$

which compares the learned and true syndrome-class error rates over all nontrivial syndrome classes \mathcal{C}^* .

First, we test on the rotated surface code with system sizes $n = 3^2, 5^2, \dots, 23^2$ and sample sizes from 1000 to 6,000,000. Each qubit is subject to a single-qubit Pauli channel, and the error rate $p \sim \mathcal{N}(\mu, \sigma^2)$ of each Pauli component is sampled from a Gaussian distribution with mean $\mu = 5/3 \times 10^{-3}$ and standard deviation $\sigma = 1/3 \times 10^{-3}$. We clip negative values to 10^{-5} . We tested the optimization method based on minimal \mathcal{M}' in Eq. (32) with uniform constraints B within each syndrome class. We fit a linear model of $\bar{\eta}_C$ as a function of sample size on the log scale and estimate the sample size needed to achieve a fixed precision. As shown in Fig. 3a, the optimization using a minimal stabilizer subset requires nearly constant sample size.

We further compare the optimization method in Eq. (33) with the analytic solution Eq. (35) and observed two main factors influencing the precision. On the one hand, the minimal stabilizer subset \mathcal{M}' used in Eq. (33) contains the least noisy syndromes due to their minimal weight, but also lacks redundancy. On the other hand, we observe that at smaller sample sizes, the system of equations (35) tends to overfit, i.e., learning the shot noise rather than the actual noise. Therefore, the gradient-descent-based optimization on linear equations provides two advantages. On the one hand, one can tune the number of stabilizers used as long as the equation satisfies the full-rank condition. Moreover, one can in

principle terminate the optimization before it starts to overfit. We adopt the simple approach of calibrating the termination point by simulating relevant error rates and recording the average number of iterations after which the average relative error starts to increase.

We test the optimization Eq. (33) on a distance-23 rotated surface code and the $[[72, 12, 6]]$ bivariate bicycle codes. We first determine a terminal step number from one fixed error rate and apply this same number of optimization steps to learn 20 other sets of error rates from the same distribution $\mathcal{N}(\mu, \sigma^2)$. In Fig. 3b, we observe that below $N = 30k$, optimization significantly outperforms the analytic solution, with the two agreeing once N becomes large. Moreover, we observe that by optimizing while minimizing overfitting, using the minimal \mathcal{M}' also has comparable performance in this low sample size regime compared with using the larger set from the analytic solution.

IV. CIRCUIT-LEVEL NOISE LEARNING

To learn circuit-level Pauli noise for Clifford circuits, we utilize the circuit-to-code mapping, a formalism of converting the problem of correcting circuit-level Pauli errors into the problem of correcting Pauli errors on the corresponding *spacetime code* [13–15]. As we focus on non-adaptive fault-tolerant Clifford circuits here, the method introduced in Section III for static codes with a single round of syndrome extraction can then be applied to the spacetime code.

We begin by reviewing the spacetime code formalism and identifying the correct noise model on the spacetime code from the circuit-level error model in Section IV A. We then demonstrate our method using simulations of circuit-level noise in Section IV, and apply it to experimental data in Section IV C.

A. Mapping to the spacetime code

We first introduce the setup of the spacetime code. Given a Clifford circuit with n qubits and T time steps, the spacetime code is a subsystem stabilizer code of $n^{(\text{ST})} = n(T + 1)$ qubits. We label each qubit by its spacetime location (q, t) where q denotes the qubit (i.e., the spatial label in the circuit) and t denotes the time-coordinate index. The first and last layer of spacetime qubits are placed before the first gate layer and after the last gate layer respectively. The temporal labels t of the spacetime qubits are $0.5, 1.5, \dots, T + 0.5$, where the 0.5 shift here emphasizes that the spacetime qubits are placed before and after the gates. We illustrate the spacetime mapping for a simple 4-qubit Clifford circuit that extracts a syndrome of the 3-qubit repetition code in Fig. 4.

We now introduce the construction of the measured stabilizer and the logical group in the spacetime code, as

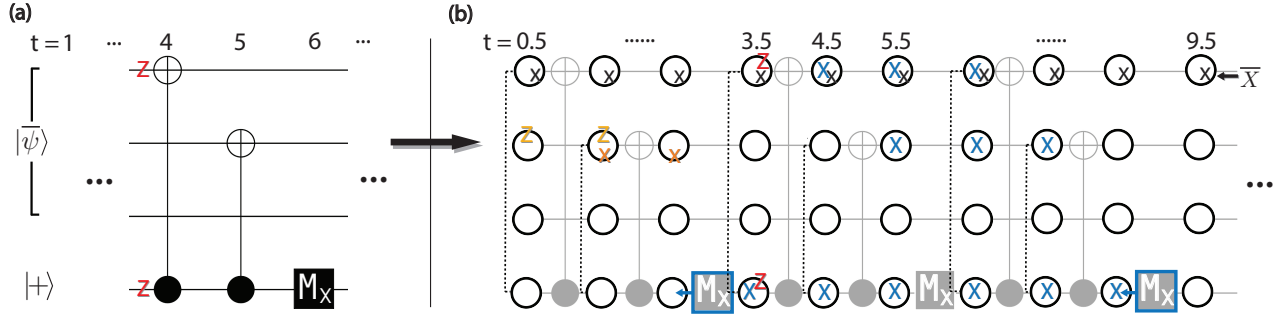


FIG. 4: Circuit-to-code mapping illustrated using a syndrome extraction circuit for the 3-qubit repetition code. (a) r rounds of 3-layer syndrome extraction circuits that measure X_1X_2 for the repetition code with stabilizer group $\mathcal{S}^{(\text{ini})} = \langle X_1X_2, X_2X_3 \rangle$. The last qubit is the ancilla qubit for syndrome readout. (b) The spacetime code with $4 \times (3r + 1)$ qubits mapped from the circuit in (a). Pauli operator in blue is a measured stabilizer generator of the spacetime code due to the parity constraints on the first and third measurement results (blue squares). The stabilizer elements are local within the associated measurements in the temporal direction. One logical representative $\overline{X}^{(\text{ST})}$ as the back-culm of \overline{X} at the last layer is shown in black. It will be a measured spacetime logical operator if the first qubit is eventually measured. Correlated ZZ error on the CNOT gate shown in (a) is mapped to ZZ errors at $t = 3.5$ (in red). Its syndrome and logical effect are given by the commutation with the spacetime stabilizer and logical operator respectively. The gauge group $\mathcal{G}^{(\text{ST})}$ contains errors with trivial syndrome and logical effect. $\mathcal{G}^{(\text{ST})}$ is non-abelian in general (see a pair of errors in light and dark orange).

these are relevant to the noise-learning algorithm. One way to capture the effect of circuit Pauli errors on syndrome and logical measurements is by checking the commutation relations of the circuit errors that are forward propagated to the syndrome and logical measurements at particular spacetime locations. A more natural way from the perspective of the noise model, however, is to capture these commutation relations in the structure of the spacetime code, while errors stay local in their spacetime location, just like in the static code case. This is possible because the same commutation holds between the errors localized at their spacetime locations and the backward-propagated measurements to the relevant layer.

Formally, the spacetime stabilizer and logical operators are objects referred to as *back-cumulant* [15] (or *spackle* [13, 14]) of some Pauli operator $O \in \mathcal{P}_{n(T+1)}$ and we denote it as \overleftarrow{O} . For $t \in \{1, \dots, T+1\}$, the components $\overleftarrow{O}_t \in \mathcal{P}_n$ of $\overleftarrow{O} \in \mathcal{P}_{n(T+1)}$ at the layer t are given by

$$(\overleftarrow{O})_{t-0.5} = \prod_{t'=T+1}^t U_{t,t'}^\dagger O_{t'-0.5} U_{t,t'}. \quad (37)$$

Here, $U_{t,t'} = \prod_{s=t}^{t'-1} U_s$ is a product of the gates U_s from layer t to $t' - 1$ and we let $U_{t,t'} = I$ if $t' \leq t$.

We begin by constructing the spacetime stabilizer operators. We assume the input to the Clifford circuit, up to a possible flip of the syndrome values, is a codeword of a stabilizer code with stabilizer group $\mathcal{S}^{(\text{ini})}$, i.e., a state $|\psi\rangle$ satisfying $S^{(\text{ini})} |\psi\rangle = \pm |\psi\rangle, \forall S^{(\text{ini})} \in \mathcal{S}^{(\text{ini})}$. We fictitiously add a layer of perfect syndrome measurement $S^{(\text{ini})} \in \mathcal{S}^{(\text{ini})}$ at $t = 0$ to record the initial syndrome. This is then followed by the Clifford gates and Pauli mea-

surements in the circuits. One can efficiently track how the stabilizer group and the group of logical operators change after each operation's action [32].

The spacetime stabilizer operators are then constructed from the linear constraints that the measurement results of a noise-free circuit satisfy. Given an initial stabilizer group with s generators and m measurements in the circuit, we denote the measured operators by $\vec{E} = (S_1^{(\text{ini})}, \dots, S_s^{(\text{ini})}, M_1^{(\text{circ})}, \dots, M_m^{(\text{circ})})$. The measurement results of these operators are stored in a binary vector $\vec{o} \in \mathbb{Z}_2^{s+m}$, where we assign $o_i = 0$ when the value of E_i is $+1$ and $o_i = 1$ if it is -1 . In the absence of circuit errors, whenever a stabilizer element is measured, the measurement result is deterministic and depends on previous measurement outcomes. The measurement result \vec{o} in the circuit therefore needs to satisfy consistency relations, or *parity checks* $\mathcal{O}^\perp = \{\vec{u}\}$, in that every set of noise-free measurement outcomes \vec{o} satisfies $\vec{u} \cdot \vec{o} = 0$ for all $\vec{u} \in \mathcal{O}^\perp$. Circuit errors can be detected from flips of those parity checks, which coincides with the notion of detector [17, 33].

The generators of the measured spacetime stabilizer group $\mathcal{M}^{(\text{ST})}$ are then constructed from the parity constraints $\vec{u} \in \mathcal{O}^\perp$ of the circuit as

$$M^{(\text{ST})}(\vec{u}) = \prod_{i=s+1}^{s+m} \kappa_{t_{E_i}-0.5}(E_i^{u_i}), \quad (38)$$

where $\kappa_t(O) \in \mathcal{P}_{n(T+1)}$ denotes the operator obtained by embedding $O \in \mathcal{P}_n$ at layer t and tensor product with identity I_n for all other layers. t_{E_i} denotes the layer where E_i is measured (for initial stabilizer generators

$S^{(\text{ini})}$, $t_{S^{(\text{ini})}} = 0$). One notable property of $M^{(\text{ST})}(\vec{u})$ is that it is bounded by the time involved in the parity constraint $\vec{u} \in \mathcal{O}^\perp$ (Lemma 8 in [15]), i.e., for all $(q, t) \in \text{supp}(M^{(\text{ST})}(\vec{u}))$ we have

$$\min_{j \in [s+m] \mid u_j=1} t_{E_j} < t < \max_{j \in [s+m] \mid u_j=1} t_{E_j}. \quad (39)$$

We now introduce the measured logical group of the spacetime code. We emphasize that we want to understand the logical errors only on the relevant logical measurements of the circuit. This makes the spacetime code a subsystem code since, in general, the set of undetectable yet logically trivial errors in the circuits corresponds to a non-abelian subgroup in $\mathcal{P}_{n(T+1)}$ for the spacetime code. See example of such errors in Fig. 4(b). These logically trivial errors generate the gauge group $\mathcal{G}^{(\text{ST})}$ of the spacetime code. See Section G for the construction.

In a subsystem code, logical Pauli operators that commute with the gauge group encode the logical information and are called the bare logical operators. In contrast, dressed logical operators commute with the stabilizer group but may anticommute with some gauge operators [34]; these are the logical errors of the code. Unless otherwise specified, we use “logical operators” to mean bare logical operators. In this work, we focus on a subgroup of spacetime logical operators $\mathcal{L}'^{(\text{ST})}$ corresponding to the logical Pauli measurements in the circuit. In a Clifford circuit with m_L logical measurements, we denote the logical measurement outcome as $\vec{o}^L \in \mathbb{Z}_2^{m_L}$. In a noiseless circuit, each logical Pauli measurement result o_i^L will depend on a set of physical measurement results as $o_i^L = \vec{u}^L \cdot \vec{o}$ for some binary vector $\vec{u}^L \in \mathbb{Z}_2^{s+m}$. Here, the non-zero elements of \vec{u}^L correspond to the physical measurements involved. \vec{u}^L corresponds to a generator

$$L'^{(\text{ST})}(\vec{u}^L) = \prod_{i=s+1}^{s+m} \kappa_{t_{E_i}-0.5}(E_i^{u_i^L}) \quad (40)$$

of the group of measured logical operators $\mathcal{L}'^{(\text{ST})}$ in the spacetime code. See Fig. 4 for an example. The detailed generic algorithm of constructing \mathcal{O}^\perp , $\mathcal{M}^{(\text{ST})}$, and $\mathcal{L}^{(\text{ST})}$ is explained in Section G.

Pauli errors in the circuit can also be mapped onto the spacetime code. A circuit error represented as $e^{(\text{circ})} = (e_t \in \mathcal{P}_n \mid t \in [T+1])$, i.e., inserting Pauli error e_t before each circuit layer t , can be mapped to the error $e^{(\text{ST})} \in \mathcal{P}_{n(T+1)}$ in the spacetime code as

$$e^{(\text{ST})} = \prod_{t \in [T+1]} \kappa_{t-0.5}(e_t). \quad (41)$$

Throughout the remainder of the text, we identify circuit errors $e^{(\text{circ})}$ with their corresponding spacetime-code Pauli errors $e^{(\text{ST})} \in \mathcal{P}_{n(T+1)}$ via equation Eq. (41) and its inverse relation $e^{(\text{circ})} = (e_t^{(\text{ST})} \mid t \in [T+1])$.

We now define the circuit-level Pauli error model in a way that admits a natural representation as a Pauli

noise model (Section II) on the spacetime code by identifying each spacetime location (q, t) in the circuit with the spacetime qubit labeled by (q, t) .

Definition 5 (Circuit-level Pauli error model). *We define a circuit-level Pauli model by a set of spacetime supports $\Gamma^{(\text{ST})} = \{\gamma_i\}_i$. Each support $\gamma \in \Gamma^{(\text{ST})}$ is a set of spacetime locations $\{(q_1, t_1), (q_2, t_2), \dots\}$ in the circuit labeling the spacetime qubits. Each support is associated with a Pauli error distribution $P_\gamma : \mathcal{P}_{n(T+1)} \rightarrow [0, 1]$ and $P_\gamma(e) = 0$ if $\text{supp}(e) \not\subseteq \gamma$. The circuit-level Pauli error model is then a distribution of Pauli errors over the whole circuit given by the convolution of local distributions $P_{\Gamma^{(\text{ST})}} = *_{\gamma \in \Gamma^{(\text{ST})}} P_\gamma$.*

Pauli error models on the spacetime code correspond to circuit-level noise models on the circuit with errors correlated in space and time, depending on the structure of the set of spacetime supports $\Gamma^{(\text{ST})}$. Therefore, a general Pauli noise model could, in principle, capture features of correlated errors, leakage errors, and non-Markovian errors, but the practical application for more complicated error models will be out of the scope of this paper. In the remaining numerical and experimental results, we instead consider the Pauli noise model on the spacetime code according to the standard circuit model in the fault-tolerance literature, where errors are only correlated between qubits involved in each circuit location defined below.

Definition 6 (Circuit location). *We define circuit locations as the indivisible operations in a circuit, including idling, state preparation, gates, and measurements. Each location is associated with a time step and a set of qubits it acts upon. Locations at the same time step do not share any qubit.*

Definition 7 (Standard circuit-level Pauli error model). *The standard circuit-level Pauli noise model is a restricted version of the circuit-level Pauli noise model in Definition 5. In this mode, a w -qubit Pauli error channel is placed before every w -qubit circuit location except for state preparation locations, where the error channel is applied afterwards. The channel acts on the same w qubits involved in the corresponding location.*

The standard circuit-level Pauli noise model, apart from the state preparations at the beginning, corresponds to a non-overlapping Pauli error channel \mathcal{N}_Γ on the spacetime code. Specifically, \mathcal{N}_Γ is the composition of w -qubit Pauli channels, each acting on the w spacetime qubits at time $t - 0.5$ corresponding to a circuit location involving those w qubits at time t . For example, a noisy CNOT gate at circuit layer t on qubit i and j corresponds to a local Pauli channel $\mathcal{N}_{\{(i, t-0.5), (j, t-0.5)\}}$ on the spacetime code.

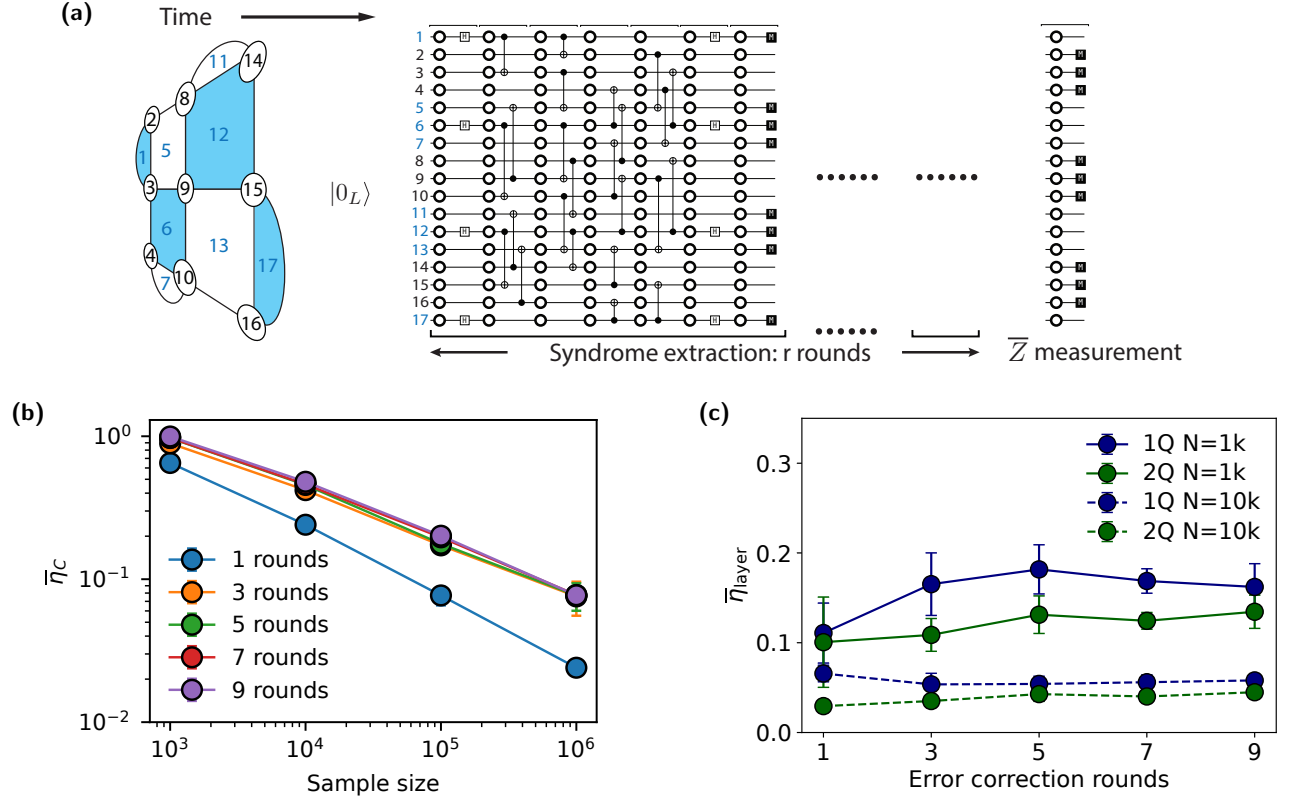


FIG. 5: (a) Error correction circuit for the 3×3 rotated surface code and its corresponding spacetime code. The surface code starts from its logical $|\bar{0}\rangle$ state and we simulate r rounds of syndrome extractions followed by a transversal Z measurement. The learning algorithm converts the whole circuit into a spacetime code where spacetime qubits (empty circles) are placed before every layer of gates. (b) The relative error $\bar{\eta}_C$ of the learned syndrome class total error rate averaged over all classes. We simulated for different rounds of syndrome extraction. (c) relative error $\bar{\eta}_{\text{layer}}$ of the estimated average single-qubit (1Q) and two-qubit (2Q) error rates per layer. The true circuit-level error rates are sampled from a Gaussian distribution ($\mu = 0.001/3, \sigma = 0.0002/3$ and $\mu = 0.01/15, \sigma = 0.002/15$ for the Pauli error components of single-qubit and two-qubit locations respectively).

B. Simulation on circuit-level noise learning

We first test our noise learning algorithm on the spacetime code of the Clifford circuits by performing simulations on surface code quantum memory circuits, constructed as follows. We initialize in the initial logical state of the 3×3 rotated surface code in the logical $|\bar{0}\rangle$ state, and place one ancilla qubit in the state $|0\rangle$ for each plaquette of the rotated surface code. A single round of syndrome measurement has seven layers of gates, consisting of performing Hadamard gates on the X syndrome ancillas, using CNOT gates to entangle ancilla and data qubits, and measuring ancilla qubits in the correct basis to read out the syndrome bits, see Fig. 5a. Here, the order of CNOTs is chosen to maximize parallelism and ensure fault tolerance [35]. We perform several rounds of syndrome extraction before a final transversal measurement in the computational basis to perform a fault-tolerant logical \bar{Z} measurement. For simplicity, we do not perform ancilla qubit reset between rounds of syn-

drome extraction, but simply keep track of all measurement records [36]. The spacetime stabilizer measurement values (detectors) are calculated based on these records.

Given a Clifford circuit, there are different ways of selecting a set of generators for the measured spacetime stabilizer group $\mathcal{M}^{(\text{ST})}$ corresponding to different bases that implement the same parity check matrix \mathcal{O}^\perp on the measurement outcomes. With the property in Eq. (39), we optimize the set of generators such that the weight of each $M^{(\text{ST})}(\vec{u})$ is constant by constructing a generating set of $\{\vec{u}\}$ for $\text{span}(\mathcal{O}^\perp)$ that involve measurements in a local time window. Specifically, for the surface code syndrome extraction circuit in Fig. 5a, we define the local spacetime stabilizer generators based on the following parity constraints: For the first two rounds ($r = 1, 2$) of syndrome extractions, we set each u to encode the parity of an ancilla measurement result and the corresponding initial stabilizer value. For syndrome measurements at round $r > 2$, we set each u to encode the parity of an ancilla result at round r and round $r - 2$. Lastly, the

transversal Z measurement at the end also creates Z type spacetime generators. For each Z stabilizer generator S_z of the surface code, we set an additional parity check u as the parity of the final data qubit bit strings for S_z and the corresponding ancilla measurement at the last two rounds. We construct the local spacetime generators with these parity checks u according to Eq. (38). A r -round 3×3 surface code EC circuit has $8r + 4$ local spacetime stabilizer generators. We feed these generators into Algorithm 1 to find the minimal set of equations in Eq. (26). Under the standard circuit-level Pauli noise model for a 9-round syndrome extraction circuit, we obtain 961 independent equations corresponding to $|\mathcal{C}^*| = 961$ non-trivial syndrome error classes.

We simulate the standard circuit-level Pauli error model where each Pauli component of single-qubit and two-qubit channels has an error rate following a Gaussian distribution centered at near-threshold error rates $0.001/3$ and $0.01/15$, fluctuating with standard deviation $0.0002/3$ and $0.002/15$ respectively. After converting the circuit into a spacetime code, we apply our learning algorithm Eq. (32) for static code under various extra constraints B using sample sizes $N = 10^3, 10^4, 10^5, 10^6$.

To evaluate the quality of circuit noise learning, we first study how well we can learn the total error rates of the syndrome class of the corresponding spacetime code. Errors within each syndrome class correspond to circuit-level errors that violate the same parity constraints (detectors) $\forall u \in \mathcal{O}^\perp$. Here, we use the optimization method Eq. (32) instead of the approximation method in Eq. (33) as we observe the result from optimization is slightly better, although the latter is more efficient in terms of classical computational cost. We use the simple extra assumption B which assumes uniform noise for all local Pauli errors, i.e. $r(e) = 1, \forall e \in \mathcal{E}_\Gamma$ in Eq. (30) and Eq. (31). In Fig. 5b, we show the average relative error $\bar{\eta}_C = \frac{1}{|\mathcal{C}^*|} \sum_{C \in \mathcal{C}^*} \eta_C$ of the predicted syndrome class total error rates to the true error rates. With around $N = 1000$ samples, the learning algorithm can learn the orders of magnitude of the syndrome class total error rates. By increasing the sample size to $N = 10^4$ to 10^5 , we achieve better relative precision, and the estimation quality remains stable as the number of syndrome extraction rounds increases. We note that we expect the accuracy can be substantially improved for sample size $N = 1000$ to 10000 if techniques of reducing shot noise are used, according to the comparison of circles and dotted lines shown in the Fig. 3b in the code capacity setting.

We also estimate the average error rate for single-qubit locations and two-qubit locations (CNOT gates) per layer, and we expect it to require a smaller sample size to reach the same relative precision compared with estimating syndrome class total error rates. We implement the optimization Eq. (32) with B following the average noise ratio of single-qubit and two-qubit gates, i.e., $r(e^{(1Q)}) = 1, r(e^{(2Q)}) = 10$. We consider $\bar{\eta}_{\text{layer}}^{(1Q)}$ and $\bar{\eta}_{\text{layer}}^{(2Q)}$ which represent the relative error of our estimated

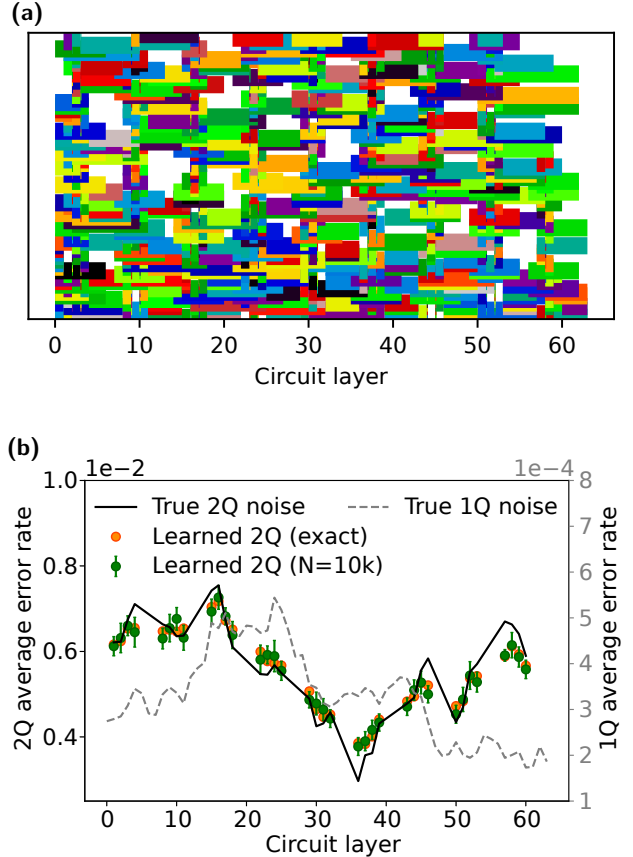


FIG. 6: (a) The temporal span of 961 non-trivial syndrome error classes \mathcal{C}^* for the 9-round 3×3 surface code EC circuit (Fig. 5a) with circuit level noise. The vertical position is arbitrary as we focus on the resolution in time, and the colors are only for distinguishing different classes. 331 classes are contained in a single layer and 297 classes involve only two consecutive layers. (b) The estimated average two-qubit (2Q) error rates per layer using the simulated syndrome data. We apply a time-varying error rate that follows a random walk for 1Q and 2Q errors independently. The extra constraints encoded in B (Eq. (32)) is set according to the initial ratio of $p_0^{(1Q)}$ and $p_0^{(2Q)}$. We observe that the learned error rates both from the exact syndrome (orange dots) and from $N = 10,000$ samples (green dots) match the true error rates and serve as good estimates of the time-dependent noise.

single-qubit and two-qubit error rates per layer averaged over all layers, and they are shown in Fig. 5c. With 1000 samples under this noise setup, the learning algorithm can estimate single-qubit and two-qubit gate average error rates per layer within 0.2 relative error.

Furthermore, we investigate how well the learning algorithm could perform under time-dependent noise. In time series analysis, one could model discrete time-dependent noise as an average over a series of Markov chains $p_t =$

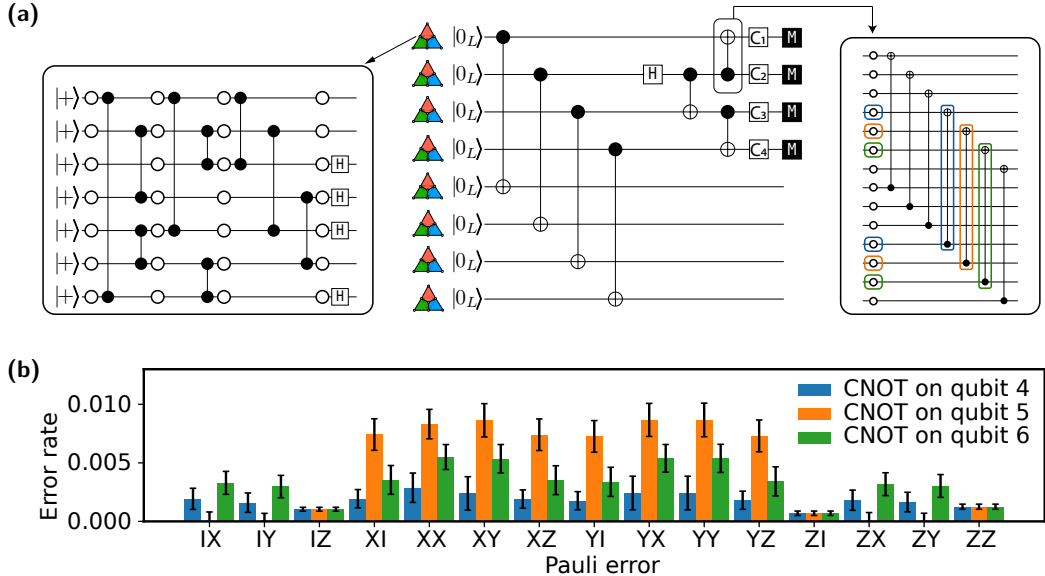


FIG. 7: Logical GHZ state preparation experiment and physical error rate learning. (a) The box on the left shows the encoding circuit for logical $|\bar{0}\rangle$ of the [[7,1,3]] Steane code. A series of logical circuits for preparing the 4-qubit encoded GHZ state and logical stabilizer measurements are shown in the middle. Here, logical Hadamard and CNOT gates are transversal gates acting on code blocks. The lower four code blocks fault-tolerantly verify the prepared $|\bar{0}\rangle$. The last two layers implement direct fidelity estimation in experiments where logical Clifford gates are applied and then qubits are measured transversally in the Z basis. The box on the right shows the physical circuit of the transversal CNOT gates of the enclosed logical CNOT gate. Empty circles shown in the physical circuits are qubits of the spacetime code, susceptible to errors from gates to their right in the diagram. (b) Learned Pauli error rates of the CNOT gates enclosed in the middle logical circuit for the logical $ZZZZ$ measurement circuits are shown. The learning algorithm is applied based on the syndrome data of the spacetime stabilizer (detectors) constructed without the knowledge of the initial logical state of the data blocks.

$\frac{1}{M} \sum_{m=1}^M p_t^m$, $t = 0, \dots, T$. Here p_t^m is of the form [37, 38]:

$$p_t^m = \theta^m p_{t-1}^m + \sigma \eta_t, \quad t = 1, \dots, T. \quad (42)$$

where η_t are i.i.d random variables following the standard normal distribution and θ^m is a parameter from 0 to 1. One could approximate the noise signal with spectral density $S(f) \sim 1/f^\alpha$ if θ^m following a certain distribution parametrized by α (Eq. (15) in [38]). With $\theta^m = 0$, we have non-correlated noise, also known as white noise, whereas when $\theta^m = 1$, we have noise exhibiting the 1D random walk ($S(f) \sim 1/f^2$). For simplicity, we simulate the 3×3 surface code circuit with unbiased Pauli errors that only distinguish single qubit operations (including measurement and idling noise) and two qubit gates with initial total error rate $p_0^{(1Q)} = 3 \times 10^{-4}$ and $p_0^{(2Q)} = 5 \times 10^{-3}$, respectively. We model 1Q and 2Q noise separately, each being uniform in every layer and evolving as a random walk with parameter $M = 1, \theta = 1, \frac{\sigma}{p_0} = 0.1$.

Similarly, we use the gate-based extra constraints in the B matrix for the optimization, i.e. $r(e^{(1Q)})/r(e^{(2Q)}) = p_0^{(1Q)}/p_0^{(2Q)}$. We note that we have worse predictions of average error rates per layer for

less noisy processes, e.g., single-qubit gates, when error rates are highly time-dependent. On the other hand, the algorithm can capture the error rates for the noisy process, i.e., two-qubit gates in this case. In Fig. 6b, we show the result of the learned two-qubit gate errors from both exact syndrome expectations and syndrome expectations from $N = 10K$ samples. The learned error rates averaged at every layer are consistent with the true error rates, even at this small sample size. This exceeds our naive expectation that noise only resolved between different syndrome extraction rounds, as we only have one round of measurement at the end of the depth-7 syndrome extraction circuit. The resolution can be explained by the short temporal span of the syndrome error classes, as shown in Fig. 6a. Out of 961 syndrome error classes, 331 classes are contained in a single layer and 297 classes involve only two consecutive layers, whereas a single EC cycle includes 7 layers of gates.

C. Learning from experimental data

We consider learning the circuit-level noise model of a fault-tolerant circuit performed on the Harvard neutral atom platform [1] that prepares a logical 4-qubit GHZ state, as shown in Fig. 7a. The logical circuit is encoded in four blocks of seven-qubit Steane code by the non-fault-tolerant $|\bar{0}\rangle$ preparation circuit and then fault-tolerantly verified by the other four blocks of logical ancillas in $|\bar{0}\rangle$. Then, the logical GHZ state is prepared using logical Hadamard and CNOT gates, which are transversal for the Steane code. To correct errors and verify logical fidelity, the direct fidelity estimation [39] on the logical level was performed by measuring all elements of the logical stabilizer group $\langle \bar{Z}ZII, \bar{IZ}ZI, \bar{II}ZZ, \bar{XXX}\rangle$ of the logical GHZ state. The logical measurements in the \bar{Z} basis, i.e. $\langle \bar{Z}ZII, \bar{IZ}ZI, \bar{II}ZZ \rangle$, can be done simultaneously with a single logical circuit; therefore, 9 logical circuits are executed in total. The initial stabilizer generators of the circuit are $X_1, X_2, X_5, X_6, X_3X_4, X_3X_7$, which propagate to the stabilizer generators of the Steane code for each data code block, along with all single-qubit X operators for the ancilla blocks. These are provided as input to Algorithm 2 to construct the measured spacetime stabilizer group of each logical circuit.

To get a reasonable estimate of gate error rates, we impose extra constraints B using previously reported gate fidelities [40] as a reference. Specifically, for errors within each syndrome class of the spacetime code, we differentiate them by the prior belief $r(e)$ Eqs. (30) and (31), i.e., a relative strength between errors of different circuit location type, as $r = 1, 3, 10, 20$ for idle, single-qubit, two-qubit, and measurement errors respectively. Each logical circuit is repeated and postselected on successful initialization, resulting in a sample size N of less than 3000 times, and these sampled measurement bitstrings are used to obtain the expectation values of the spacetime code syndrome, i.e., the empirical Pauli eigenvalues. Part of the learned logical CNOT gate error rates are shown in Fig. 7b. To estimate the uncertainty of the learned noise, we simulate sampling syndrome with the same number of samples as in the experiment and apply the learning procedure to these simulated syndrome data. The resulting error bars represent the standard deviation of the learned error rates over 30 repetitions. We can distinguish the relative noise strength of different gates and Pauli components with a certain confidence. This can be useful to identify potential circuit defects to perform gate tune-up. One of the features we observe in common with the learned error rates in this collection of circuits is that the gate fidelity tends to diminish over time. We hypothesized that this is caused by atom loss. See Section K for the complete estimated error rates for the \bar{ZZZZ} measurement circuit.

V. LEARNING LOGICAL ERROR RATES AND LOGICAL FIDELITY FROM SYNDROME DATA

In the previous section, we showed how to explicitly characterize physical circuit-level errors in fault-tolerant circuits using syndrome data. In this section, we ask if that same data can also be used to benchmark the quality of the implemented *logical circuits*. We extend the results of Wagner *et al.* [12] from the channel-coding setting to non-adaptive Clifford circuits, allowing arbitrary stabilizer code codewords as inputs and logical measurements. Given a Clifford circuit that is fault-tolerant to the assumed circuit-level Pauli error model (Definitions 5 and 9), we first prove that with respect to the set of logical measurements, the total error rate of the classes of logically equivalent errors with a given syndrome is learnable using the syndrome expectation values. We emphasize that this is a decoder-independent quantity.

Consequently, with a decoder, we show that logical error rates for the set of logical measurements are learnable. In practice, we take the estimated physical error rates that satisfy the syndrome expectation, as described in Section III C, and perform Monte Carlo simulations using any relevant decoder to learn the logical error rates. Notably, the input state of the circuit can be any codeword (e.g., non-stabilizer state) since characterizing errors of logical measurements in Clifford circuits can be determined from the commutation relation between circuit errors and the spacetime code logical operators (see Section G).

A. Logical error rate learnability

We consider an ideal logical circuit with a set of m_L logical measurements $\mathcal{M}_L = \{\bar{M}_i\}_i$ implemented by a physical fault-tolerant Clifford circuit. For example, for the logical GHZ preparation circuit shown in Fig. 7a with Z basis measurements, the set of logical measurements is $\mathcal{M}_L = \{\bar{Z}III, \bar{IZ}II, \bar{II}ZI, \bar{III}Z\}$ at the final layer. The ideal logical circuits can be thought of as a quantum-to-classical channel. Given an input state, the channel can be described by a distribution over the output classical bitstrings $\bar{o}_L^{(\text{ideal})} \in \mathbb{Z}_2^{m_L}$ corresponding to the ideal logical measurement outcome. When there is a circuit-level Pauli error channel, the logical output is obtained by first applying additional Pauli correction to the circuit based on the observed syndrome using a decoder and then determining the corrected logical outcome. The errors and the subsequent correction introduce an additional bit-flip channel on the ideal logical measurement outcomes, which can be described by a distribution P_{fail} over the possible logical errors, i.e., bit flips $\vec{f}_L \in \mathbb{Z}_2^{m_L}$. The final logical output is then given by $\bar{o}_L^{(\text{ideal})} \oplus \vec{f}_L$. We now show that given any decoder, the bit-flip channel on logical measurement outcome, described by the logical error rate $P_{\text{fail}}(\vec{f}_L)$, is learnable from syndrome data under a

fault-tolerant condition.

Given the physical error rates, we quantify the probability of a logical error happening for logical measurements using the spacetime code picture introduced in Section IV A. We map the physical circuit into an $n^{(\text{ST})}$ -qubit spacetime subsystem code. In particular, we have the parity checks \mathcal{O}^\perp in the physical measurements mapped to the measured spacetime stabilizer group $\mathcal{M}^{(\text{ST})}$, and the logical measurements \mathcal{M}_L mapped to the group of measured spacetime logical operators $\mathcal{L}'^{(\text{ST})}$ using Algorithm 2. The effect of any circuit Pauli error on the syndrome and logical measurement can be captured by the commutation between the corresponding error $e \in \mathcal{P}_{n^{(\text{ST})}}$ in the spacetime code and the spacetime stabilizer and logical elements (see Lemma G.3 and Lemma G.4 in Section G). As a result, an error $e \in \mathcal{P}_{n^{(\text{ST})}}$ is undetectable and logically trivial to the logical measurements if and only if e is in the gauge group $\mathcal{G}'^{(\text{ST})} = N(\mathcal{L}'^{(\text{ST})})$ of the spacetime code. Therefore, any two Pauli errors that differ by elements of the spacetime code gauge group are indistinguishable and logically equivalent. For each Pauli error e in the spacetime code, we define its *logical error class* as the coset $e\mathcal{G}'^{(\text{ST})}$ in $\mathcal{P}_{n^{(\text{ST})}}$ and we denote it as $\overline{C}_{\vec{s}, \vec{\ell}}$. Here, $\vec{s} \in \mathbb{Z}_2^r$ and $\vec{\ell} \in \mathbb{Z}_2^{m_L}$ are the syndrome and logical component of the error e respectively:

$$s_i(e) = \langle e, M_i^{(\text{ST})} \rangle \quad (43)$$

$$\ell_i(e) = \langle e, L_i^{(\text{ST})} \rangle, \quad (44)$$

where $\{M_i^{(\text{ST})}\}_i^r$ generates the measured stabilizer group. $\{L_i^{(\text{ST})}\}_i^{m_L}$ is the set of measured spacetime logical operators from the logical measurements. Furthermore, we denote the probability of each logical error class as

$$\overline{P}(\vec{s}, \vec{\ell}) = \sum_{e \in \overline{C}_{\vec{s}, \vec{\ell}}} P(e) = \sum_{g \in \mathcal{G}'^{(\text{ST})}} P(e_{\vec{s}, \vec{\ell}} g), \quad (45)$$

where $e_{\vec{s}, \vec{\ell}}$ is any error satisfying $\vec{s}(e) = \vec{s}$ and $\vec{\ell}(e) = \vec{\ell}$. Note that the number of degrees of freedom of \overline{P} is the numbers of cosets of $\mathcal{G}'^{(\text{ST})}$, i.e., reduced by a factor of $|\mathcal{G}'^{(\text{ST})}|$ compared with the physical error rate $P(e)$. In contrast to generic physical error rates that is determined by all Pauli eigenvalues in $\mathcal{P}_{n^{(\text{ST})}}$, one only needs Pauli eigenvalues $\Lambda_{\mathcal{L}'}$ of the logical operators in $\mathcal{L}'^{(\text{ST})}$ to determine \overline{P} . In fact, they are related by a Walsh-Hadamard transform W :

$$\overline{P} \xleftarrow{W} \Lambda_{\mathcal{L}'} \quad (46)$$

See [12] and Section H for details. Wagner *et al.* [12] showed the sufficient condition of the learnability of \overline{P} in the channel coding setting.

Theorem 8 (Wagner *et al.* [12]). *Let a Pauli error channel \mathcal{N}_Γ be a composition of Pauli channels with support $\gamma \in \Gamma$ as defined in Eq. (3). The probabilities \overline{P} of logical*

error classes are learnable from the syndrome data if any union $\gamma_1 \cup \gamma_2$ of two channel supports $\gamma_1, \gamma_2 \in \Gamma$ only supports trivial logical operators.

We emphasize that the values of $\overline{P}(\vec{s}, \vec{\ell})$ are decoder-independent quantities that depend only on the logical equivalence relation in the code, i.e., the gauge group and the physical error rates. To define the logical error rate P_{fail} of the logical measurements, we need a decoder. A decoder takes the syndrome \vec{s} of the circuit as input and returns a logical class $\vec{\ell}_{\text{dec}}(\vec{s})$. Then, the probability of a logical error corresponds to the bit-flip $\vec{f}_L \in \mathbb{Z}_2^{m_L}$ of the ideal logical measurement outcome average over all possible syndromes is

$$P_{\text{fail}}(\vec{f}_L) = \sum_{\vec{s}} \overline{P}(\vec{s}, \vec{f}_L \oplus \vec{\ell}_{\text{dec}}(\vec{s})). \quad (47)$$

We show that syndrome expectation values in the circuit suffice to determine the logical error class probability, and hence the logical error rates, of fault-tolerant Clifford circuits (in the sense of Definition 9) under the assumed circuit-level Pauli noise model.

Definition 9 (Fault tolerance). *Consider a circuit-level Pauli error model defined by a set of spacetime supports $\Gamma^{(\text{ST})}$ as in Definition 5. We denote the set of individual spacetime Pauli errors of the model by $\mathcal{E}_{\Gamma^{(\text{ST})}}$. We say a non-adaptive Clifford circuit is fault tolerant to a circuit-level Pauli error model for a set of logical measurements \mathcal{M}_L if and only if for any undetectable error e , either in $\mathcal{E}_{\Gamma^{(\text{ST})}}$ or as a product $e = e_1 e_2$ for any $e_1, e_2 \in \mathcal{E}_{\Gamma^{(\text{ST})}}$, the error e on the circuit does not change the distribution of logical measurements outcome in \mathcal{M}_L for any input codeword to the circuit.*

Theorem 10 (Learnability of logical errors). *Given a non-adaptive Clifford circuit with a set of logical measurements \mathcal{M}_L under a circuit-level Pauli noise model (satisfies Assumption 1 on the spacetime code), the logical error class probabilities \overline{P} for \mathcal{M}_L can be learned from the syndrome expectation value if and only if the circuit is fault-tolerant (Definition 9) to the noise model for \mathcal{M}_L . As a consequence, given a decoder of the circuit, the associated logical error rates P_{fail} for the set of logical measurements \mathcal{M}_L can be learned from the syndrome data if the circuit is fault-tolerant to the noise model for \mathcal{M}_L .*

The proof using the spacetime code mapping is in Section H. A naive way of learning the logical error rate would be to solve for $\Lambda_{\mathcal{L}'}$ from the syndrome expectation values and then performing the inverse Walsh-Hadamard transformation in Eq. (46) involving an exponentially large matrix. In practice, we first learn any set of physical error rates compatible with the syndrome expectations and then perform Monte Carlo simulations to estimate the logical error rate.

In addition to benchmarking logical measurements, estimating the fidelity of a prepared logical state is also of

interest. We show that given the learned logical noise rates, we can estimate the logical fidelity [1, 3, 41, 42] of the noisy output state $\tilde{\rho}$ with the target output state $\rho = |\bar{\psi}\rangle\langle\bar{\psi}|$, which is assumed to be pure. We define the logical fidelity F_L as the physical fidelity after correcting the output state $\tilde{\rho}$ back to the code space, see [41] for a detailed discussion. We denote by \mathcal{S} the stabilizer group of the output state ρ , and by $\mathcal{L} = N(\mathcal{S})$ the group of logical operators. We denote the set of representatives of each coset of \mathcal{S} in \mathcal{L} as $\hat{\mathcal{L}}$. In the case when the logical circuits are performing direct fidelity estimation by measuring logical operators in different bases [39], we have

$$F_L = \text{Tr}\{R(\tilde{\rho})\rho\} \quad (48)$$

$$= \frac{1}{2^n} \sum_{O \in \mathcal{P}_n} \langle O \rangle_{R(\tilde{\rho})} \langle O \rangle_{\rho} \quad (49)$$

$$= \frac{1}{2^k} \sum_{L' \in \hat{\mathcal{L}}} \langle L' \rangle_{R(\tilde{\rho})} \langle L' \rangle_{\rho}. \quad (50)$$

Here, R is the CPTP map of syndrome measurement followed by error correction, and we denote by $\langle O \rangle_{\rho}$ the expectation value of O with respect to the target output state ρ . We can learn the logical fidelity F_L from the syndrome data of the family of circuits. This is because P_{fail} can be learned according to Theorem 10, and $\langle L' \rangle_{R(\tilde{\rho})}$ depends on the Walsh-Hadamard transformation of P_{fail} and the ideal expectation value $\langle L' \rangle_{\rho}$ as

$$\langle L' \rangle_{R(\tilde{\rho})} = \left(\sum_{\vec{f}_L \in \mathbb{Z}_2^{m_L}} (-1)^{\vec{\alpha}(L') \cdot \vec{f}_L} P_{\text{fail}}(\vec{f}_L) \right) \langle L' \rangle_{\rho}. \quad (51)$$

where $\vec{\alpha}(L') \in \mathbb{Z}_2^{m_L}$ is the binary vector whose nonzero entries indicate which measurement outcomes are used to compute $\langle L' \rangle$. When ρ is a stabilizer state, denote its full stabilizer group as $\mathcal{S}_{\rho} > \mathcal{S}$ and denote by $\hat{\mathcal{S}}_{\rho}$ a set of representatives of the cosets of \mathcal{S} in \mathcal{S}_{ρ} , then the logical fidelity reduces to $F_L = \frac{1}{2^k} \sum_{S \in \hat{\mathcal{S}}_{\rho}} \langle S \rangle_{R(\tilde{\rho})}$. In Section V C, we compared the learned logical fidelity from syndrome data with the experimentally measured fidelity (Fig. 7a) of the logical GHZ state from logical direct fidelity estimation.

When there is no sufficient set of logical measurement bases implemented at the end, syndrome constraints will not be sufficient to uniquely identify the logical fidelity. One can still estimate the logical fidelity by using additional constraints (Eq. (31)) to first estimate all physical error rates and simulate the noisy circuit with a final round of perfect syndrome measurement and recovery. This is still expected to be accurate, particularly when several rounds of error correction are performed to accumulate sufficient syndrome data, except for the final round.

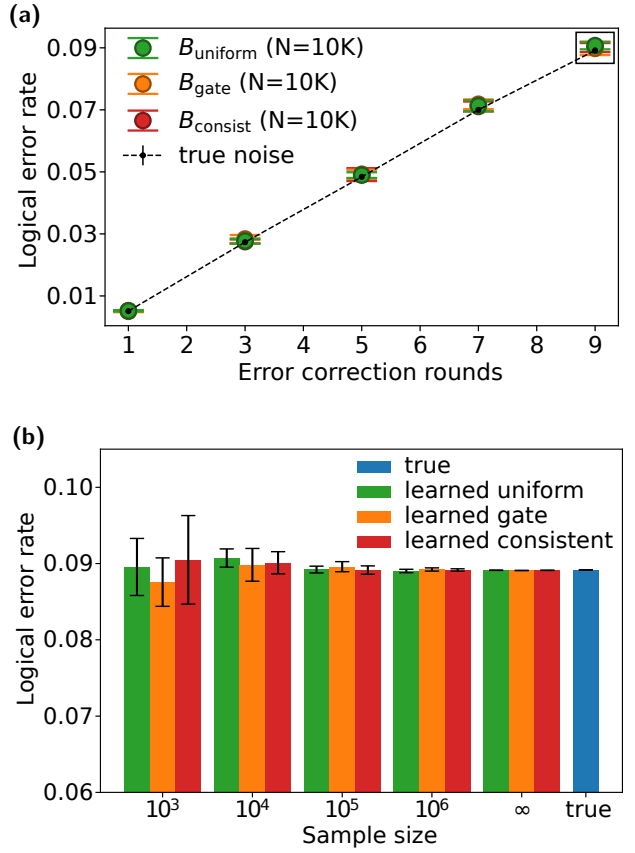


FIG. 8: (a) Logical error rate estimation from simulation of surface code error correction circuits. We apply two-qubit Pauli error channels on two-qubit gates and single-qubit Pauli channels on other locations with near-threshold error rates fluctuating (20%) around 0.01 and 0.001, respectively. Logical error rates are estimated by Monte Carlo sampling. (b) A zoomed-in plot of the learned logical error rates corresponds to 9 rounds of syndrome extraction (box in (a)) for different extra constraints B and sample sizes. Learned logical error rates for different B constraints match the true value.

B. Benchmarks

We first test the logical error rate learning with the data from various simulated surface code syndrome extraction circuits in Section IV B, ranging from a single round $r = 1$ up to $r = 9$ rounds of syndrome extractions. The logical error rate at the end of the 9 circuits is evaluated from the simulation of the syndrome measurement, decoding, and final correction of the whole circuit with Stim and Pymatching [43, 44]. The physical error rates are estimated using Eq. (32), where we use different B matrices for the extra constraints. We denote by B_{gate} the one that assumes a fixed ratio between pairs of errors in each syndrome error class consistent with the error rates without added Gaussian fluctuation. The other matrix asserts uniform noise within each syndrome error

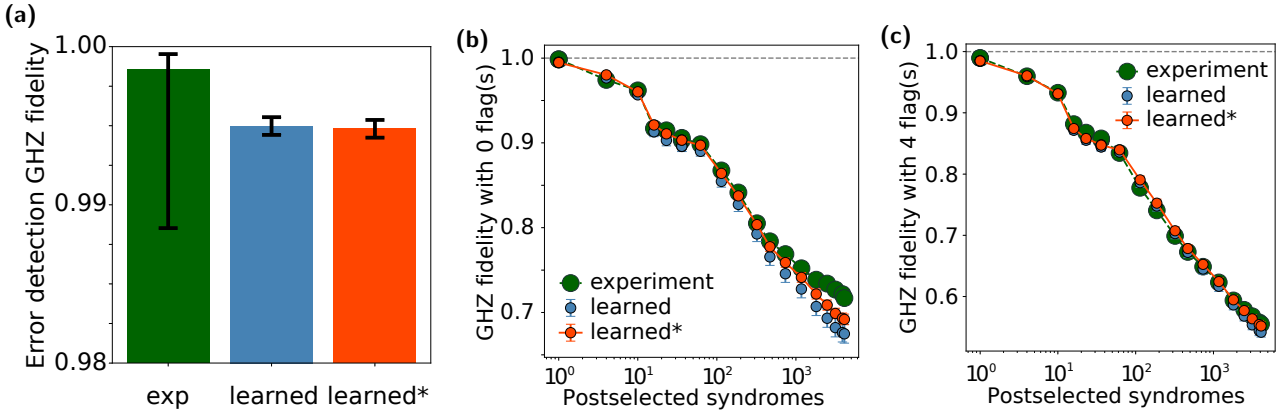


FIG. 9: Comparison of logical direct fidelity estimation between experimental results and learned noise models from syndromes. The left plot shows the error detecting results for the Logical GHZ fidelity from experimental measurement, learned logical fidelity, and the learned fidelity with extra uniformity constraints, denoted with *. Where on the right plot, the same comparison of the partial postselection on syndrome is performed conditioned on the number of ancilla blocks having non-trivial syndrome (flag), see Fig. 18 for results of postselection on various numbers of flags.

class, denoted as B_{uniform} . Finally, we use B_{consist} , which asserts constraints consistent with the true noise. As shown in Fig. 8, the learned circuit noise predicts the logical error rate well with uncertainty $\epsilon_{P_{\text{fail}}} \leq \pm 3 \cdot 10^{-4}$ for a single round syndrome extraction, and $\epsilon_{P_{\text{fail}}} \leq \pm 2.2 \cdot 10^{-3}$ for nine rounds of syndrome extractions. Importantly, notice that the logical failure rate is independent of the extra constraints used to fix the error rates of individual Pauli errors in the same syndrome classes.

C. Logical error rates in experiments

We now use our algorithm to learn the logical error rates from the syndrome data of the experiments reported in Ref. [1]. We estimate the logical fidelity from the learned physical error rates (using Eq. (32)) of all 9 logical GHZ preparation circuits with different logical measurement bases shown in Fig. 7a, Section IV C. We perform Monte Carlo simulations on stim [44] to sample measurement bitstrings from our estimated physical error rates of all the circuits. The simulated logical measurement results, corrected using the correlated decoding technique [1, 45], are extracted. We note that these simulated logical measurement results encode the learned logical error rates, and the logical bitstrings from the experimental data are never used. In addition, we implemented “sliding-scale error detection”, where we rank data block syndromes based on the probability of their most likely error and perform partial postselection based on a cutoff threshold, see [1] for details. To mitigate shot noise from the syndrome expectation value due to the small sample size, we also implemented the optimization in Eq. (32) with added intraclass uniformity constraints (Section J) denoted by ** in Figs. 9b and 9c.

Comparing our learned GHZ state logical fidelity from

the circuit syndrome with the experimental result obtained from direct fidelity estimation, we find them in good agreement, as shown in Fig. 9. For postselection on the trivial syndrome, the estimated logical fidelity is within the experimental error bars. The protocol also gives a good estimation in the case of error correction with partial postselection, as most experimental results fall in the range error bar of the learned data, and we see better agreement for the learned data with extra uniformity constraints. We speculate that the deviation from the experimental result is due to shot noise from the limited sample size and our simplified noise model. Nevertheless, the overall good agreement shows that the local Pauli error model is a valid error model in the setting of error-corrected logical quantum information processing for these experiments.

D. Exponential sample complexity advantage at very low logical error rates

The threshold theorem of fault-tolerant quantum computation [8, 28, 31] shows that there exist families of codes with growing distance d , such that if the physical error rate p is below some threshold p_{th} then one can exponentially suppress the logical error rate as a function of the distance of the code. Under the uniform single-qubit error model assumption and in the asymptotically low physical error rate regime, the logical error rate follows the formula [46, 47]:

$$P_{\text{fail}} = A_d \left(\frac{p}{p_{\text{th}}} \right)^{\frac{d+1}{2}}, \quad (52)$$

where $A_d = \text{poly}(d)$ is some constant independent of p . When estimating such exponentially suppressed logical

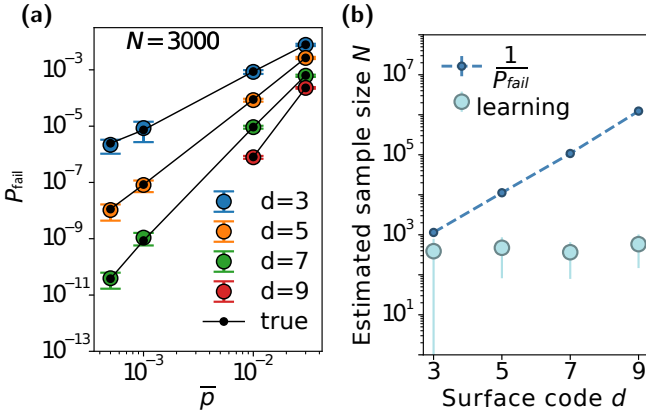


FIG. 10: (a) Rotated surface code logical error rate P_{fail} initialized in $|\bar{0}\rangle$ for various distances d and physical single-qubit error rates in the code capacity setting (average error rate \bar{p} with $\sigma = 0.3 \bar{p}$). The black markers are the true logical error rates from the minimum weight perfect matching (MWPM) decoder. The colored markers are the learned values from $N = 3000$ samples of syndrome data. (b) Estimated sample size needed for direct fidelity estimation at the logical level (dark blue) versus the one needed (from interpolation of results shown in (a) with different N at average physical error rate 10^{-2}) for the logical error rate learning algorithm (light blue) if one requires $\eta = 1$ relative error.

error rates directly at the logical level, for example, using direct fidelity estimation, an exponential number of samples is required to resolve the signal. Quantitatively, sampling from a binomial distribution with probability p_{bin} , the sample size N needed to obtaining an estimation of p_{bin} with relative error η is given by

$$N = \frac{1 - p_{\text{bin}}}{\eta^2 p_{\text{bin}}} \approx \frac{1}{\eta^2 p_{\text{bin}}}. \quad (53)$$

Since multiplicative errors scale linearly under exponentiation, the asymptotic formula in Eq. (52) suggests that achieving a logical-level relative error within η_L only requires improving the physical-level multiplicative precision by a factor proportional to the code distance. This is much more desirable since the physical error rates typically do not decrease with increasing number of qubits, and we have

$$N_{\text{physical}} \approx \frac{d^2}{\eta_L^2 p}. \quad (54)$$

In this section, we make the statement precise for Clifford circuits under the local sparse Pauli error model described in Section II.

Theorem 11 (Sample complexity of logical error estimation). *Consider a non-adaptive logical Clifford circuit*

with n physical qubits and of physical depth T that corresponds to a qLDPC spacetime code. We assume the circuit is fault-tolerant to a circuit-level noise that corresponds to a local sparse Pauli channel \mathcal{N}_Γ on the spacetime code, for a set of logical measurements \mathcal{M}_L . Denote the vector of true error rates by \vec{p} and the minimal syndrome class error rate by $P_{C\min}$. Then we can learn the logical error rates P_{fail} for \mathcal{M}_L with relative error within η_L using a sample size

$$N = \tilde{\mathcal{O}}\left(\frac{n^2 T^2}{\eta_L^2 P_{C\min}^2}\right), \quad (55)$$

if

$$\|\vec{p}\|_\infty \leq \min\left(\frac{2}{L_H, K_{G_B}}, \left(\frac{\eta_L P_{C\min}}{4|\Gamma| C_c}\right)^{\frac{1}{2}}\right), \quad (56)$$

for constants L_H, K_{G_B}, C_c defined in Eqs. (F27), (F28) and (I18).

See Section I2 for details of the proof. Again, applying the Chernoff bound gives a more precise scaling $N = \tilde{\mathcal{O}}(\frac{p_{\max}}{P_{C\min}^2})$, where $p_{\max} = \|\vec{p}\|_\infty$, with respect to the physical error rates. It reduces to $\mathcal{O}(1/p)$ under the uniform error rate case as expected.

The logical error rate estimation method considered in the proof makes use of the solution in Eq. (35) and approximates the syndrome-class error rate to first order via $P_C = -\frac{1}{2} \log \nu_C + \mathcal{O}(\|\vec{p}\|^2)$. Since better physical error rate learning precision is required as spacetime volume increases in the proof, we require the upper bound on $\|\vec{p}\|_\infty$ to decrease as $\sim 1/(nT)$. This is reflected in the number of local channels $|\Gamma|$ in the denominator of the upper bound in Eq. (56). Nevertheless, for a fixed sufficiently low physical error rate, the theorem still yields an exponential sampling advantage for finite-size systems. This first-order approximation can be avoided by using optimization methods to solve Eq. (32). Therefore, we believe the sampling advantage holds more generally in this case.

In the regime where the physical error rate is well below the fault tolerance threshold, the sample complexity scaling approaches $\mathcal{O}(d^2)$ instead of $\mathcal{O}(n^2 T^2)$. This scaling arises because the fault patterns are dominated by the minimum weight uncorrectable errors in the circuit, which require $\mathcal{O}(d)$ independent error events happening in the set of local errors \mathcal{E}_Γ .

To test if the advantage holds in practice, we perform numerical simulations to study the accuracy of logical error rate learning on rotated surface codes of distance $d = 3, 5, 7, 9$ in the code capacity setting. We sample single-qubit error rates from a gaussian distribution $\mathcal{N} \sim (\mu = 10^{-3}, \sigma = \frac{1}{2} \times 10^{-3})$. As shown in Section VD, with $N = 3000$ samples, one can estimate the logical error rate with good relative precision at the order of 10^{-11} if the code/circuit is fault-tolerant to the noise model. We simulate learning error rates with different sample sizes and different surface code distances and perform a linear

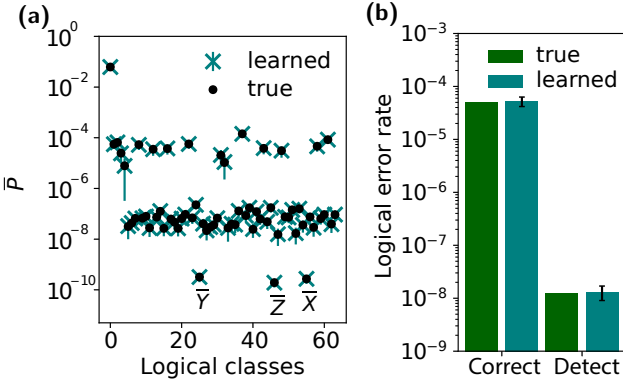


FIG. 11: (a) Learned 64 logical class error rate of the $[[5, 1, 3]]$ code. Each true single-qubit Pauli error rate is sampled from $p \sim \mathcal{N}(\mu, \sigma^2)$, where $\mu = 10^{-3}, \sigma = 5 \times 10^{-4}$. With $N = 8000$ samples of syndrome data, every logical class error rate can be estimated close to the true value in multiplicative precision. (b) The logical error rate of both error correction and error detection in (a) can be estimated to high precision.

fit of the multiplicative precision with the sample size for each code on the log scale. In Fig. 10b, we show the estimated samples needed for relative error $\eta = 1$ and see a clear advantage compared to $1/P_{\text{fail}}$ as in Eq. (53).

Finally, learning the probability of different logical error classes corresponding to different Pauli errors with a certain syndrome is also of interest. This is because post-selection on syndromes is also widely used in many protocols and is a general means of improving logical fidelity in the near term [1, 48–51]. All logical error class probabilities can be learned with good relative precision since they can all be written as a polynomial in the physical error rates, similarly to the logical error rate averaged over syndromes. We observed from numerical simulations, as shown in Fig. 11, that all 64 logical class error rates \bar{P} of the $[[5, 1, 3]]$ of different orders of magnitude can be learned with $N = 8000$ samples to good relative precision. This allows one to estimate the logical error rate conditioned on any subset of syndromes one postselects on, using syndrome data from a small number of samples.

VI. DISCUSSION

In this paper, we study the problem of learning Pauli noise in fault-tolerant Clifford circuits from syndrome data. To this end, we analyze the noise-learning problem for general subsystem codes and map Clifford circuits to spacetime (subsystem) codes. We rigorously show that the total error rates of every equivalence class of circuit-level Pauli noise, i.e., the syndrome class where errors have the same syndrome, can be learned from the syndrome data of a fault-tolerant Clifford circuit. In fact, we are able to prove that local sparse Pauli channels in the

circuit can be learned from a constant number of samples when the spacetime code of the circuit is qLDPC.

Complementing these analytical results, we design a general algorithm to estimate circuit-level Pauli error rates of Clifford circuits given syndrome data. We do so by turning the noise learning problem into a least square optimization on a system of noisy non-linear equations (without approximation)/linear equations (with approximation), which allows us to adaptively adjust the redundancy as well as terminate early to reduce overfitting. To improve the accuracy of our learning algorithm, one could design better optimization schemes and potentially dynamically adjust the effective degrees of freedom in the noise model to further reduce overfitting from shot noise.

Our work provides a complementary method for benchmarking gate errors compared to randomized benchmarking, gate-set tomography, and cycle error reconstruction [52–56]. These methods effectively magnify physical error rates by increasing the number of gate layers. In the context of our work, this is essentially trading measurements with gates, thus holding an advantage if measurements are slower than gate implementations. However, compared to these methods, our approach requires no pre-calibration and provides in situ estimates of the gate error rate for the target computational task. In addition, our method is able to capture non-Markovian or time-dependent effects such as drift, while offline benchmarking methods typically make a Markovian or time-independent assumption about the noise.

We further show that the logical error rate of the circuit is determined by the syndrome data if the circuit is fault-tolerant to the noise model we are learning. This allows us to learn logical error rates and estimate the logical fidelity of circuits without information from a logical measurement. This includes logical circuits with Clifford gates encoded in any stabilizer code, subsystem codes, and dynamical codes containing rounds of fault-tolerant syndrome extraction. Notably, we show that our method of extracting logical error rates from syndrome information provides an exponential sample advantage compared with tomography/fidelity estimation at the logical level only. This becomes important when logical error rates are suppressed by larger code distances. We do so using numerics and give a proof in the regime of low error rates. We note that an important problem remains unsolved: developing efficient classical algorithms to estimate the logical error rate of larger systems given the learned physical error rates. A series of work based on the splitting method and Metropolis sampling algorithms can potentially be such a complementary tool to our work [46, 57, 58].

Our work opens up several directions for future research. Learning circuit-level noise directly benefits decoding since one could obtain a more accurate prior for the decoder. The improvement for the optimal decoder will be optimal within the learned noise model, since we uniquely determine the total Pauli error rates for each logical error class. On the other hand, one could develop

a framework beyond the standard Pauli noise model to account for more realistic and specific noise models, such as coherent errors and crosstalk, where syndrome data may not provide enough information but will still be an important input to the learning protocol. Moreover, our logical error rate learnability condition can break down if there are correlated errors with higher weights outside the code's correctability. Since our framework assumes a certain locality structure of the noise, there can be extra identification work to validate the noise structure assumption based on other detection [59] or the syndrome itself [19, 35, 60]. If such long-range correlated events are rare, one can postselect on their absence and still learn the Pauli error model describing the background physical error rates and the corresponding logical error rates.

An exciting future direction is to go beyond non-adaptive Clifford circuits and estimate physical and logical errors in circuits with quantum advantage or circuits enabling universal quantum computation. In our upcoming work, Part II, [16], we progress towards this goal by adapting the noise-learning algorithm to verify logical Clifford circuits with magic state injection and extending Pauli noise learning to non-Clifford circuits. Investigat-

ing these future directions would potentially lead to a more comprehensive noise learning algorithm and an efficient verification of quantum advantage in the context of encoded logical circuits.

Note: After finalizing this work, we became aware of Ref. [61], where the authors study learning the logical error rate from syndrome data.

ACKNOWLEDGMENTS

We thank Steven Flammia and Martin Kliesch for helpful discussions. This research was supported in part by NSF QLCI grant OMA-2120757, the Defense Advanced Research Projects Agency (DARPA) under Agreement No. HR00112490357, and ARO grant W911NF-23-1-0258. DH is grateful for support from a Simons postdoctoral fellowship through DOE QSA and NSF QLCI Grant No. 2016245, and from the Swiss National Science Foundation through Ambizione Grant No. 223764. We acknowledge the use of large language models to improve clarity and grammar of original text.

[1] D. Bluvstein, S. J. Evered, A. A. Geim, S. H. Li, H. Zhou, T. Manovitz, S. Ebadi, M. Cain, M. Kalinowski, D. Hangleiter, *et al.*, Logical quantum processor based on reconfigurable atom arrays, *Nature* **626**, 58 (2024).

[2] R. Acharya, L. Aghababaie-Beni, I. Aleiner, T. I. Andersen, M. Ansmann, F. Arute, K. Arya, A. Asfaw, N. Asatrakhantsev, J. Atalaya, *et al.*, Quantum error correction below the surface code threshold, *arXiv preprint arXiv:2408.13687* (2024).

[3] S. Krinner, N. Lacroix, A. Remm, A. Di Paolo, E. Genois, C. Leroux, C. Hellings, S. Lazar, F. Swiadek, J. Herrmann, *et al.*, Realizing repeated quantum error correction in a distance-three surface code, *Nature* **605**, 669 (2022).

[4] C. Ryan-Anderson, N. Brown, C. Baldwin, J. Dreiling, C. Foltz, J. Gaebler, T. Gatterman, N. Hewitt, C. Hollliman, C. Horst, *et al.*, High-fidelity and fault-tolerant teleportation of a logical qubit using transversal gates and lattice surgery on a trapped-ion quantum computer, *arXiv preprint arXiv:2404.16728* (2024).

[5] M. Da Silva, C. Ryan-Anderson, J. Bello-Rivas, A. Chernoguzov, J. Dreiling, C. Foltz, J. Gaebler, T. Gatterman, D. Hayes, N. Hewitt, *et al.*, Demonstration of logical qubits and repeated error correction with better-than-physical error rates, *arXiv preprint arXiv:2404.02280* (2024).

[6] K. Mayer, C. Ryan-Anderson, N. Brown, E. Durso-Sabina, C. H. Baldwin, D. Hayes, J. M. Dreiling, C. Foltz, J. P. Gaebler, T. M. Gatterman, *et al.*, Benchmarking logical three-qubit quantum fourier transform encoded in the steane code on a trapped-ion quantum computer, *arXiv preprint arXiv:2404.08616* (2024).

[7] A. G. Fowler, A. M. Stephens, and P. Groszkowski, High-threshold universal quantum computation on the surface code, *Physical Review A—Atomic, Molecular, and Optical Physics* **80**, 052312 (2009).

[8] A. G. Fowler, Proof of finite surface code threshold for matching, *Physical review letters* **109**, 180502 (2012).

[9] C. Chamberland and M. E. Beverland, Flag fault-tolerant error correction with arbitrary distance codes, *Quantum* **2**, 53 (2018).

[10] S. Bravyi, A. W. Cross, J. M. Gambetta, D. Maslov, P. Rall, and T. J. Yoder, High-threshold and low-overhead fault-tolerant quantum memory, *Nature* **627**, 778 (2024).

[11] T. Wagner, H. Kampermann, D. Bruß, and M. Kliesch, Pauli channels can be estimated from syndrome measurements in quantum error correction, *Quantum* **6**, 809 (2022).

[12] T. Wagner, H. Kampermann, D. Bruß, and M. Kliesch, Learning logical pauli noise in quantum error correction, *Physical review letters* **130**, 200601 (2023).

[13] D. Bacon, S. T. Flammia, A. W. Harrow, and J. Shi, Sparse quantum codes from quantum circuits, *IEEE Transactions on Information Theory* **63**, 2464 (2017).

[14] D. Gottesman, Opportunities and challenges in fault-tolerant quantum computation, *arXiv preprint arXiv:2210.15844* (2022).

[15] N. Delfosse and A. Paetznick, Spacetime codes of clifford circuits, *arXiv preprint arXiv:2304.05943* (2023).

[16] X. Xiao, D. Hangleiter, D. Bluvstein, M. D. Lukin, and M. J. Gullans, In-situ benchmarking of fault-tolerant quantum circuits. II. classically-hard circuits, *in preparation*.

[17] A. G. Fowler, D. Sank, J. Kelly, R. Barends, and J. M. Martinis, Scalable extraction of error models from the output of error detection circuits, *arXiv preprint arXiv:1405.1454* (2014).

[18] S. T. Spitz, B. Tarasinski, C. W. Beenakker, and T. E. O'Brien, Adaptive weight estimator for quantum error correction in a time-dependent environment, *Advanced Quantum Technologies* **1**, 1800012 (2018).

[19] Exponential suppression of bit or phase errors with cyclic error correction, *Nature* **595**, 383 (2021).

[20] I. Hesner, B. Hetényi, and J. R. Wootton, Using detector likelihood for benchmarking quantum error correction, *arXiv preprint arXiv:2408.02082* (2024).

[21] M.-X. Huo and Y. Li, Learning time-dependent noise to reduce logical errors: real time error rate estimation in quantum error correction, *New Journal of Physics* **19**, 123032 (2017).

[22] E. Takou and K. R. Brown, Estimating decoding graphs and hypergraphs of memory qec experiments, *arXiv preprint arXiv:2504.20212* (2025).

[23] A. Remm, N. Lacroix, L. Bödeker, E. Genois, C. Hellings, F. Swiadek, G. J. Norris, C. Eichler, A. Blais, M. Müller, *et al.*, Experimentally informed decoding of stabilizer codes based on syndrome correlations, *arXiv preprint arXiv:2502.17722* (2025).

[24] R. Blume-Kohout and K. Young, Estimating detector error models from syndrome data, *arXiv preprint arXiv:2504.14643* (2025).

[25] R. Chao, M. E. Beverland, N. Delfosse, and J. Haah, Optimization of the surface code design for majorana-based qubits, *Quantum* **4**, 352 (2020).

[26] T. Wagner, H. Kampermann, D. Bruß, and M. Kliensch, Optimal noise estimation from syndrome statistics of quantum codes, *Physical review research* **3**, 013292 (2021).

[27] Y. Mao and F. R. Kschischang, On factor graphs and the fourier transform, *IEEE Transactions on Information Theory* **51**, 1635 (2005).

[28] E. Dennis, A. Kitaev, A. Landahl, and J. Preskill, Topological quantum memory, *Journal of Mathematical Physics* **43**, 4452 (2002).

[29] D. Horsman, A. G. Fowler, S. Devitt, and R. Van Meter, Surface code quantum computing by lattice surgery, *New Journal of Physics* **14**, 123011 (2012).

[30] A. M. Steane, Error correcting codes in quantum theory, *Physical Review Letters* **77**, 793 (1996).

[31] A. G. Fowler, M. Mariantoni, J. M. Martinis, and A. N. Cleland, Surface codes: Towards practical large-scale quantum computation, *Physical Review A—Atomic, Molecular, and Optical Physics* **86**, 032324 (2012).

[32] S. Aaronson and D. Gottesman, Improved simulation of stabilizer circuits, *Physical Review A—Atomic, Molecular, and Optical Physics* **70**, 052328 (2004).

[33] P.-J. H. Derk, A. Townsend-Teague, A. G. Burchards, and J. Eisert, Designing fault-tolerant circuits using detector error models, *arXiv preprint arXiv:2407.13826* (2024).

[34] F. Pastawski and B. Yoshida, Fault-tolerant logical gates in quantum error-correcting codes, *Physical Review A* **91**, 012305 (2015).

[35] Suppressing quantum errors by scaling a surface code logical qubit, *Nature* **614**, 676 (2023).

[36] G. P. Gehér, M. Jastrzebski, E. T. Campbell, and O. Crawford, To reset, or not to reset—that is the question, *arXiv preprint arXiv:2408.00758* (2024).

[37] C. W. Granger, Long memory relationships and the aggregation of dynamic models, *Journal of econometrics* **14**, 227 (1980).

[38] S. Erland and P. E. Greenwood, Constructing $1/\omega\alpha$ noise from reversible markov chains, *Physical Review E—Statistical, Nonlinear, and Soft Matter Physics* **76**, 031114 (2007).

[39] S. T. Flammia and Y.-K. Liu, Direct fidelity estimation from few pauli measurements, *Physical review letters* **106**, 230501 (2011).

[40] S. J. Evered, D. Bluvstein, M. Kalinowski, S. Ebadi, T. Manovitz, H. Zhou, S. H. Li, A. A. Geim, T. T. Wang, N. Maskara, *et al.*, High-fidelity parallel entangling gates on a neutral-atom quantum computer, *Nature* **622**, 268 (2023).

[41] D. Hangleiter, M. Kalinowski, D. Bluvstein, M. Cain, N. Maskara, X. Gao, A. Kubica, M. D. Lukin, and M. J. Gullans, Fault-tolerant compiling of classically hard iqp circuits on hypercubes, *arXiv preprint arXiv:2404.19005* (2024).

[42] J. Combes, C. Granade, C. Ferrie, and S. T. Flammia, Logical randomized benchmarking, *arXiv preprint arXiv:1702.03688* (2017).

[43] O. Higgott, Pymatching: A python package for decoding quantum codes with minimum-weight perfect matching, *ACM Transactions on Quantum Computing* **3**, 1 (2022).

[44] C. Gidney, Stim: a fast stabilizer circuit simulator, *Quantum* **5**, 497 (2021).

[45] M. Cain, C. Zhao, H. Zhou, N. Meister, J. Ataides, A. Jaffe, D. Bluvstein, and M. D. Lukin, Correlated decoding of logical algorithms with transversal gates, *arXiv preprint arXiv:2403.03272* (2024).

[46] S. Bravyi and A. Vargo, Simulation of rare events in quantum error correction, *arXiv preprint arXiv:1308.6270* (2013).

[47] A. G. Fowler, Analytic asymptotic performance of topological codes, *arXiv preprint arXiv:1208.1334* (2012).

[48] D. Bluvstein, A. A. Geim, S. H. Li, S. J. Evered, J. Ataides, G. Baranes, A. Gu, T. Manovitz, M. Xu, M. Kalinowski, *et al.*, Architectural mechanisms of a universal fault-tolerant quantum computer, *arXiv preprint arXiv:2506.20661* (2025).

[49] C. Gidney, N. Shutty, and C. Jones, Magic state cultivation: growing t states as cheap as cnot gates, *arXiv preprint arXiv:2409.17595* (2024).

[50] E. Rosenfeld, C. Gidney, G. Roberts, A. Morvan, N. Lacroix, D. Kafri, J. Marshall, M. Li, V. Sivak, D. Abanin, *et al.*, Magic state cultivation on a superconducting quantum processor, *arXiv preprint arXiv:2512.13908* (2025).

[51] P. Sales Rodriguez, J. M. Robinson, P. N. Jepsen, Z. He, C. Duckering, C. Zhao, K.-H. Wu, J. Campo, K. Bagnall, M. Kwon, *et al.*, Experimental demonstration of logical magic state distillation, *Nature* **645**, 620 (2025).

[52] E. Knill, D. Leibfried, R. Reichle, J. Britton, R. B. Blakestad, J. D. Jost, C. Langer, R. Ozeri, S. Seidelin, and D. J. Wineland, Randomized benchmarking of quantum gates, *Physical Review A—Atomic, Molecular, and Optical Physics* **77**, 012307 (2008).

[53] S. T. Merkel, J. M. Gambetta, J. A. Smolin, S. Poletto, A. D. Córcoles, B. R. Johnson, C. A. Ryan, and M. Steffen, Self-consistent quantum process tomography, *Physical Review A—Atomic, Molecular, and Optical Physics* **87**, 062119 (2013).

[54] E. Nielsen, J. K. Gamble, K. Rudinger, T. Scholten, K. Young, and R. Blume-Kohout, Gate set tomography, *Quantum* **5**, 557 (2021).

- [55] A. Carignan-Dugas, D. Dahlen, I. Hincks, E. Ospadov, S. J. Beale, S. Ferracin, J. Skanes-Norman, J. Emerson, and J. J. Wallman, The error reconstruction and compiled calibration of quantum computing cycles, arXiv preprint arXiv:2303.17714 (2023).
- [56] N. Fazio, R. Freund, D. Sannamoth, A. Steiner, C. D. Marcinia, M. Rispler, R. Harper, T. Monz, J. Emerson, and S. D. Bartlett, Characterizing physical and logical errors in a transversal cnot via cycle error reconstruction, arXiv preprint arXiv:2504.11980 (2025).
- [57] C. Mayer, A. Ganti, U. Onunkwo, T. Metodi, B. Anker, and J. Skryzalin, Rare event simulation of quantum error-correcting circuits, arXiv preprint arXiv:2509.13678 (2025).
- [58] M. E. Beverland, M. Carroll, A. W. Cross, and T. J. Yoder, Fail fast: techniques to probe rare events in quantum error correction, arXiv preprint arXiv:2511.15177 (2025).
- [59] P. M. Harrington, M. Li, M. Hays, W. Van De Pontseele, D. Mayer, H. D. Pinckney, F. Contipelli, M. Gingras, B. M. Niedzielski, H. Stickler, *et al.*, Synchronous detection of cosmic rays and correlated errors in superconducting qubit arrays, *Nature Communications* **16**, 6428 (2025).
- [60] S. J. S. Tan, C. A. Pattison, M. McEwen, and J. Preskill, Resilience of the surface code to error bursts, arXiv preprint arXiv:2406.18897 (2024).
- [61] H. Zheng, A. Chu, S. Chen, A. G. Manes, S.-u. Lee, S. Zhou, and L. Jiang, Efficient learning of logical noise from syndrome data, in preparation.
- [62] S. T. Flammia and J. J. Wallman, Efficient estimation of pauli channels, *ACM Transactions on Quantum Computing* **1**, 1 (2020).
- [63] P. Abbeel, D. Koller, and A. Y. Ng, Learning factor graphs in polynomial time and sample complexity, *The Journal of Machine Learning Research* **7**, 1743 (2006).
- [64] W. Xinghua, Convergence of newton's method and inverse function theorem in banach space, *Mathematics of Computation* **68**, 169 (1999).

APPENDIX A: Overview

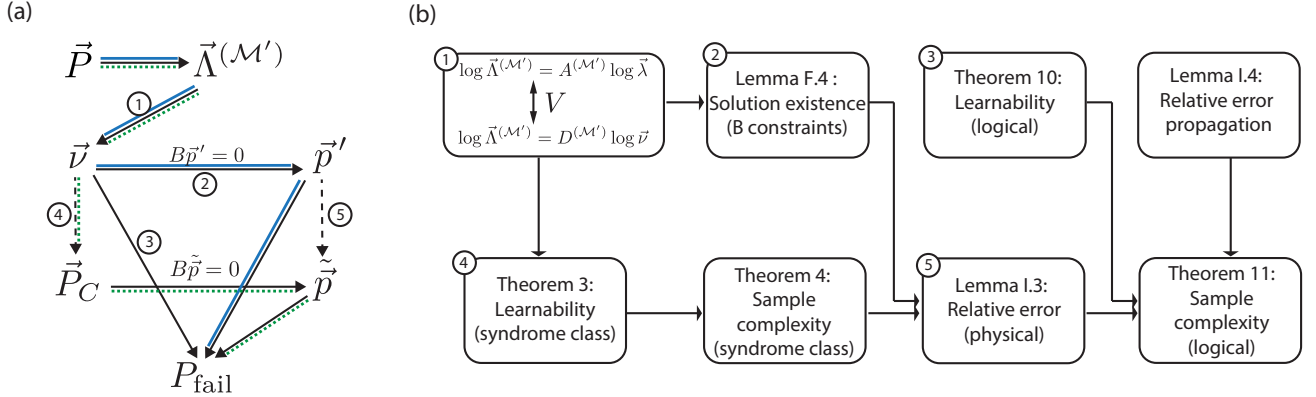


FIG. 12: An overview of the structure of the lemma and theorems. (a) The graph relates different quantities throughout the physical and logical-level noise learning process. \vec{p} are the true physical error rates. $\vec{\Lambda}$ are the syndrome expectation values (Pauli eigenvalues of the channel). \vec{v} are the learnable transformed eigenvalues that approximate the syndrome class error rates $\vec{P}_C \approx -\frac{\log \vec{v}}{2}$. \vec{p}' are the error rates that are consistent with \vec{v} and the extra constraints $B\vec{p}' = 0$ within each syndrome class. \vec{p} are the estimated physical error rates based on the estimated \vec{P}_C and the same extra constraints. A solid black arrow from A to B indicates that B can be derived from A , whereas a dashed black arrow indicates that A and B are approximately related in the low-error regime. Some edges are labeled with the lemmas and theorems used in (b). The solid blue line shows the path of learning the logical error rate without low-error rate approximation by solving the non-linear equation (circled 1 and 2) using optimization methods, but we don't have a proof for the sample complexity in this case. The dotted green line shows the path along which one can linearize $\log \vec{v}$ and ignore second-order corrections to obtain error rates from linear equations; we can then prove the sample complexity in this case for sufficiently low physical error rates. (b) Lemmas and theorems, starting from the syndrome equations, eventually lead to the sample-complexity scaling for learning the logical error rate from the syndrome.

The appendices present the proofs of the theorems in the main text, along with the lemmas used in the proofs and the algorithms used for noise learning. Fig. 12 illustrates the structure of the main results in this paper. In particular, we show two routes that start from the syndrome expectation values generated from the true error rates to learning physical error rates, and eventually learning the logical error rates. The first route, in solid blue lines, represents an exact solution that uses nonlinear equation solving via optimization. The second route in dotted green lines represents the first-order linear approximation method, where we are able to prove, in a certain error regime, an exponential advantage of sampling complexity in learning the logical error rate from syndrome data, compared with learning from logical measurement results.

We now explain the structure of the appendices. The essential results are represented by Theorem 3, Theorem 10, Theorem 4, Theorem 11. These are results on the learnability at the physical and logical levels, along with their sample complexities.

Section B introduces the basis transform from Pauli eigenvalues Λ to the transformed eigenvalues U , which allows us to have a minimal set of parameters describing the total error channel and the local channels. The matrix D of the linear equations matrix in this new basis has a nice structure that allows us to prove learnability conditions. Section C describes the structure of the linear equations from syndrome data, and proves the rank of the corresponding matrices, i.e., the minimum number of irredundant stabilizer elements needed to extract noise information from a given Pauli noise model. Section D describes an efficient algorithm to find the minimal subset of stabilizer elements.

Section E presents the proof of Theorem 3, where we show that syndrome-class error rates can be approximately determined from the syndrome data under the assumption of low error rates. This observation also provides a way to linearize the equation between syndrome class error rates and syndrome data directly. We show that in the case of the detector error model/inclusive error model [22, 23] where all errors are assumed to be uncorrelated, the detector error rate, i.e., probability that an odd number of errors occur for each syndrome class, can be learned exactly for any stabilizer code.

Section F proves Lemma F.4, which shows that there always exist error rates that satisfy both the syndrome constraints and extra constraints under low physical error rates. Section G describes the spacetime code formulation that maps Clifford circuits to stabilizer/subsystem codes in more detail, and we give an algorithm that generates the stabilizer and logical operators of the spacetime code. Section H proves Theorem 10, which shows that if the Clifford circuit is fault-tolerant to the Pauli error model we consider, then any error rates in this model that satisfy the syndrome constraints must give rise to the same true logical error rate with respect to the logical measurements in the circuit.

Section I proves the sample complexity scaling for learning physical syndrome class error rate (Theorem 4) and logical error rates (Theorem 11) in the low physical error rate regime. We show that the original solution [23] for solving detector error models assuming independent error mechanisms can be used to learn syndrome class error in our more general Pauli model with constant sample complexity (with increasing system size) if the spacetime code of the circuit is qLDPC and the Pauli channel is local and sparse. On top of that, we show that the logical error rate can be learned with a polynomial sample size, where the polynomial overhead arises from the relative error propagation from the physical to the logical levels. This then has the exponential advantage in sample complexity for learning logical error rates from syndrome data over direct fidelity/tomography estimation at the logical level. This is because logical error rates decrease exponentially with the distance of the code and therefore require an exponentially large sample size to learn the logical error rate within a finite relative error. The proof requires a decreasing upper bound on the physical error rates as the system size increases; in the practically relevant case when physical error rates are fixed, this sample-complexity advantage is only proven up to some finite size. However, we believe this advantage holds in general when using the non-linear optimization method without a first-order approximation. Finally, Section J describes a method used in the experimental analysis of adding intraclass uniform constraints that reduce overfitting in the higher shot noise regime.

APPENDIX B: The transformed eigenvalue basis

One of the central questions we want to understand is given the Pauli eigenvalues $\Lambda(M)$ of the Pauli channel \mathcal{N}_Γ for elements in the measured stabilizer group \mathcal{M} , what can we learn about the total channel \mathcal{N}_Γ and the individual noise channels $\mathcal{N}_\gamma, \forall \gamma \in \Gamma$? Wagner *et al.* [11, 12] used the canonical factors F of the Pauli eigenvalues, which is a linear transformation $\log \Lambda \rightarrow \log F$, to parametrize the total error channel \mathcal{N}_Γ and showed that there is effectively $|\mathcal{E}_\Gamma|$ degrees of freedom. They further proved the sufficient condition of learnability of \mathcal{N}_Γ . Our work is based on another linear transformation of $\log \Lambda$, denoted as $\log U$, and we refer to U as the transformed eigenvalues. $\log U$ serve as another parametrization of the channel \mathcal{N}_Γ and shares similar properties to the canonical factors $\log F$. Based on $\log U$, we have a simple proof of the learnability results Theorem 2 with the additional necessary condition for learnability, and more importantly, answer the questions (Theorem 3) of what we can generally learn about the parameters of the local channels \mathcal{N}_γ , when the learnability condition in Theorem 2 is not satisfied. See Fig. 13 for an illustration of the basis transforms. In this appendix section, we first introduce the canonical factors $\log F$ [11, 12], and then introduce the transformed eigenvalues $\log U$ used in this work.

$$\begin{array}{c}
 \log F = \sum_{\gamma \in \Gamma} \log F_\gamma \\
 \nearrow [12] \\
 \vec{P} \xrightarrow{W} \vec{\Lambda} \longrightarrow \log \vec{\Lambda} \\
 \searrow W^{-1} \\
 \log U = \sum_{\gamma \in \Gamma} \log U_\gamma \\
 \downarrow \quad \downarrow \\
 \bar{\mu} \quad \mu
 \end{array}$$

FIG. 13: An overview of the basis transform to the transformed eigenvalues U . The Pauli eigenvalues $\vec{\Lambda}$ of the error channel are obtained from the Walsh-Hadamard transform of the true physical error rates. Wagner *et al.* [12] performs a transformation to get the canonical moments F that parametrize the total channel \mathcal{N}_Γ . Our work performs an inverse Hadamard transform on $\log \vec{\Lambda}$ instead and obtains the transformed eigenvalues $\bar{\mu}$ and μ as parametrization of the total channel \mathcal{N}_Γ and the local channels \mathcal{N}_γ respectively.

1. $\log F$: Basis of the canonical factor [12]

Given the convolutional factor graph structure Fig. 1 of the noise model, we have the eigenvalue $\Lambda(O)$ of any Pauli $O \in \mathcal{P}_n$ for the total error channel \mathcal{N}_Γ decomposed as a factor graph (see Fig. 1):

$$\Lambda(O) = \prod_{\gamma \in \Gamma} \Lambda_\gamma(O) = \prod_{\gamma \in \Gamma} \Lambda_\gamma(O_\gamma) \quad (\text{B1})$$

where the local eigenvalues $\Lambda_\gamma(O)$ of O only depends on its restriction on the support γ , i.e. $\Lambda_\gamma(O) = \Lambda_\gamma(O_\gamma)$.

To understand the degrees of freedom in both the total Pauli error rates P and in each local error rate P_γ , Wagner *et al.* [12] considers factors in another basis where we refer to the canonical basis from the canonical factors as defined typically in a factor graph [12, 62, 63].

Definition B.1 (Canonical factor [12]). *The canonical factors $F(O), \forall O \in \mathcal{P}_n$ of the total Pauli channel with eigenvalues $\Lambda(O), \forall O \in \mathcal{P}_n$ is defined as:*

$$F(O) = \prod_{O' \leq O} \Lambda^{(-1)^{|O|-|O'|}}(O'). \quad (\text{B2})$$

where $a \leq b$ if and only if a is a Pauli substring of b , i.e., $b_{\text{supp}(a)} = a$.

Equivalently, this can be written as a linear transformation of $\log \Lambda(O), \forall O \in \mathcal{P}_n$:

$$\log F(O) = \sum_{O' \leq O} (-1)^{|O|-|O'|} \log \Lambda(O') \quad (\text{B3})$$

Similarly, the local canonical factors $F_\gamma(O), \forall O \in \mathcal{P}_n$ of a local Pauli channels in a system of n qubits with support γ with eigenvalues $\Lambda_\gamma(O) = \Lambda_\gamma(O_\gamma), \forall O \in \mathcal{P}_n$ is defined as:

$$\log F_\gamma(O) = \sum_{O' \leq O} (-1)^{|O|-|O'|} \log \Lambda_\gamma(O'). \quad (\text{B4})$$

Property B.2. *The (local) canonical factors F (F_γ) have the following properties [12]:*

1. *The canonical factors are the product of local canonical factors, or equivalently:*

$$\log F(O) = \sum_{\gamma \in \Gamma} \log F_\gamma(O). \quad (\text{B5})$$

2. *Local canonical factors $\log F_\gamma(O) = 0$, if $\text{supp}(O) \not\subseteq \gamma$. For the global canonical factors we have $\log F(O) = 0$, if $\text{supp}(O) \not\subseteq \gamma, \forall \gamma \in \Gamma$.*

3. *The linear transformation in Eq. (B3) and Eq. (B5) is full rank. The eigenvalue of local Pauli channels for operator O can be written as products of all the canonical factors of substrings of O : $\log \Lambda_\gamma(O) = \sum_{O' \leq O} \log F_\gamma(O')$. Similarly, the eigenvalues of the total channel are given by [12]: $\log \Lambda(O) = \sum_{O' \leq O} \log F(O')$.*

As a result, $\{F(e) | \forall e \in \mathcal{E}_\Gamma\}$ is an irredundant set that parametrizes the total Pauli channel \mathcal{N}_Γ . Similarly, for each local channel $\gamma \in \Gamma$, $\{F_\gamma(e) | e \in \mathcal{E}_\gamma\}$ parametrizes the local channel \mathcal{N}_γ . Note that there is gauge freedom in general for each local channel if one only fixes the total channel \mathcal{N}_Γ . One benefit of looking at the canonical factors F as opposed to the Pauli eigenvalue Λ is that the gauge freedom is straightforward, as shown in Eq. (B5). More explicitly, whenever we have two non-overlapping distinct channel supports $\gamma_1, \gamma_2 \in \Gamma$ and Pauli error e such that $\text{supp}(e) \subseteq \gamma_1 \cap \gamma_2$, we have associated gauge freedom α :

$$\log F_{\gamma_1}(e) \longrightarrow \log F_{\gamma_1}(e) + \alpha \quad \text{and} \quad \log F_{\gamma_2}(e) \longrightarrow \log F_{\gamma_2}(e) - \alpha, \quad (\text{B6})$$

such that the total channel stays invariant. And given the total Pauli channel \mathcal{N}_Γ , one could determine the local Pauli channel \mathcal{N}_γ if and only if $\gamma \cap \gamma' = \emptyset$ for all other local supports $\gamma' \in \Gamma$. This is the case mostly considered in the main text when mapping standard circuit-level Pauli noise to the spacetime code.

2. $\log U$: Basis of the transformed eigenvalues

Here, we introduced the alternative basis that allows us to design the linearized approximate algorithm for noise learning and prove the theorems in this work. In the main text, we defined the set of transformed local eigenvalues μ , used to approximate the physical error rates. In this section, we introduce the formalism more systematically by first introducing the associated global quantities, the transformed eigenvalues of the total channel $U(O), \forall O \in \mathcal{P}_n$, whose logarithm is the inverse Walsh-Hadamard transform of the Pauli eigenvalues $\log \Lambda$ of the total channel \mathcal{N}_Γ :

$$\log U(O) = -\frac{2}{|\mathcal{P}_n|} \sum_{O' \in \mathcal{P}_n} [[O', O]] \log \Lambda(O'_\gamma). \quad (\text{B7})$$

The extra -2 factor here is a convention that gives a simple binary form of the matrix D in Eq. (23). For each individual channel \mathcal{N}_γ , we similarly define the transformed eigenvalues $U_\gamma(O)$ of the individual channel, or simply the transformed eigenvalues as

$$\log U_\gamma(O) = -\frac{2}{|\mathcal{P}_n|} \sum_{O' \in \mathcal{P}_n} [[O', O]] \log \Lambda_\gamma(O'_\gamma). \quad (\text{B8})$$

Here are some properties of the transformed eigenvalues U and U_γ analogous to Property B.2:

Lemma B.3 (Properties of U and U_γ). *For any $O \in \mathcal{P}_n$:*

1. $\log U(O) = \sum_{\gamma \in \Gamma} \log U_\gamma(O)$.
2. *For any local support $\gamma \in \Gamma$, $\log U_\gamma(O) = 0$, if $\text{supp}(O) \not\subseteq \gamma$. And $\log U(O) = 0$, if $\forall \gamma \in \Gamma$, $\text{supp}(O) \not\subseteq \gamma$.*

Proof. To prove the first property, note that for the Pauli eigenvalues $\Lambda(O) = \prod_{\gamma \in \Gamma} \Lambda_\gamma(O)$, therefore we have $\log \Lambda(O) = \sum_{\gamma \in \Gamma} \log \Lambda_\gamma(O)$. Since the logarithm of the transformed eigenvalues $\log U$ and $\log U_\gamma$ are the same linear transformation of $\log \Lambda$ and $\log \Lambda_\gamma$ respectively, property 1 follows directly.

To prove property 2, for any support $\gamma \in \Gamma$:

$$\log U_\gamma(O) = -\frac{2}{|\mathcal{P}_n|} \sum_{O' \in \mathcal{P}_n} [[O', O]] \log \Lambda_\gamma(O'_\gamma) \quad (\text{B9})$$

$$= -\frac{2}{|\mathcal{P}_n|} \sum_{O'_{\gamma^c} \in \mathcal{P}_{\gamma^c}} [[O'_{\gamma^c}, O_{\gamma^c}]] \sum_{O'_\gamma \in \mathcal{P}_\gamma} [[O'_\gamma, O_\gamma]] \log \Lambda_\gamma(O'_\gamma) \quad (\text{B10})$$

$$= \frac{-2}{4|\gamma|} \sum_{O'_\gamma \in \mathcal{P}_\gamma} [[O'_\gamma, O_\gamma]] \log \Lambda_\gamma(O'_\gamma). \quad (\text{B11})$$

where we denote the complement of the support γ as $\gamma^c = [n] \setminus \gamma$, and \mathcal{P}_γ is the subgroup of \mathcal{P}_n containing all Pauli operators supported on γ . Since $\sum_{O'_{\gamma^c} \in \mathcal{P}_{\gamma^c}} [[O'_{\gamma^c}, O_{\gamma^c}]] = 0$ if $O \notin \mathcal{E}_\gamma$, $\log U_\gamma(O) = 0$ if $\text{supp}(O) \not\subseteq \gamma$. And if $\forall \gamma \in \Gamma$, $\text{supp}(O) \not\subseteq \gamma$, then $\log U(O) = 0$ due to property 1. \square

This motivates us to define the set of transformed local eigenvalues for the total channel as $\bar{\mu} = \{U(e) | e \in \bar{\mathcal{E}}_\Gamma\}$ and the corresponding vector $\vec{\mu} = (U(e) | e \in \bar{\mu})$ with entries in the order of Eq. (15). This set of transformed local eigenvalues is the set of values of $\log U(e)$ of the local errors $e \in \bar{\mathcal{E}}_\Gamma$, and it is the set of non-trivial factors that determines the total channel \mathcal{N}_Γ . This is because for all $e \notin \mathcal{E}_\Gamma \cup \{I\}$, we have $\log U(e) = 0$ according to Lemma B.3, while for $e = I$, $\log U(I)$ depends on the values in μ :

$$\log U(I) = -\sum_{e \in \bar{\mathcal{E}}_\Gamma} \log U(e), \quad (\text{B12})$$

since $\log \Lambda(I) \propto \sum_{e \in \mathcal{P}_n} \log U(e) = \sum_{e \in \bar{\mathcal{E}}_\Gamma + \{I\}} \log U(e) = 0$. In particular, for any Pauli eigenvalue $\Lambda(e), \forall e \in \mathcal{P}_n$ we

have:

$$\log \Lambda(e) = -\frac{1}{2} \sum_{e' \in \mathcal{P}_n} [[e', e]] \log U(e') \quad (\text{B13})$$

$$= -\frac{1}{2} \left(\log U(I) + \sum_{e' \in \bar{\mathcal{E}}_\Gamma} [[e', e]] \log U(e') \right) \quad (\text{B14})$$

$$= \sum_{e' \in \bar{\mathcal{E}}_\Gamma} \frac{-[[e', e]] + 1}{2} \log U(e') \quad (\text{Eq. (B12)}) \quad (\text{B15})$$

$$= \sum_{e' \in \bar{\mathcal{E}}_\Gamma} \langle e', e \rangle \log U(e') \quad (\text{B16})$$

$$= \sum_{e' \in \bar{\mathcal{E}}_\Gamma} \langle e', e \rangle \log \bar{\mu}_{e'}. \quad (\text{B17})$$

Here, we define the binary commutator for Pauli operators $\langle A, B \rangle$ as

$$\langle A, B \rangle = \begin{cases} 0 & \text{if } A, B \text{ commute} \\ 1 & \text{else.} \end{cases} \quad (\text{B18})$$

Therefore, for any set \mathcal{H} of Pauli operators, we can write

$$\log \vec{\Lambda}^{(\mathcal{H})} = \overline{D}^{(\mathcal{H})} \log \vec{\mu}, \quad (\text{B19})$$

where $\overline{D}^{(\mathcal{H})}$ is a $|\mathcal{H}|$ by $|\bar{\mathcal{E}}_\Gamma|$ matrix with entries: $\overline{D}^{(\mathcal{H})}[h, e] = \langle h, e \rangle, h \in \mathcal{H}, e \in \bar{\mathcal{E}}_\Gamma$.

Similarly, to parametrize local channels, we define the set $\mu = \{U_{\gamma_e}(e) | e \in \mathcal{E}_\Gamma\}$ and the corresponding vector $\vec{\mu} = (U(e) | e \in \mu)$ and we have

$$\log \vec{\Lambda}^{(\mathcal{H})} = D^{(\mathcal{H})} \log \vec{\mu}, \quad (\text{B20})$$

where $D^{(\mathcal{H})}$ is a $|\mathcal{H}|$ by $|\mathcal{E}_\Gamma|$ matrix with entries: $D^{(\mathcal{H})}[h, e] = \langle h, e \rangle, h \in \mathcal{H}, e \in \mathcal{E}_\Gamma$. We refer to the matrix D as the *syndrome matrix* for the collection of local channels.

Note that there is intrinsic gauge freedom in $\log \mu$ of the form similar to Eq. (B6):

$$\log U_{\gamma_1}(e) \longrightarrow \log U_{\gamma_1}(e) + \alpha \quad \text{and} \quad \log U_{\gamma_2}(e) \longrightarrow \log U_{\gamma_2}(e) - \alpha, \quad (\text{B21})$$

whenever we have two non-overlapping distinct channel supports $\gamma_1, \gamma_2 \in \Gamma$ and Pauli error e such that $\text{supp}(e) \subseteq \gamma_1 \cap \gamma_2$. However, working with the local channels using the transformed local eigenvalues $\log \mu$ is more natural for physical level benchmarking, since $\log \mu$ is an approximation of the Pauli error rates associated with physical circuit operation (see Section E).

In Section C, we prove the rank of matrices A and D , which gives the minimal number of measured stabilizer elements needed to solve for the system of linear equations.

APPENDIX C: Rank of matrix A and D

Given a Pauli error model with a set of supports Γ and the group of measured stabilizer \mathcal{M} , we constructed Eq. (18) that connects local Pauli eigenvalues to the syndrome expectation values. In this section, we present more details of the structure of this system of linear equations represented by the matrix $A^{(\mathcal{M})}$ by performing a basis transform to the syndrome matrix $D^{(\mathcal{M})}$ (Eq. (B20) in Section B) and show that the rank of $A^{(\mathcal{M})}$ and $D^{(\mathcal{M})}$ is the number of non-trivial syndrome classes $|\mathcal{C}^*|$. Therefore one only need to select a subset $\mathcal{M}' \subseteq \mathcal{M}$ of $|\mathcal{C}^*|$ many stabilizer elements such that the rows among $A^{(\mathcal{M}')}$ and $D^{(\mathcal{M}')}$ are all independent. We give a formal definition of syndrome class with respect to a set of Pauli operators:

Definition C.1 (Syndrome error class). *Given a set of Pauli operators \mathcal{H} and the set of Pauli errors \mathcal{E}_Γ , we define the syndrome vector for any $e \in \mathcal{E}_\Gamma$ as $\vec{s}(e) = (\langle e, h \rangle)_{h \in \mathcal{H}}$. We define the set of syndrome classes $\mathcal{C}^{(\mathcal{H})}$ of \mathcal{E}_Γ with respect to \mathcal{H} as a set of equivalent classes of \mathcal{E}_Γ induced by the relation $e \sim e'$ if and only if $\vec{s}(e) = \vec{s}(e')$. We denote by C_0 the trivial syndrome class in $\mathcal{C}^{(\mathcal{H})}$, i.e. the class $\{e \in \mathcal{E}_\Gamma | \vec{s}(e) = \vec{0}\}$. And we denote the set of non-trivial classes $\mathcal{C}^{*(\mathcal{H})} = \mathcal{C}^{(\mathcal{H})} \setminus \{C_0\}$. When the set \mathcal{H} is the measured stabilizer group \mathcal{M} , we omit the superscript.*

From Eq. (B15), we note that matrix A and the syndrome matrix D differ by a full rank transformation:

Lemma C.2. $\text{rank } D^{(\mathcal{H})} = \text{rank } A^{(\mathcal{H})}$ for any set of Pauli operators \mathcal{H} .

Proof. The full rank matrix V of the linear transformation $D^{(\mathcal{H})} = A^{(\mathcal{H})}V$ is given by:

$$V = \bigoplus_{\gamma \in \Gamma} (J_{4^{|\gamma|}-1} - W'_{4^{|\gamma|}})/2 \quad (\text{C1})$$

where we denote $W'_{4^{|\gamma|}}$ as the order $4^{|\gamma|}$ Walsh-Hadamard matrix deleting the first row and first column. J_n is a n by n matrix with all entries being 1. For example, consider V on a single qubit, then we have

$$W_4 = \begin{pmatrix} 1 & 1 & 1 & 1 \\ 1 & 1 & -1 & -1 \\ 1 & -1 & 1 & -1 \\ 1 & -1 & -1 & 1 \end{pmatrix} \mapsto W'_4 = \begin{pmatrix} 1 & -1 & -1 \\ -1 & 1 & -1 \\ -1 & -1 & 1 \end{pmatrix} \quad (\text{C2})$$

and

$$V = \frac{1}{2} \begin{pmatrix} 1 & 1 & 1 \\ 1 & 1 & 1 \\ 1 & 1 & 1 \end{pmatrix} - \frac{1}{2} \begin{pmatrix} 1 & -1 & -1 \\ -1 & 1 & -1 \\ -1 & -1 & 1 \end{pmatrix} = \begin{pmatrix} 0 & 1 & 1 \\ 1 & 0 & 1 \\ 1 & 1 & 0 \end{pmatrix}. \quad (\text{C3})$$

For example, the syndrome matrix $D^{(\mathcal{H})}$ of single-qubit errors can be constructed in such a way where we look at the three columns of any qubit, its X column is the sum of the Y and Z column of $A^{(\mathcal{H})}$, its Y column is the sum of the X and Z column of $A^{(\mathcal{H})}$, and its Z column is the sum of the X and Y column of $A^{(\mathcal{H})}$. Eq. (C1) generalizes this procedure to an arbitrary set of local channel supports Γ . \square

Since $D^{(\mathcal{M})}$ encodes the commutation of each error with the measured stabilizer group, the columns of D for errors in the same syndrome error class are identical. We define the reduced syndrome matrix D' by removing columns of these redundant errors in D :

Definition C.3. The reduced syndrome matrix $D'^{(\mathcal{H})}$ of a given set of Pauli error support Γ and a set of Pauli operators \mathcal{H} is a $|\mathcal{H}|$ by $|\mathcal{C}^{*(\mathcal{H})}|$ matrix where each column correspond to one representative in every non-trivial syndrome error class $C \in \mathcal{C}^{*(\mathcal{H})}$, and the syndrome classes are defined for the set \mathcal{E}_Γ . The reduced syndrome matrix $\overline{D}'^{(\mathcal{H})}$ for the total channel is defined similarly but the syndrome classes $\mathcal{C}^{*(\mathcal{M})}$ is defined for the error set $\overline{\mathcal{E}}_\Gamma$ instead.

Lemma C.4. $\text{rank } \overline{D}^{(\mathcal{M})} = \text{rank } \overline{D}'^{(\mathcal{M})} = \text{rank } D^{(\mathcal{M})} = \text{rank } D'^{(\mathcal{M})} = |\mathcal{C}^{*(\mathcal{M})}|$ for any subgroup of the Pauli group $\mathcal{M} \leq \mathcal{P}_n$, where $\mathcal{C}^{*(\mathcal{M})}$ is the set of non-trivial syndrome classes (Definition C.1) for the set of errors \mathcal{E}_Γ .

Proof. The first three equalities are trivial from Definition C.3 and Eqs. (B19) and (B20). For the last equality, one could show that $(D'^{(\mathcal{M})})^T (D'^{(\mathcal{M})})$ is full rank. The observation is that

$$[(D'^{(\mathcal{M})})^T (D'^{(\mathcal{M})})]_{i,j} \quad (\text{C4})$$

$$= |\{M \in \mathcal{M} | [[M, e_i]] = [[M, e_j]] = -1\}| \quad (\text{C5})$$

$$= \begin{cases} |\mathcal{M}|/2 & \text{if } i = j, \\ |\mathcal{M}|/4 & \text{if } i \neq j. \end{cases} \quad (\text{C6})$$

Here, e_i is the error correspond to the i th column of $D'^{(\mathcal{M})}$. To justify the last equality Eq. (C6), we select a generating set \mathcal{Q} of \mathcal{M} such that $\mathcal{M} = \langle \mathcal{Q} \rangle$ and so that $|\mathcal{M}| = 2^{|\mathcal{Q}|}$. Then every $M \in \mathcal{M}$ corresponds to an element $\mathcal{Q}^{(M)}$ of the power set $2^{\mathcal{Q}}$:

$$M = \prod_{Q \in \mathcal{Q}^{(M)}} Q. \quad (\text{C7})$$

We define $\mathcal{Q}_{e_k} = \{Q \in \mathcal{Q} | [[Q, e_k]] = -1\}$, i.e. the set of generators that anticommute with e_k . To find the number of M that anticommute with e_i , $\mathcal{Q}^{(M)}$ has to satisfy:

$$|\mathcal{Q}^{(M)} \cap \mathcal{Q}_{e_i}| \equiv 1 \pmod{2}, \quad (\text{C8})$$

so the number of choices of $\mathcal{Q}^{(M)}$ is:

$$2^{|\mathcal{Q}|-|\mathcal{Q}_{e_i}|} \sum_{\text{odd } j} \binom{|\mathcal{Q}_{e_i}|}{j} = 2^{|\mathcal{Q}|-1} = |\mathcal{M}|/2. \quad (\text{C9})$$

We denote by $\mathcal{Q}_1 \setminus \mathcal{Q}_2$ the relative complement of \mathcal{Q}_1 and \mathcal{Q}_2 , i.e., the set of elements in \mathcal{Q}_1 that are not in \mathcal{Q}_2 . To find the number of M that anticommute with e_i and e_j ($i \neq j$), $\mathcal{Q}^{(M)}$ has to satisfy:

$$|\mathcal{Q}^{(M)} \cap \mathcal{Q}_{e_i} \cap \mathcal{Q}_{e_j}| + |\mathcal{Q}^{(M)} \cap (\mathcal{Q}_{e_i} \setminus \mathcal{Q}_{e_j})| \equiv |\mathcal{Q}^{(M)} \cap \mathcal{Q}_{e_i} \cap \mathcal{Q}_{e_j}| + |\mathcal{Q}^{(M)} \cap (\mathcal{Q}_{e_j} \setminus \mathcal{Q}_{e_i})| \equiv 1 \pmod{2}, \quad (\text{C10})$$

so one could first choose any subset of generators in $(\mathcal{Q}_{e_i} \cup \mathcal{Q}_{e_j})^c$ and $\mathcal{Q}_{e_i} \cap \mathcal{Q}_{e_j}$, and then select generators in $\mathcal{Q}_{e_i} \setminus \mathcal{Q}_{e_j}$ and $\mathcal{Q}_{e_j} \setminus \mathcal{Q}_{e_i}$ accordingly to satisfy Eq. (C10). The number of choices of $\mathcal{Q}^{(M)}$ is therefore:

$$2^{|\mathcal{Q}|-|\mathcal{Q}_{e_i} \cup \mathcal{Q}_{e_j}|+|\mathcal{Q}_{e_i} \cap \mathcal{Q}_{e_j}|} \left(\sum_{\text{odd (even) } r} \binom{|\mathcal{Q}_{e_i} \setminus \mathcal{Q}_{e_j}|}{r} \right) \left(\sum_{\text{odd (even) } s} \binom{|\mathcal{Q}_{e_j} \setminus \mathcal{Q}_{e_i}|}{s} \right) \quad (\text{C11})$$

$$= |\mathcal{M}|/4. \quad (\text{C12})$$

Therefore from Eq. (C6) we have:

$$(D'^{(\mathcal{M})})^T (D'^{(\mathcal{M})}) = \frac{|\mathcal{M}|}{4} (J_{|\mathcal{C}^*|} + I_{|\mathcal{C}^*|}), \quad (\text{C13})$$

where J_n is the n by n matrix of all ones and I_n is the n by n identity matrix. As a result, $(D'^{(\mathcal{M})})^T (D'^{(\mathcal{M})})$ is full rank thus $D'^{(\mathcal{M})}$ has full column rank which is $|\mathcal{C}^{*(\mathcal{M})}|$. \square

Corollary C.5. $\text{rank } A^{(\mathcal{M})} = \text{rank } D^{(\mathcal{M})} = |\mathcal{C}^{*(\mathcal{M})}|$.

Proof. This follows directly from Lemma C.2 and Lemma C.4. \square

APPENDIX D: Minimal number of equations for the syndrome data

In this section, we explain the algorithm used to find the minimum subset \mathcal{M}' of stabilizer elements needed for the noise learning. This is motivated because to solve Eq. (18) or Eq. (22):

$$\log \vec{\Lambda}^{(\mathcal{M})} = A^{(\mathcal{M})} \log \vec{\lambda}, \quad (\text{D1})$$

$$\log \vec{\Lambda}^{(\mathcal{M})} = D^{(\mathcal{M})} \log \vec{\mu}, \quad (\text{D2})$$

we encounter the scaling issue as there are exponentially many equations ($|\mathcal{M}| = 2^{n-k}$) if assuming full syndrome is measured, i.e., $\mathcal{M} = \mathcal{S}$. (See the relation of the two sets of equations in Section E). However, we focus on the case when \mathcal{N}_Γ is a (r_Γ, c_Γ) -Pauli channel, i.e. local Pauli noise models with $|\gamma|_{\max} = r_\Gamma = O(1)$ and $|\Gamma| = O(n)$. In this local noise model setting, the total number of noise model parameters scales linearly with the system size n . From Definition C.3, Lemma C.2, Lemma C.4, and Corollary C.5 we have:

$$\text{rank } A^{(\mathcal{M})} = \text{rank } D^{(\mathcal{M})} = \text{rank } A^{(\mathcal{M}') \text{ }} = \text{rank } D^{(\mathcal{M}') \text{ }} = \text{rank } D'^{(\mathcal{M}') \text{ }} = |\mathcal{C}^*| \quad (\text{D3})$$

where $|\mathcal{C}^*|$ is the number of non-trivial syndrome classes that also scales linearly with n in this setting.

Here, we show an algorithm to select a subset $\mathcal{M}' \subseteq \mathcal{M}$ of size $|\mathcal{C}^*|$ satisfying $\text{rank } A^{(\mathcal{M}') \text{ }} = |\mathcal{C}^*|$ so that one could solve the following linear size system of equations (Eq. (26) in main text) instead:

$$\log \vec{\Lambda}^{(\mathcal{M}') \text{ }} = A^{(\mathcal{M}') \text{ }} \log \vec{\lambda} \quad (\text{D4})$$

$$\log \vec{\Lambda}^{(\mathcal{M})} = D^{(\mathcal{M}') \text{ }} \log \vec{\mu}. \quad (\text{D5})$$

We find \mathcal{M}' in the reduced search space since one only needs to consider products of "correlated" stabilizer generators, as shown in proposition D.1.

Lemma D.1. *Given a set of generators of \mathcal{M} and the set of error supports Γ , we call a pair of elements in \mathcal{M} "correlated" if they both overlap with some region $\gamma \in \Gamma$. To construct matrix $A^{(\mathcal{M}') \text{ }}$ with maximal rank, it suffices to pick stabilizer elements from a product of generators such that for any M_i in the product, there exists $M_j \neq M_i$ in the factors of the product that is correlated with M_i .*

Proof. We denote the row corresponding to element $H \in \mathcal{H}$ of the matrix $A^{(\mathcal{H})}$ as $A^{(\mathcal{H})}[H]$. For any $M \in \mathcal{M}$ that corresponds to an independent row of A and can be written as $M = M_i M_j$ for some uncorrelated pair $M_i, M_j \in \mathcal{M}$, i.e. $\text{supp}(M_i) \cap \text{supp}(M_j) \cap \gamma = \emptyset, \forall \gamma \in \Gamma$, we have $\Lambda(M) = \Lambda(M_i)\Lambda(M_j)$ and $A[M] = A[M_i] + A[M_j]$. Therefore, replacing M by M_i is a row operation on A unless M_i is linearly dependent on other rows, in which case one could replace M by M_j . We could repeat the process until all rows of A are the product of overlapping stabilizer generators without decreasing the rank of A . \square

This motivates us to define the stabilizer correlation graph which the algorithm 1 utilizes, a graph that encodes the correlation between a set of measured stabilizer generators given the individual error events determined by Γ :

Definition D.2 (Stabilizer correlation graph). *Given a set of measured stabilizer generators, the stabilizer correlation graph G is a graph with vertices corresponding to the measured stabilizer generators. Two vertices share an edge if and only if the two generators have overlapping support $\gamma \in \Gamma$.*

Given the graph G , all elements of \mathcal{M} satisfying the condition of Lemma D.1 correspond to the connected subgraphs of G . One can implement the algorithm below and guarantee to output a subset $\mathcal{M}' \subseteq \mathcal{M}$ with $A^{(\mathcal{M}')} \in \mathcal{M}'$ reaches the maximal rank $\text{rank } A^{(\mathcal{M}')} = \text{rank } A^{(\mathcal{M})} = |\mathcal{C}^*|$. One can use similar algorithms based on the reduced syndrome matrix D' .

Algorithm 1: Constructing the matrix $A^{(\mathcal{M}')}$

Input:

1. Local generators of S
2. Syndrome error classes $\mathcal{C}(\mathcal{S}, \Gamma)$ and its non-trivial classes \mathcal{C}^* .

- 1 Construct the stabilizer correlation graph G from Def. D.2.
- 2 Let $v = 0, \mathcal{M}' = \{\}$.
- 3 Let $A^{(\mathcal{M}')} = \text{empty matrix}$.
- 4 **while** $\text{rank } A^{(\mathcal{M}')} < |\mathcal{C}^*|$ **do**
- 5 $v = v + 1$
- 6 **for** connected subgraph g of order v in G **do**
- 7 Add stabilizer elements M that correspond to g to \mathcal{M}' .
- 8 Construct matrix $A^{(\mathcal{M}')}$.
- 9 **return** \mathcal{M}' and $A^{(\mathcal{M}')}$

Lemma D.3. *The runtime of Algorithm 1 is $\text{Poly}(n)$ for qLDPC codes under local sparse Pauli channel \mathcal{N}_Γ .*

Proof. The upper bound of the order v_{\max} of the connected subgraph needed is given by the maximum number of stabilizer generators that a single local error can flip, as shown in Eq. (35) and proven in Lemma I.1. \square

For each order v of the connected subgraphs being searched, the runtime of the algorithm scales $\text{Poly}(n)$ and $\exp(v)$. However, the upper bound of the order v_{\max} of the connected subgraph needed is given by the maximum number of stabilizer generators that a single local error can flip, as shown in Eq. (35) in Lemma I.1. Therefore, the maximum order v_{\max} of the search is a constant for qLDPC codes. For example, the upper bound of the order v is 4 for single-qubit errors on the rotated surface code of any size using the typical local stabilizer generators.

The learning algorithm can be summarized as solving two sets of equations, one is the system of equations characterized by $A^{(\mathcal{M}')}$ or $D'^{(\mathcal{M}')}$ in Eqs. (26) and (27) with respect to the log of the local Pauli eigenvalues $\log \vec{\lambda}$. The other one is the extra constraints characterized by matrix B in Eq. (29), which are linear constraints in the probability distribution/local Pauli eigenvalues $\vec{\lambda}$. The number of rows of B , i.e. the total number of these extra constraints, is $|\mathcal{C}_0| + \sum_{C \in \mathcal{C}^*} (|C| - 1)$. The number of independent equations from syndrome expectation values is $|\mathcal{C}^*|$. As a result, the total number of constraints equals:

$$\# \text{constraints} \quad (\text{D6})$$

$$= |\mathcal{C}_0| + \sum_{C \in \mathcal{C}^*} (|C| - 1) + |\mathcal{C}^*| \quad (\text{D7})$$

$$= |\mathcal{E}_\Gamma| - 1 \quad (\text{D8})$$

which is exactly the degrees of freedom in the Pauli noise model. In Section F, we prove that a solution under these two sets of equations must exist for low error rates.

APPENDIX E: Proof of syndrome class error rate learnability condition

To understand the learnability of the total channel, we first look at the parametrization of the total channel \mathcal{E}_Γ with the set of transformed local eigenvalues of the total channel $\vec{\mu}$ defined from the $\log U$ basis. In particular, we have the logarithm of Pauli eigenvalues of \mathcal{N}_Γ written as a linear function of $\log \vec{\mu}$ as in Eq. (B19):

$$\log \vec{\Lambda}^{(\mathcal{H})} = \overline{D}^{(\mathcal{H})} \log \vec{\mu}. \quad (\text{E1})$$

Lemma E.1. *For a Pauli channel \mathcal{N}_Γ with a set of support Γ satisfies that for any $\gamma \in \Gamma, e \in \mathcal{E}_\gamma$ $P_\gamma(e) > 0$ and $P_\gamma(I) > 1/2$ (Assumption 1), then the set of transformed eigenvalues $\vec{\mu}$ for the collection of individual channels $\{\mathcal{N}_\gamma\}_{\gamma \in \Gamma}$ is an open set in $\mathbb{R}^{|\mathcal{E}_\Gamma|}$. Similarly, the set of transformed eigenvalues $\vec{\mu}$ for the total channel \mathcal{N}_Γ is an open set in $\mathbb{R}^{|\overline{\mathcal{E}}_\Gamma|}$.*

Proof. Given Assumption 1, we have all the possible local error rates \vec{p} as an open set in $\mathbb{R}^{|\mathcal{E}_\Gamma|}$. And we have

$$\vec{\mu} = V^{-1} \log \vec{\lambda} = V^{-1} \log (\vec{I} - 2V\vec{p}) \quad (\text{E2})$$

where V is the invertible matrix in Eq. (C1). Therefore, the map between \vec{p} and $\vec{\mu}$ is a continuous bijection, and therefore the set of possible transformed eigenvalues $\vec{\mu}$ is also an open set in $\mathbb{R}^{|\mathcal{E}_\Gamma|}$.

In addition, the logarithm of the transformed eigenvalues for the total $\log \vec{\mu}$ of the total channel is related to $\log \vec{\mu}$ by a surjective maps (see the first properties of Lemma B.3), so the set of possible $\vec{\mu}$ is also an open set, in $\mathbb{R}^{|\overline{\mathcal{E}}_\Gamma|}$. \square

Theorem 3 (Restated). Let a total Pauli error channel \mathcal{N}_Γ be a composition of Pauli channels \mathcal{N}_γ with support $\gamma \in \Gamma$. Under Assumption 1, we have:

1. The total channel \mathcal{N}_Γ can be learned if and only if every error $e \in \overline{\mathcal{E}}_\Gamma$ has a unique and nontrivial syndrome.
2. Each individual channel \mathcal{N}_γ is learnable if and only if every $e \in \mathcal{E}_\gamma$ produces a syndrome that is non-trivial and unique among the syndromes of all errors in \mathcal{E}_Γ .
3. For all non-trivial syndrome error classes $C \in \mathcal{C}^*$, the sum of syndrome error class error rates $P_C = \sum_{e \in C} p_e$ can be learned up to an $\mathcal{O}(\|\vec{p}^{(\Gamma_C)}\|^2)$ deviation.

Proof. To prove the first statement regarding the learnability condition of the total channel \mathcal{N}_Γ , note that there is an invertible linear map (Walsh-Hadamard transform) between the logarithm of Pauli eigenvalues $\log \Lambda(e)$ of \mathcal{N}_Γ and the transformed eigenvalues $\log U(e)$ for all $e \in \mathcal{P}_n$. On the other hand, given the restricted structure of the total channel \mathcal{N}_Γ with the set of support Γ , we proved in Section B that the transformed eigenvalues $\log U(e) = 0$ if $e \neq I$ and $e \notin \overline{\mathcal{E}}_\Gamma$, and $\log U(I)$ depends on $\{\log U(e) | e \in \overline{\mathcal{E}}_\Gamma\}$. Therefore, we define a local subset of the transformed eigenvalues $\vec{\mu} = \{\log U(e) | e \in \overline{\mathcal{E}}_\Gamma\}$ and two total channels \mathcal{N}_Γ and \mathcal{N}'_Γ are equal if and only if their corresponding " $\vec{\mu}$ set" $\vec{\mu}$ and $\vec{\mu}'$ are equal.

On the other hand, we have the relation between the syndrome expectation and the transformed local eigenvalues $\vec{\mu}$ for the total channel

$$\log \vec{\Lambda}^{(\mathcal{M})} = \overline{D}^{(\mathcal{M})} \vec{\mu}. \quad (\text{E3})$$

where $\overline{D}^{(\mathcal{M})}$ is the $|\mathcal{M}|$ by $|\overline{\mathcal{E}}_\Gamma|$ syndrome matrix of the error set $\overline{\mathcal{E}}_\Gamma$. First, note that the set of expectation values of all the measured stabilizer elements $\vec{\Lambda}^{(\mathcal{M})}$ is a sufficient statistic of the syndrome data. This is because it is a Walsh-Hadamard transformation of the probability distribution over the m -bit syndrome, where m is the number of generators of the measured stabilizer group \mathcal{M} .

According to Lemma C.4, the rank of $\overline{D}^{(\mathcal{M})}$ is the number of non-trivial syndrome classes of \mathcal{E}_Γ (or equivalently $\overline{\mathcal{E}}_\Gamma$). In addition, if the values of the transformed local eigenvalues $\vec{\mu}$ is valid given the assumption about the channel \mathcal{N}_Γ , then the neighborhood of $\vec{\mu}$ is also valid according to Lemma E.1. As a result, given the syndrome expectation values $\vec{\Lambda}^{(\mathcal{M})}$, we have a continuous family of valid parametrization $\log \vec{\mu}' = \log \vec{\mu} + \vec{\epsilon}$ around a valid point $\log \vec{\mu}$, where $\vec{\epsilon} \in \ker(\overline{D}^{(\mathcal{M})})$. Therefore, we can conclude that $\vec{\mu}$ and thus the total channel \mathcal{N}_Γ is learnable if and only if the number of non-trivial syndrome classes is equal to $|\overline{\mathcal{E}}_\Gamma|$, i.e. all syndromes in $\overline{\mathcal{E}}_\Gamma$ are non-trivial and distinct. The second statement regarding the learnability of local channels can be proven similarly by arguing that all transformed local eigenvalues μ from a local channel \mathcal{N}_γ can be learned if and only if the errors in \mathcal{E}_γ has distinct and non-trivial syndrome among all syndromes of \mathcal{E}_Γ by looking at columns of the syndrome matrix $D^{(\mathcal{M})}$ in Eq. (22).

To prove what we can learn about the local channels when the necessary and sufficient condition of learnability potentially fails, we look at the transformation of the basis in Eq. (18) regarding all the local Pauli eigenvalues $\vec{\lambda}$:

$$\log \vec{\Lambda}^{(\mathcal{M})} = A^{(\mathcal{M})} \log \vec{\lambda}. \quad (\text{E4})$$

to this basis of the syndrome matrix $D^{(\mathcal{H})}$ with the transformed eigenvalues in Eq. (B20):

$$\log \vec{\Lambda}^{(\mathcal{M})} = D^{(\mathcal{M})} \log \vec{\mu}, \quad (\text{E5})$$

where the transformation V is given in Eq. (C1) so that we have:

$$D^{(\mathcal{M})} = A^{(\mathcal{M})} V \quad (\text{E6})$$

$$\log \vec{\mu} = V^{-1} \log \vec{\lambda}. \quad (\text{E7})$$

Explicitly, V^{-1} is the direct sum of a constant times the Walsh-Hadamard matrix (Eq. (C2)):

$$V^{-1} = -2 \bigoplus_{\gamma \in \Gamma} \frac{1}{4^{|\gamma|}} W'_{4^{|\gamma|}}. \quad (\text{E8})$$

In general, for an error e supported on $\gamma \in \Gamma$, the transformed eigenvalues μ_e can be written as a fraction where the numerator/denominator are products of Pauli eigenvalues of errors supported on γ that anticommute/commute with e respectively, then raised the power of $\frac{1}{2^{(2|\gamma|-1)}}$. Moreover, if e has a unique syndrome, then the column of $D^{(\mathcal{M})}$ corresponding to e is independent of other columns (Lemma C.4). Since $D^{(\mathcal{M})}$ encodes the syndrome of all local errors $e \in \mathcal{E}_\Gamma$ in its columns, the learnable quantities are therefore the sum of $\log \mu$ of each syndrome error class. Denoting \mathcal{C}^* as the set of non-trivial syndrome classes, we can learn

$$\left\{ \sum_{e \in C} \log \mu_e \mid C \in \mathcal{C}^* \right\}. \quad (\text{E9})$$

At low physical error rate for each local channel $\gamma \in \Gamma$, $\log \lambda = \lambda - 1 + \mathcal{O}(\|\vec{p}\|^2)$ and $\log \mu$ is just the local Walsh-Hadamard transform of $\log \lambda$. Therefore according to Eq. (E8) we have:

$$-\frac{1}{2} \log \mu_e = p_e + \mathcal{O}(\|\vec{p}^{(\gamma)}\|^2) \quad (\text{E10})$$

for any $e \in \mathcal{E}_\Gamma$, where $\vec{p}^{(\gamma)} = (p_e)_{e \in \mathcal{E}_\gamma}$. For each syndrome error class $C \in \mathcal{C}^*$, we have the learnable quantity referred to as the learnable eigenvalues

$$\log \nu_C = \sum_{e \in C} \log \mu_e = -2 \sum_{e \in C} p_e + \mathcal{O}(\|\vec{p}^{(\Gamma_C)}\|^2). \quad (\text{E11})$$

A straightforward approximate estimator for the sum of syndrome class error rates is given by

$$\sum_{e \in C} \tilde{p}_e = -\frac{1}{2} \log \nu_C \quad (\text{E12})$$

and the magnitude of the bias is of second order in the local error rates, i.e., $|\sum_{e \in C} \tilde{p}_e - \sum_{e \in C} p_e| = \mathcal{O}(\|\vec{p}^{(\Gamma_C)}\|^2)$. \square

Lemma E.2 (Independent detector error model learnability). *If the local Pauli channel can be written as a composition of independent single-Pauli channels:*

$$\mathcal{N}(\rho) = \circ_{e \in \mathcal{E}_\Gamma} \mathcal{N}^{(e)}(\rho) \quad (\text{E13})$$

where $\mathcal{N}^{(e)}(\rho) = (1 - p_e)\rho + p_e e \rho e^\dagger$. Then the probability of an odd number of errors in each syndrome error class, or the detector error rate [22], can be exactly learned.

Proof. Note that if each local channel can be further decomposed into a composition of channels $\mathcal{N}^{(e)}$ involving a single Pauli error e , then each transformed eigenvalue $\mu^{(e)}$ is of the simple form:

$$\mu_{e'}^{(e)} = \begin{cases} 1 - 2p_e & \text{if } e = e', \\ 1 & \text{else.} \end{cases} \quad (\text{E14})$$

Then the detector error rate associated with the syndrome error class C is:

$$P_C^{\text{detect}} = \frac{1 - \prod_{e \in C} (1 - 2p_e)}{2} = \frac{1}{2}(1 - \nu_C) \quad (\text{E15})$$

which is learnable as shown in Eq. (24). \square

Example E.3. For single-qubit Pauli channels $\mathcal{N}_{\{1\}}(\rho) = \sum_{e \in \{I, X_1, Y_1, Z_1\}} p_e e \rho e^\dagger$, the transformed eigenvalue μ_{X_1} is

$$\mu_{X_1} = \left(\frac{\Lambda(Y_1)\Lambda(Z_1)}{\Lambda(X_1)} \right)^{\frac{1}{2}}. \quad (\text{E16})$$

But when the Pauli channel contains only one error, e.g. $\mathcal{N}^{(X_1)}(\rho) = (1 - p_{X_1})\rho + p_{X_1}X_1\rho X_1^\dagger$, we have

$$\Lambda^{(X_1)}(e) = (-1)^{\langle X_1, e \rangle} (1 - 2p_{X_1}) = \begin{cases} 1 & \text{if } X_1 \text{ and } e \text{ commute,} \\ 1 - 2p_{X_1} & \text{if } X_1 \text{ and } e \text{ anticommute.} \end{cases} \quad (\text{E17})$$

So we have $\mu_{X_1}^{(X_1)} = 1 - 2p_{X_1}$ and $\mu_P^{(X_1)} = 1$ for other single-qubit Pauli P .

As a result, given a set of local errors \mathcal{E}_Γ , Eq. (22) can be reduced to:

$$\log \begin{bmatrix} \Lambda(M_1) \\ \Lambda(M_2) \\ \vdots \end{bmatrix} = \begin{bmatrix} \langle M_1, e_1 \rangle & \langle M_1, e_2 \rangle & \cdots \\ \langle M_2, e_1 \rangle & \langle M_2, e_2 \rangle & \cdots \\ \vdots & \vdots & \ddots \end{bmatrix} \log \begin{bmatrix} \mu_{e_1} \\ \mu_{e_2} \\ \vdots \end{bmatrix} = \begin{bmatrix} \langle M_1, e_1 \rangle & \langle M_1, e_2 \rangle & \cdots \\ \langle M_2, e_1 \rangle & \langle M_2, e_2 \rangle & \cdots \\ \vdots & \vdots & \ddots \end{bmatrix} \log \begin{bmatrix} 1 - 2p_{e_1} \\ 1 - 2p_{e_2} \\ \vdots \end{bmatrix}. \quad (\text{E18})$$

where each e_i are in the set \mathcal{E}_Γ . As a result, what we could learn is

$$\nu_C = \prod_{e \in C} \mu_e = \prod_{e \in C} (1 - 2p_e) = \exp(D'^+ \log \vec{\Lambda}^{(\mathcal{M}')}). \quad (\text{E19})$$

where D'^+ is the pseudoinverse of D' in Eq. (25). The probability of a syndrome of C being flipped (the detector error rates associated with the hyperedges in a decoder graph) is

$$P_C^{\text{detect}} = \frac{1}{2}(1 - \nu_C). \quad (\text{E20})$$

APPENDIX F: Existence of a family of logically equivalent physical error rates

In this section, we prove that under certain low-error-rate conditions for the true error rates, there exists a family of error rates parametrized by the extra constraints B matrix, i.e. Eq. (29), and satisfies the system of equations given by the ideal syndrome expectations, i.e. Eq. (26) or Eq. (27).

By grouping error rates into equivalence classes $C \in \mathcal{C}$ according to their syndrome, we see in Corollary C.5 that the syndrome data gives us $|\mathcal{C}^*|$ independent linear equations. Here $\mathcal{C}^* = \mathcal{C} \setminus \mathcal{C}_0$ is the set of non-trivial syndrome error classes. And in Theorem 3, we show that we can learn the sum of the error rates P_C in each class $C \in \mathcal{C}^*$ up to a second-order deviation in the physical error rates. However, we would like to estimate each error rate associated with each local error $\mathcal{N}_\gamma, \forall \gamma \in \Gamma$ for several reasons. For one, it gives us a direct sense of gate fidelity in the circuit, rather than syndrome-class error rates (or detector error rates), which are only natural in decoding because they are related to the weights of edges in the decoder graph. Secondly, fixing a set of error rates from a family of possible error rates determined by the syndrome data is part of the logical error rate learning algorithm, since we estimate the logical error rate via Monte Carlo sampling. Finally, as shown in Section I.2, our proof of the bounds on the sampling complexity for learning the logical error rate is based on a single instance (determined by extra constraints) of all possible error rates.

We view the system of equations Eqs. (27) and (29) as a vector-valued function on a real vector space and prove the existence of such a family of error rates using a simplified version of a general quantitative inverse function theorem:

Lemma F.1 (Theorem 4.1 of Xinghua [64]). *Let X, Y be Banach spaces and let $f : D \subset X \rightarrow Y$ be differentiable. Fix $x_0 \in D$ and assume $f'(x_0)^{-1}$ exists. $\mathcal{B}_r(x_0)$ denotes the ball of radius r , centered at x_0 . Let $L > 0$ be such that $\mathcal{B}_{\frac{1}{L}}(x_0) \subset D$ and*

$$\|f'(x_0)^{-1}f'(x) - I\| \leq L\|x - x_0\|, \quad \forall x \in \mathcal{B}_{\frac{1}{L}}(x_0). \quad (\text{F1})$$

Then the local inverse $f_{x_0}^{-1}$ exists and is differentiable on the open ball of radius $r = \frac{1}{2L\|f'(x_0)^{-1}\|}$:

$$\mathcal{B}_r(f(x_0)) \subset f\left(\mathcal{B}_{\frac{1}{L}}(x_0)\right). \quad (\text{F2})$$

Lemma F.2 (Quantitative inverse function theorem for C^1 functions over \mathbb{R}^n). *Let $f : \mathbb{R}^n \rightarrow \mathbb{R}^n$ be continuously differentiable (C^1) and $\|\cdot\|$ be a norm on \mathbb{R}^n and also its induced operator norm on matrices. Write $J_f(\vec{x})$ as the Jacobian matrix at \vec{x} , and $\vec{x}_0 \in \mathbb{R}^n$ is a point such that $J_f(\vec{x}_0)$ is invertible. Define $\delta = \frac{1}{\|J_f(\vec{x}_0)^{-1}\|} > 0$. Let $R > 0$ and a constant K be such that*

$$\|J_f(\vec{x}) - J_f(\vec{x}_0)\| \leq K\|\vec{x} - \vec{x}_0\|, \quad \forall \vec{x} \in \mathcal{B}_R(\vec{x}_0). \quad (\text{F3})$$

If $R \geq \frac{\delta}{K}$, then there exists a function $g : \mathcal{B}_{\frac{\delta^2}{2K}}(f(\vec{x}_0)) \rightarrow \mathbb{R}^n$ such that

$$f(g(\vec{y})) = \vec{y} \quad \text{for all } \vec{y} \in \mathcal{B}_{\frac{\delta^2}{2K}}(f(\vec{x}_0)).$$

Proof. Let $f'(x) = J_f(x)$ so that the notation matches the one used in the general case in Lemma F.1. If $\|J_f(x) - J_f(x_0)\| \leq K\|x - x_0\|, \in \mathcal{B}_R(x_0)$, then we have

$$\|f'(x_0)^{-1}f'(x) - I\| = \|f'(x_0)^{-1}(f'(x) - f'(x_0))\| \quad (\text{F4})$$

$$\leq \|f'(x_0)^{-1}\| \|f'(x) - f'(x_0)\| \quad (\text{F5})$$

$$\leq K\|f'(x_0)^{-1}\| \|x - x_0\| \quad (\text{F6})$$

$$= L\|x - x_0\| \quad (\text{F7})$$

for any $x \in \mathcal{B}_R(x_0)$, where we define $L = K\|f'(x_0)^{-1}\| = \frac{K}{\delta}$. Moreover, if $R \geq \frac{\delta}{K}$, then $R \geq \frac{1}{L}$. Therefore according to Lemma F.1, there exists inverse $g = f^{-1}$ in open ball of radius $\frac{1}{2L\|f'(x_0)^{-1}\|} = \frac{\delta^2}{2K}$. \square

Define the detectable local error rates as $\vec{p}^* = (P_{\gamma_e}(e) | e \in \mathcal{E}_\Gamma^*)$, where $\mathcal{E}_\Gamma^* = \mathcal{E}_\Gamma \setminus C_0$ is the set of detectable local errors. Define a function $H : R^{|\mathcal{E}_\Gamma^*|} \rightarrow R^{|\mathcal{C}^*|}$ being the map to the values of the learnable eigenvalues in Theorem 3, as a function of the local error rates of the detectable errors

$$H(\vec{p}^*) = \log \vec{\nu}(\vec{p}^*). \quad (\text{F8})$$

We denote H_i as the component of the function H for the syndrome class $C_i \in \mathcal{C}^*$. To use Lemma F.2, we define another function $G_B(x) : R^{|\mathcal{C}^*|} \rightarrow R^{|\mathcal{C}^*|}$ and

$$G_B(\vec{x}) = H(K_B \vec{x}) = \log \vec{\nu}. \quad (\text{F9})$$

Here \vec{x} refers to the non-trivial syndrome error class error rates and $x_i = P_{C_i}$ denotes the syndrome class error rate for the i th syndrome class C_i . K_B is a matrix such that $\vec{p}^* = K_B \vec{x}$. To be more specific, note that the function G_B depends on the extra constraints $\vec{B} \vec{p}^* = \vec{0}$ and it gives rise to a linear map from syndrome error rate to the detectable error rates $\vec{p}^* = K_B \vec{x}$. Here, each row i of the matrix K_B has a single element at column j , corresponding to the fraction of the error rate p_i^* in its syndrome class P_{C_j} :

$$[K_B]_{i,j} = \frac{r_{e_i}}{\sum_{e \in C_j} r_e} \mathbb{I}_{C_j}(e_i), \quad (\text{F10})$$

where r_e are the relative strengths of the errors e that construct matrix B in Eqs. (30) and (31), and \mathbb{I}_C is the indicator function for the syndrome class, i.e. $\mathbb{I}_C(e) = 1$ if error e is in the syndrome class C , and 0 otherwise.

We define the second-order derivative, i.e., Hessian, of a function $f(\vec{x}) : \mathbb{R}^n \rightarrow \mathbb{R}^n$ as $J_f^2(\vec{x})$, which is a rank-3 tensor with entries:

$$[J_f^2(\vec{x})]_{i,j,k} = \frac{\partial f_i}{\partial x_j \partial x_k}. \quad (\text{F11})$$

We define the induced norm $\|J_f^2\|_\infty$ as

$$\|J_f^2\|_\infty = \max_{\|\vec{v}\|_\infty=1} \|J_f^2 \vec{v}\|_\infty, \quad (\text{F12})$$

where the norm on the RHS is the usual vector-induced norm for matrices, and $J_f^2 \vec{v}$ is a matrix obtained by the tensor contraction $(J_f^2 \vec{v})_{i,j} = \sum_k [J_f^2]_{i,j,k} v_k$. The norm can be written explicitly as

$$\|J_f^2\|_\infty = \max_i \sum_{j,k} \left| \frac{\partial f_i}{\partial x_j \partial x_k} \right|. \quad (\text{F13})$$

Lemma F.3. *Consider a local sparse (r_Γ, c_Γ) -Pauli channel on an n -qubit qLDPC code under Assumption 1. Then $\|J_H\|_\infty = \mathcal{O}(1)$ and $\|J_{G_B}^2\|_\infty = \mathcal{O}(1)$ for any extra constraints $B\vec{p} = 0$.*

Proof. For a local sparse (r_Γ, c_Γ) -Pauli channel on an LDPC code, the size of the syndrome class $C \in \mathcal{C}^*$ is bounded by a constant $|C|_{\max}$. For each syndrome class C , the collection of all errors in the involved channels $\Gamma_C = \{\gamma | \mathcal{E}_\gamma \cap C \neq \emptyset\}$, denoted by \mathcal{E}_{Γ_C} , is also of constant size. Due to Assumption 1, we assume the total error rate of each channel $\sum_{e \in \mathcal{E}_\gamma} p_e < \frac{1}{2}$, we have each local Pauli eigenvalue lower bounded by a positive constant λ_{\min} : $\lambda_e = 1 - 2 \sum_{e' \in \mathcal{E}_\gamma, [[e, e']] = -1} p_{e'} \geq \lambda_{\min} > 0$ for all local channel $\gamma \in \Gamma$ and $e \in \mathcal{E}_\gamma$.

For a syndrome class $C_i \in \mathcal{C}$, we first look at each term $\log \mu_e$ of the component of the function $H_i = \log \nu_{C_i} = \sum_{e \in C_i} \log \mu_e$. Note that for any error $e \in C_i$ with its individual channel \mathcal{N}_{γ_e} ,

$$\log \mu_e = \frac{2}{4^{|\gamma_e|}} \sum_{e' \in \mathcal{E}_{\gamma_e}} [[e', e]] \log \lambda_{e'} \quad (\text{F14})$$

and

$$\left| \frac{\partial \log \mu_e}{\partial p_i^*} \right| \leq \sum_{e' | e' \text{ anticommute } e_i} \frac{4}{4^{\gamma_e}} \lambda_{e'}^{-1} \leq \frac{4}{\lambda_{\min}}. \quad (\text{F15})$$

Therefore for each component H_i , we have

$$\left| \frac{\partial H_i}{\partial p_j^*} \right| = \sum_{e \in C_i} \left| \frac{\partial \log \mu_e}{\partial p_j^*} \right| \leq \frac{4|C|_{\max}}{\lambda_{\min}} \quad (\text{F16})$$

So we have an upper bound for the Jacobian

$$\|J_H\|_\infty \leq \sum_{e \in \mathcal{E}_{\Gamma_C}} \frac{4|C|_{\max}}{\lambda_{\min}} = \mathcal{O}(1). \quad (\text{F17})$$

For the second-order derivative

$$\left| \frac{\partial \log \mu_e}{\partial p_i^* \partial p_j^*} \right| \leq \sum_{e' | e' \text{ anticommute } e_i, e_j} \frac{8}{4^{\gamma_e}} \lambda_{e'}^{-2} \leq \frac{8}{\lambda_{\min}^2}. \quad (\text{F18})$$

Similarly,

$$\|J_H^2\|_\infty \leq \sum_{e, e' \in \mathcal{E}_{\Gamma_C}} \frac{8|C|_{\max}}{\lambda_{\min}^2} = \mathcal{O}(1). \quad (\text{F19})$$

To upperbound $\|J_{G_B}^2\|_\infty$, we use the chain rule:

$$\|J_{G_B}(\vec{x}) - J_{G_B}(\vec{y})\|_\infty = \|(J_H(K_B \vec{x}) - J_H(K_B \vec{y})) K_B\|_\infty \quad (\text{F20})$$

$$\leq \|J_H^2\|_\infty \|K_B\|_\infty \|\vec{x} - \vec{y}\|_\infty \|K_B\|_\infty \quad (\text{F21})$$

$$= \|J_H^2\|_\infty \|K_B\|_\infty^2 \|\vec{x} - \vec{y}\|_\infty \quad (\text{F22})$$

$$\leq \|J_H^2\|_\infty \|\vec{x} - \vec{y}\|_\infty \quad (\text{F23})$$

where we used the fact that $\|K_B\|_\infty \leq 1$, since each row of K_B has a single non-zero element less than 1 (Eq. (F10)). Therefore, we have $\|J_{G_B}^2\|_\infty \leq \|J_H^2\|_\infty = \mathcal{O}(1)$. \square

Lemma F.4 (Existence of physical error under B constraints). *Consider a local sparse Pauli channel $\mathcal{N}_\Gamma = \circ_{\gamma \in \Gamma} \mathcal{N}_\gamma$, which acts on a qLDPC stabilizer/subsystem code with measured stabilizer subgroup \mathcal{M} . There exists a constant $0 < p_{\max} \leq \frac{1}{4^{r_\Gamma}}$ such that if the true error rates \vec{p} in \mathcal{N}_Γ satisfy $\|\vec{p}^*\|_\infty < p_{\max}$, where \vec{p}^* denotes the detectable error rates, then there exists a solution for \vec{p}^* of the system of equations that consists of Eq. (25):*

$$\log \vec{\Lambda}^{(\mathcal{M})} = D'^{(\mathcal{M})} \log \vec{\nu}, \quad (\text{F24})$$

and any set of extra constraints Eq. (29):

$$B\vec{p} = \vec{0}. \quad (\text{F25})$$

Proof. According to Theorem 3, we have the Taylor expansion $G_B(\vec{x}) = -2\vec{x} + \mathcal{O}(\|\vec{p}\|^2)$. Therefore at $\vec{x}_0 = \vec{0}$, the Jacobian $J_{G_B}(\vec{x}_0) = -2I$ is invertible and

$$\delta_{G_B} = \frac{1}{\|J_{G_B}(\vec{x}_0)^{-1}\|_\infty} = 2. \quad (\text{F26})$$

Since the size of each syndrome class is bounded by a constant in the qLDPC code and local sparse Pauli channel setting, there is a constant P_{\max}^C for the syndrome class error rates, i.e., we consider $\|\vec{x}\|_\infty \leq P_{\max}^C$ for the function $G_B(\vec{x})$.

We define an upperbound K_{G_B} of the norm of the second-order derivative of G_B as

$$K_{G_B} = \max \left(\max_{\vec{x} \in \mathcal{B}_{P_{\max}^C}(\vec{0})} \|J_{G_B}^2(\vec{x})\|_\infty, \frac{\delta_{G_B}}{P_{\max}^C} \right). \quad (\text{F27})$$

Let $R_p = \frac{1}{4^{r_\Gamma}}$, we define an upperbound L_H of the norm of the Jacobian of H as:

$$L_H = \max \left(\max_{\vec{x} \in \mathcal{B}_{R_p}(\vec{0})} \|J_H(\vec{x})\|_\infty, \frac{\delta_{G_B}^2}{2K_{G_B}R_p} \right). \quad (\text{F28})$$

Both K_{G_B} and L_H is $\mathcal{O}(1)$ according to Lemma F.3. Therefore, we have,

$$\|J_{G_B}(\vec{x}) - J_{G_B}(\vec{0})\|_\infty \leq K_{G_B} \|\vec{x}\|_\infty, \quad \forall \vec{x} \in \mathcal{B}_{P_{\max}^C}(\vec{0}) \quad (\text{F29})$$

and $P_{\max}^C \geq \frac{\delta_{G_B}}{K_{G_B}}$ according to Eq. (F27). As a result, $G_B(\vec{x}) = \vec{y}$ has unique solution when $\vec{y} \in \mathcal{B}_{r_y}(\vec{0})$ where the radius $r_y = \frac{\delta_{G_B}^2}{2K_{G_B}} = \frac{2}{K_{G_B}}$ according to Lemma F.2. To show the radius for \vec{p}^* around $\vec{0}$ such that $\vec{y} = H(\vec{p}^*) \in \mathcal{B}_{r_y}(\vec{0})$, note that we have

$$\|J_H(\vec{p}^*)\| \leq L_H, \quad \forall \vec{p}^* \in \mathcal{B}_{R_p}(\vec{0}). \quad (\text{F30})$$

Let $p_{\max} = \frac{r_y}{L_H} = \frac{2}{K_{G_B}L_H}$ then $p_{\max} \leq R_p = \frac{1}{4^{r_\Gamma}}$ according to Eq. (F28). $\|\vec{y}\|_\infty = \|H(\vec{p}^*)\|_\infty \leq \|J_H(\vec{p}^*)\|_\infty \|\vec{p}^*\|_\infty \leq L_H \|\vec{p}^*\|_\infty$ will be within radius r_y around $\vec{0}$ if $\|\vec{p}^*\|_\infty < p_{\max}$, thus a solution exists. \square

APPENDIX G: Spacetime code

We can map a non-adaptive Clifford circuit into a spacetime code [13–15], which we introduce briefly in this section. We also note that the spacetime code is highly related to the detector error model that is being widely used in the field of fault tolerance [17, 33]. In particular, the measurement result of the generators of the measured stabilizer group in the spacetime code corresponds to the detectors in the detector error model. Here, we used the spacetime code formalism since the learning protocol in the static code case can be carried out here directly. For simplicity, we omit the superscript ^(ST) here for operators in the spacetime code.

Given a circuit with n qubits and T time steps, the spacetime code constructed from the Clifford circuit is a subsystem stabilizer code of $n(T+1)$ qubits, where we put layers of n qubits in between every pair of neighboring circuit layers, as well as a layer before and a layer after the circuit. We assign a temporal label $t = 0.5, 1.5, \dots, T+0.5$ for each layer of spacetime qubits. We borrow the notation (change from η to κ) in [13, 15] and denote $\kappa_{t-0.5}(O) \in \mathcal{P}_{n(T+1)}$ as the Pauli operator in the spacetime code by placing Pauli $P \in \mathcal{P}_n$ at t th layer of the spacetime code tensor product

with $I_n \in \mathcal{P}_n$ on all other layers. For any spacetime operator $O \in \mathcal{P}_{n(T+1)}$, $O_{t-0.5} \in \mathcal{P}_n$ denotes the component of O at the t th layer of the spacetime code. Moreover, let $t \in [T]$, $t \leq t' \leq T+1$, and we denote the unitary gate at layer t as U_t , the product of gates from layer t to $t' - 1$ as $U_{t,t'}$, and let $U_{t,t'} = I$ if $t' \leq t$.

The goal of the construction is that circuit-level Pauli errors can be considered as errors acting on these spacetime qubits such that both the syndrome and logical effect of the error can be captured in the static spacetime code. As a subsystem code, the structure of the conventional spacetime code is typically defined via the gauge group \mathcal{G} of the spacetime code [13, 14]. It is defined as the set of Pauli errors in the spacetime code for which the corresponding errors in the circuit do not trigger any detection events and are logically trivial. In the conventional case, when one wants to preserve all logical operators of the input state stabilizer code, or simply the input code, \mathcal{G} can be constructed by adding the following Pauli operators as generators:

1. At the input layer, include the input code stabilizer generators as $\kappa_{0.5}(S_i^{(\text{ini})})$ in $\mathcal{G}^{(\text{ST})}$.
2. For each measurement $M^{(\text{circ})}$ in the circuit at layer $t = t(M^{(\text{circ})})$, include $\kappa_{t+0.5}(M^{(\text{circ})})$.
3. For each layer $t = 1, \dots, T$, add $\kappa_{t-0.5}(P_i)\kappa_{t+0.5}(U_{t,t+1}P_iU_{t,t+1}^\dagger)$, where P_i runs over a generating set of $N(\mathcal{M}_t^{(\text{circ})})$, i.e., the normalizer of the group of the measured operator \mathcal{M}_t at layer t . For example, if there is no measurement at layer t , then we let P_i be $X_1, Z_1, \dots, X_n, Z_n$, and if there is a Y_2Z_3 measurement at layer t , P_i runs over $\{X_1, Z_1, Y_2, Z_3, X_2X_3, X_4, Z_4, \dots, Z_n\}$.

As in Section V of the main text, we are only interested in the logical errors affecting the circuit's logical measurement. This motivates us to extend the gauge group introduced above. We will first construct the measured stabilizer group \mathcal{M} and the measured logical group \mathcal{L}' (Eq. (G7)) using the output of Algorithm 2. Then concretely, the extended gauge group can be obtained by replacing operators in step 1 with operators of the form $\kappa_{0.5}(O)$ where O goes over a generating set of $N(\mathcal{L}'^{(\text{ini})})$. Here we define $\mathcal{L}'^{(\text{ini})} = \{L'_{0.5} \mid L' \in \mathcal{L}'\}$ as the subgroup of the logical group of the input code associated with the logical measurement of the circuit.

We now introduce Algorithm 2 below. The algorithm keeps track of the stabilizer group, destabilizer group, and the logical group at each layer and records the relevant measurement indices whenever a stabilizer or logical operator is measured. These records, in the form of two matrices \mathcal{O}^\perp and \mathcal{K}^L are then used to construct the measured stabilizer and logical group of the spacetime code. The stabilizer group \mathcal{S} of the spacetime code is the center of the conventional gauge group \mathcal{G} , but in general, not all elements in \mathcal{S} are measured, and the measured stabilizer group \mathcal{M} is a subgroup of \mathcal{S} . Similarly, for a Clifford circuit, the logical measurements only correspond to a subset of the initial logical operators, and therefore, the measured logical operators in the spacetime code are only a subset of the normalizer of the conventional gauge group. We use the following notation in the algorithm below: For a binary vector $\vec{a} \in \mathbb{Z}_2^m$, we use the notation $S^{\vec{a}} = [S^{a_1}, S^{a_2}, \dots, S^{a_m}]$, and $\mathcal{S} \leftarrow \mathcal{S} \odot S'^{\vec{a}}$ represents the process of replacing the list of operators $\mathcal{S} = [S_1, \dots, S_m]$ by $\mathcal{S} \odot S'^{\vec{a}} = [S_1 S'^{a_1}, S_2 S'^{a_2}, \dots, S_m S'^{a_m}]$.

Algorithm 2: Measured stabilizer generators and logical generators for the spacetime code

Input:

1. The Clifford circuit with m measurements $\{M_1^{(\text{circ})}, \dots, M_m^{(\text{circ})}\}$ with input state encoded in a $[[n,k]]$ stabilizer code.
2. Initial stabilizer: $\mathcal{S} = [S_1^{(\text{ini})}, \dots, S_s^{(\text{ini})}]$ and initial destabilizer: $\mathcal{D} = [D_1^{(\text{ini})}, \dots, D_s^{(\text{ini})}]$.
3. Initial X logical operators: $\overline{\mathcal{X}} = [\overline{X}_1^{(\text{ini})}, \dots, \overline{X}_k^{(\text{ini})}]$ and initial Z logical operators: $\overline{\mathcal{Z}} = [\overline{Z}_1^{(\text{ini})}, \dots, \overline{Z}_k^{(\text{ini})}]$.

Output:

1. \mathcal{O}^\perp , parity checks of the output bitstrings.
2. \mathcal{K}^L , sets of operator indices of measured logical operators.

```

1 Initialize  $\vec{c}_s, \vec{c}_d \in \mathbb{Z}_2^s, \vec{c}_{\overline{x}}, \vec{c}_{\overline{z}} \in \mathbb{Z}_2^k$ . Let  $\{\vec{e}_i\}_i^{s+m}$  be the set of unit vectors in  $\mathbb{Z}_2^{s+m}$ .
2 Initialize two sets  $\mathcal{O}^\perp = \{\}$  and  $\mathcal{K}^L = \{\}$ .
3 for  $i = 1, \dots, s$  do
4   Initialize  $\vec{v}_s^{(i)} = \vec{e}_i \in \mathbb{Z}_2^{s+m}$ .
5 for  $i = 1, \dots, k$  do
6   Initialize  $\vec{v}_{\overline{x}}^{(i)} = \vec{v}_{\overline{z}}^{(i)} = \vec{0} \in \mathbb{Z}_2^{s+m}$ .
7 for  $r = 1, \dots, m$  do
8   Propagate  $M_r^{(\text{circ})}$  to the beginning of the circuit as  $M_*$ .
9   Let  $\vec{c}_s = (\langle M_*, \mathcal{D}[i] \rangle)_{i=1}^s, \vec{c}_d = (\langle M_*, \mathcal{S}[i] \rangle)_{i=1}^s, \vec{c}_{\overline{x}} = (\langle M_*, \overline{\mathcal{Z}}[i] \rangle)_{i=1}^k, \vec{c}_{\overline{z}} = (\langle M_*, \overline{\mathcal{X}}[i] \rangle)_{i=1}^k$ .
10  if  $\vec{c}_d \neq \vec{0}$  (destabilizer measurement) then
11    Let  $i^* := \min\{i \in [s] : (c_d)_i = 1\}$  and  $D_* = S_{i^*}$ .
12    Update tableau  $\mathcal{S} \leftarrow \mathcal{S} \odot D_*^{\vec{c}_d}, \mathcal{D} \leftarrow \mathcal{D} \odot D_*^{\vec{c}_s}, \overline{\mathcal{X}} \leftarrow \overline{\mathcal{X}} \odot D_*^{\vec{c}_{\overline{x}}}, \overline{\mathcal{Z}} \leftarrow \overline{\mathcal{Z}} \odot D_*^{\vec{c}_{\overline{z}}}$ .
13    For all  $i = 1, \dots, s, j = 1, \dots, k$ , update operation vectors  $\vec{v}_s^{(i)} += (c_d)_i \cdot \vec{v}_s^{(i^*)}, \vec{v}_{\overline{x}}^{(j)} += (c_{\overline{z}})_j \cdot \vec{v}_s^{(i^*)}, \vec{v}_{\overline{z}}^{(j)} += (c_{\overline{x}})_j \cdot \vec{v}_s^{(i^*)}$ .
14    Delete the  $i^*$ th element of  $\mathcal{S}$  and  $\mathcal{D}$ , append  $M_*, D_*$  to  $\mathcal{S}$  and  $\mathcal{D}$  respectively.
15    Update  $\vec{v}_s^{(i)} \leftarrow \vec{v}_s^{(i+1)}$  for  $i = i^*, \dots, s-1$ . Let  $\vec{v}_s^{(s)} = \vec{e}_{s+r}$ .
16  if  $\vec{c}_d = \vec{0}$  and  $\vec{c}_{\overline{x}} \neq \vec{0}$  (or  $\overline{\mathcal{X}} \leftrightarrow \overline{\mathcal{Z}}$  if  $\vec{c}_{\overline{x}} = \vec{0}$  and  $\vec{c}_{\overline{z}} \neq \vec{0}$ ) (logical measurement) then
17    Let  $i^* := \min\{i \in [k] : (c_{\overline{x}})_i = 1\}$  and  $D_* = \overline{Z}_{i^*}$ .
18    Update tableau  $\mathcal{D} \leftarrow \mathcal{D} \odot D_*^{\vec{c}_s}, \overline{\mathcal{X}} \leftarrow \overline{\mathcal{X}} \odot D_*^{\vec{c}_{\overline{x}}}, \overline{\mathcal{Z}} \leftarrow \overline{\mathcal{Z}} \odot D_*^{\vec{c}_{\overline{z}}}$ .
19    For all  $j = 1, \dots, k$ , update operation vectors  $\vec{v}_{\overline{x}}^{(j)} += (c_{\overline{z}})_j \cdot \vec{v}_{\overline{x}}^{(i^*)}, \vec{v}_{\overline{z}}^{(j)} += (c_{\overline{x}})_j \cdot \vec{v}_{\overline{x}}^{(i^*)}$ .
20    Delete the  $i^*$ th element of  $\overline{\mathcal{X}}$  and  $\overline{\mathcal{Z}}$ , append  $M_*, D_*$  to  $\mathcal{S}$  and  $\mathcal{D}$  respectively.
21    Append  $\vec{u}^L = \vec{e}_{s+r} + \sum_i^s (c_s)_i \vec{v}_s^{(i)} + \sum_i^k [(c_{\overline{x}})_i \vec{v}_{\overline{x}}^{(i)} + (c_{\overline{z}})_i \vec{v}_{\overline{z}}^{(i)}]$  to  $\mathcal{K}^L$ .
22    Update  $\vec{v}_{\overline{x}}^{(i)} \leftarrow \vec{v}_{\overline{x}}^{(i+1)}, \vec{v}_{\overline{z}}^{(i)} \leftarrow \vec{v}_{\overline{z}}^{(i+1)}$  for  $i = i^*, \dots, k-1$ . Let  $\vec{v}_s^{(s)} = \vec{e}_{s+r}$ .
23     $s \leftarrow s+1, k \leftarrow k-1$ .
24  if  $\vec{c}_d = \vec{c}_{\overline{x}} = \vec{c}_{\overline{z}} = \vec{0}$  (stabilizer measurement) then
25    Let  $i^* := \min\{i \in [s] : (c_s)_i = 1\}$  and  $D_* = D_{i^*}$ .
26    Update tableau  $\mathcal{D} \leftarrow \mathcal{D} \odot D_*^{\vec{c}_s}$ .
27    Delete the  $i^*$ th element of  $\mathcal{S}$  and  $\mathcal{D}$ , append  $M', D_*$  to  $\mathcal{S}$  and  $\mathcal{D}$  respectively.
28    Append  $\vec{u} = \vec{e}_{s+r} + \sum_i^s (c_s)_i \vec{v}_s^{(i)}$  to  $\mathcal{O}^\perp$ .
29    Update  $\vec{v}_s^{(i)} \leftarrow \vec{v}_s^{(i+1)}$  for  $i = i^*, \dots, s-1$ . Let  $\vec{v}_s^{(s)} = \vec{e}_{s+r}$ .
30 return  $\mathcal{O}^\perp, \mathcal{K}^L$ 

```

Algorithm 2 is an extended version of Algorithm 1 in Ref. [15], as we also included the necessary information to construct the spacetime logical operators. Moreover, this also improves the classical computation cost from $O(n^3)$ to $O(n^2)$ by keeping track of destabilizers and calculating commutation instead of doing Gaussian elimination.

A key operation on spacetime Pauli operators is called (back-)cumulant [15] (spackle [13]), which is used to construct spacetime stabilizer and logical generators. The cumulant and back-cumulant of a spacetime operator F denoted by

\vec{F} and \overleftarrow{F} are defined by

$$(\vec{F})_{l-0.5} = \prod_{l'=1}^{l'<l} U_{l',l} F_{l'-0.5} U_{l',l}^\dagger, \quad (\text{G1})$$

$$(\overleftarrow{F})_{l-0.5} = \prod_{l'=T+1}^{l'>l} U_{l,l'}^\dagger F_{l'-0.5} U_{l,l'}. \quad (\text{G2})$$

Consider a Clifford circuit with initial stabilizer generators $\mathcal{S} = \{S_1^{(\text{ini})}, \dots, S_s^{(\text{ini})}\}$, destabilizer: $\mathcal{D} = \{D_1^{(\text{ini})}, \dots, D_s^{(\text{ini})}\}$, X logical operators: $\overline{\mathcal{X}} = \{\overline{X}_1^{(\text{ini})}, \dots, \overline{X}_k^{(\text{ini})}\}$ and Z logical operators: $\overline{\mathcal{Z}} = \{\overline{Z}_1^{(\text{ini})}, \dots, \overline{Z}_k^{(\text{ini})}\}$. We define a tuple of operators of the circuit with length $s+m$:

$$\vec{E} = (S_1^{(\text{ini})}, \dots, S_s^{(\text{ini})}, M_1^{(\text{circ})}, \dots, M_m^{(\text{circ})}) \quad (\text{G3})$$

and define the i th operator in \vec{E} as E_i . We denote t_j as the temporal index of operator E_j in the circuit, and for initial stabilizer and logical operators, $t_j = 0$. The measured spacetime stabilizer generators $M \in \mathcal{M}$ are given by

$$M(\vec{u}) = \overleftarrow{\prod_{j=s+1}^{s+m} \kappa_{t_j-0.5}(E_j^{u_j})}, \forall \vec{u} \in \mathcal{O}^\perp. \quad (\text{G4})$$

The measured spacetime logical generators $L' \in \mathcal{L}'$ are

$$L'(\vec{u}^L) = \overleftarrow{\prod_{j=s+1}^{s+m} \kappa_{t_j-0.5}(E_j^{u_j})}, \forall \vec{u}^L \in \mathcal{K}^L. \quad (\text{G5})$$

There can also be unmeasured logical operators in the spacetime code. Given any initial logical operator $L^{(\text{ini})}$ that has not been measured, we have the corresponding spacetime logical operator $L = \overrightarrow{\kappa_{0.5}(L^{(\text{ini})})}$.

The measured stabilizer group of the spacetime code is given by

$$\mathcal{M} = \langle M(\vec{u}) \rangle_{\vec{u} \in \mathcal{O}^\perp}. \quad (\text{G6})$$

The measured logical operators $\mathcal{L}'^{(\text{ST})}$ is the group generated by all the measured stabilizer generators and the relevant spacetime logical generators $\{L'_1, \dots, L'_{m_L}\}$ in Eq. (G5):

$$\mathcal{L}' = \langle M_1, \dots, L'_1, \dots, L'_{m_L} \rangle. \quad (\text{G7})$$

Below is a summary of the structure of the spacetime code in our work. Given a set of logical operators measured in the circuit, we map them to a generating set of measured spacetime logical operators according to Algorithm 2 and Eq. (G5). These operators generate the abelian subgroup of measured spacetime logical operators \mathcal{L}' according to Eq. (G7). The linear constraints ('detectors') $\vec{u} \in \mathcal{O}^\perp$ of the measurements in the ideal circuits are mapped to the measured spacetime stabilizer group \mathcal{M} . The group of dressed logical operators \mathcal{L}'_{dr} contains all the undetectable operators. It is defined as the normalizer of the measured spacetime stabilizer $\mathcal{L}'_{\text{dr}} = N(\mathcal{M})$. The gauge group \mathcal{G}' for \mathcal{L}' corresponds to the set of errors in the circuit that are undetectable, but also logically trivial with respect to the logical measurements. It is defined as $\mathcal{G}' = N(\mathcal{L}')$, i.e., it consists of operators in the spacetime code that commute with the measured logical group \mathcal{L}' , which encompasses the measured stabilizer group \mathcal{M} . See diagram in Fig. 14.

We note the two distinct roles/perspectives of Pauli operators here. Pauli operators, on the one hand, are Hermitian operators that can encode the information about the state, e.g., stabilizers of a state or Pauli measurement of a state. On the other hand, it is a unitary operator that acts on the state as an operation/error. The (bare) logical group \mathcal{L}' is the first case where it encodes the logical information being measured, whereas the dressed logical group \mathcal{L}'_{dr} , or more precisely the quotient group $\mathcal{L}'_{\text{dr}}/\mathcal{G}'$, can be interpreted as the logical operation/error on the logical states. Although the construction of measured spacetime logical operators \mathcal{L}' is not necessary in the physical error rate learning algorithm, \mathcal{L}' is needed in the proof of logical error learnability in Theorem 10 in Section H.

We prove below the equivalent condition of error detectability and logical errors on logical measurements in the circuit, in terms of the commutation relation between errors and measured stabilizer/logical operators in the spacetime code.

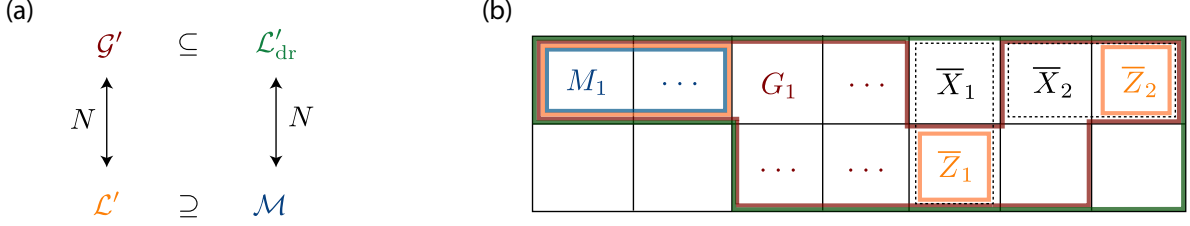


FIG. 14: (a) Four subgroups of the spacetime subsystem codes and their relation with the diagram in [12]. \mathcal{M} is the measured spacetime stabilizer group, which is contained in the measured spacetime logical subgroup \mathcal{L}' . $\mathcal{L}'_{\text{dr}} = N(\mathcal{M})$ is the dressed logical subgroup, which contains the gauge group $\mathcal{G}' = N(\mathcal{L}')$. N here denotes the normalizer in the Pauli group, and we have $A = N(B) \iff B = N(A)$ for any two Pauli subgroups A, B . (b) Example of the commutation between generators of different subgroups in (a) and the inclusion relation of these subgroups (colored boundaries). Each box represents a Pauli operator, and each column represents a pair of anticommuting operators, while operators in the same row commute. Here we consider an n -qubit spacetime code of a circuit with two logical qubits, and we measure \bar{Z}_1 at an odd time step while measuring \bar{Z}_2 at an even time step. The resulting spacetime logical Pauli \bar{X}_2 and \bar{Z}_2 for the second logical qubit commute. However, we can still define distance as $d^{(\mathcal{L}')} = \min_{e \in \mathcal{L}'_{\text{dr}} \setminus \mathcal{G}'} \text{weight}(e)$, and the inclusion relation in (a) still holds.

Lemma G.1 (Delfosse and Paetznick [15] Adjoint of the accumulator). *For any pair of spacetime operators $A, B \in \mathcal{P}_{n(T+1)}$, we have*

$$\langle \vec{A}, B \rangle = \langle A, \vec{B} \rangle. \quad (\text{G8})$$

Lemma G.2 (Delfosse and Paetznick [15] Effect of faults). *Given an Clifford circuit with m measurements $\{M_1^{(\text{circ})}, \dots, M_m^{(\text{circ})}\}$ and circuit-level Pauli error $e \in \mathcal{P}_{n(T+1)}$ in the spacetime code, define the output measurement bitstrings in the circuit as $\vec{o}^{(\text{circ})} \in \mathbb{Z}_2^m$ and its probability distribution with and without error e as $\mathbb{P}^{(e)}(\vec{o}^{(\text{circ})})$ and $\mathbb{P}(\vec{o}^{(\text{circ})})$ respectively, we have*

$$\mathbb{P}^{(e)}(\vec{o}^{(\text{circ})}) = \mathbb{P}(\vec{o}^{(\text{circ})} + \vec{f}^{(\text{circ})}(e)), \quad (\text{G9})$$

where $\vec{f}^{(\text{circ})}(e) = (f^{(\text{circ})}(e)_1, \dots, f^{(\text{circ})}(e)_m) \in \mathbb{Z}_2^m$, $f^{(\text{circ})}(e)_j = \langle \vec{e}_{t(M_j^{(\text{circ})})-0.5}, M_j^{(\text{circ})} \rangle$, and we denote $t(M_j^{(\text{circ})})$ as the temporal label when $M_j^{(\text{circ})}$ occurs in the circuit.

Let the initial stabilizer generator values be $\vec{o}^{(\text{ini})} = (o_1^{(\text{ini})}, \dots, o_s^{(\text{ini})})$ and let the measurement outcome of the m measurements $\{M_1^{(\text{circ})}, \dots, M_m^{(\text{circ})}\}$ be $\vec{o}^{(\text{circ})} = (o_1^{(\text{circ})}, \dots, o_m^{(\text{circ})})$. For a parity check $\vec{u} \in \mathcal{O}^\perp$, let $\vec{u}^{(\text{ini})} = (u_1, \dots, u_s)$, and $\vec{u}^{(\text{circ})} = (u_{s+1}, \dots, u_{s+m})$. Similarly, for $\vec{u}^L \in \mathcal{K}^L$, let $\vec{u}^{L(\text{circ})} = (u_{s+1}^L, \dots, u_{s+m}^L)$.

Lemma G.3 (Equivalence of syndrome in circuit and spacetime code). *For any circuit-level Pauli error corresponding to $e \in \mathcal{P}_{n(T+1)}$ in the spacetime code in a Clifford circuit, its syndrome bitstring $\vec{s}(e)$ corresponding to the parity check \mathcal{O}^\perp of the outcome measurements in the circuit is equal to the scalar commutator with the measured stabilizer generators in the spacetime code ($\langle e, M(\vec{u}) \rangle_{\vec{u} \in \mathcal{O}^\perp}$).*

Proof. The syndrome bitstring, by construction, is deterministically $\vec{0}$ for an noiseless circuit, i.e. $\mathbb{P}(\vec{o}) \neq 0$ if and only if $\vec{o} \in \ker \mathcal{O}^\perp$. With error e , according to Lemma G.2, $\mathbb{P}^{(e)}(\vec{o}^{(\text{circ})}) = \mathbb{P}(\vec{o}^{(\text{circ})} + \vec{f}^{(\text{circ})}(e))$. Equivalently, we have

$$\mathbb{P}^{(e)}(\vec{o}) = \mathbb{P}(\vec{o} + \vec{f}(e)), \quad (\text{G10})$$

where $\vec{f}(e)$ is obtained by prepending $\vec{f}^{(\text{circ})}(e)$ with $\vec{0} \in \mathbb{Z}_2^s$. Therefore, \vec{o} must satisfy $\vec{o} + \vec{f}(e) \in \ker \mathcal{O}^\perp$, which

means $\vec{s}(e) = (\vec{u} \cdot \vec{o})_{\vec{u} \in \mathcal{O}^\perp} = (\vec{u} \cdot \vec{f}(e))_{\vec{u} \in \mathcal{O}^\perp}$. For every $\vec{u} \in \mathcal{O}^\perp$, we also have

$$\vec{u} \cdot \vec{f}(e) = \vec{u}^{(\text{circ})} \cdot \vec{f}^{(\text{circ})}(e) \quad (\text{G11})$$

$$= \sum_{i=1}^m u_i^{(\text{circ})} \left\langle \vec{e}_{t(M_i^{(\text{circ})})-0.5}, M_i^{(\text{circ})} \right\rangle \text{ (from Lemma G.2)} \quad (\text{G12})$$

$$= \sum_{i=s}^{s+m} \left\langle \vec{e}_{t_i-0.5}, E_i^{u_i} \right\rangle \quad (\text{G13})$$

$$= \left\langle \vec{e}, \prod_{i=s}^{s+m} \kappa_{t_i-0.5}(E_i^{u_i}) \right\rangle \quad (\text{G14})$$

$$= \left\langle e, \overbrace{\prod_{i=s}^{s+m} \kappa_{t_i-0.5}(E_i^{u_i})}^{\text{from Lemma G.1}} \right\rangle \quad (\text{G15})$$

$$= \langle e, M(\vec{u}) \rangle. \quad (\text{G16})$$

□

Lemma G.4 (Equivalence of logical error in the spacetime code). *Denote as $\vec{o}_L \in \mathbb{Z}_2^{m_L}$ the logical measurement results after syndrome measurement and correction in a Clifford circuit with some input codeword. Consider any undetectable circuit-level Pauli error corresponding to $e \in \mathcal{P}_{n(T+1)}$ in the spacetime code due to the circuit error and subsequent correction from some decoder. We have the logical outcome distribution*

$$\mathbb{P}_L^{(e)}(\vec{o}_L) = \mathbb{P}_L(\vec{o}_L + \vec{f}_L(e)), \quad (\text{G17})$$

where \mathbb{P}_L is the ideal logical outcome distribution and we refer to $\vec{f}_L(e) \in \mathbb{Z}_2^{m_L}$ as the logical error on the logical measurements. Moreover, $\vec{f}_L(e)$ is equal to the binary commutation of e with the measured logical operators $\vec{f}_L(e) = \langle e, L'(\vec{u}^L) \rangle_{\vec{u}^L \in \mathcal{K}^L}$.

Proof. Given the corrected circuit outcome \vec{o} , the logical measurement result is $\vec{o}_L = (\vec{u}^L \cdot \vec{o})_{\vec{u}^L \in \mathcal{K}^L}$. If the circuit has m_L independent logical measurements, then \mathcal{K}^L has full row rank with $\text{rank } \mathcal{K}^L = m_L$. Therefore, the logical output distribution is

$$\mathbb{P}_L^{(e)}(\vec{o}_L) = \sum_{\vec{o}' \in \ker \mathcal{K}^L} \mathbb{P}^{(e)}((\mathcal{K}^L)^+ \vec{o}_L + \vec{o}') \quad (\text{G18})$$

$$= \sum_{\vec{o}' \in \ker \mathcal{K}^L} \mathbb{P}\left((\mathcal{K}^L)^+ \vec{o}_L + \vec{o}' + \vec{f}(e)\right) \quad (\text{from Eq. (G10)}) \quad (\text{G19})$$

$$= \sum_{\vec{o}' \in \ker \mathcal{K}^L} \mathbb{P}\left((\mathcal{K}^L)^+ (\vec{o}_L + \mathcal{K}^L \vec{f}(e)) + \vec{o}'\right) \quad (\text{G20})$$

$$= \mathbb{P}_L(\vec{o}_L + \vec{f}_L(e)) \quad (\text{G21})$$

where $(\mathcal{K}^L)^+$ is any right inverse of \mathcal{K}^L , i.e., $\mathcal{K}^L (\mathcal{K}^L)^+ = I_{m_L}$ and the logical error $\vec{f}_L(e) = \mathcal{K}^L \vec{f}(e)$. Similar to the derivation of Eq. (G16), we have $\vec{u}^L \cdot \vec{f}(e) = \langle e, L'(\vec{u}^L) \rangle$, $\forall \vec{u}^L \in \mathcal{K}^L$. □

Corollary G.5 (Correctness condition for spacetime code). *For any circuit-level Pauli error corresponding to $e \in \mathcal{P}_{n(T+1)}$ in the spacetime code, e is undetectable from the circuit measurements if and only if e commutes with all elements $M \in \mathcal{M}$ in the measured spacetime stabilizer group. An undetectable error e (from decoding and correction) does not affect the distribution of logical measurement results for any input codeword, if and only if e commutes with all elements in the measured spacetime logical group \mathcal{L}' .*

APPENDIX H: Logical error rate learnability

In this section, we prove Theorem 10 in the main text regarding the learnability of logical error rate for a group of logical measurements in the non-adaptive Clifford circuit from syndrome data. Using the transformed eigenvalue basis introduced in the Section B together with the spacetime code formalism introduced in Section G, we give a

simpler proof with both sufficient and necessary conditions of the logical error class probability learnability results in the context of fault-tolerant circuits with logical measurements, compared to the proof of Ref. Wagner *et al.* [12] for sufficient condition in the code capacity setting. We note that with a circuit decoder, the learnability of the logical class error rate implies the learnability of the logical error rate. We omit the superscript ^(ST) for operators in the spacetime codes.

Theorem 10 (Restated). Given a non-adaptive Clifford circuit with a set of logical measurements \mathcal{M}_L under a circuit-level Pauli noise model (satisfies Assumption 1 when mapped to noise model on spacetime code), the logical error class probabilities \bar{P} for \mathcal{M}_L can be learned from the syndrome expectation value of the circuit if and only if the circuit is fault-tolerant (Definition 9) to the noise model for \mathcal{M}_L . As a consequence, given a decoder of the circuit, the associated logical error rates P_{fail} for the set of logical measurements \mathcal{M}_L can be learned from the syndrome data if the circuit is fault-tolerant to the noise model for \mathcal{M}_L .

Proof. We map linear constraints of the measurement in the circuits to the measured spacetime stabilizer group \mathcal{M} and map measured logical operators in the circuit to the group of spacetime logical operators \mathcal{L}' . The gauge group \mathcal{G}' is given by $\mathcal{G}' = N(\mathcal{L}')$. We denote as $P_L(e)$ the logical error class probability for the error $e \in \mathcal{P}_{n(T+1)}$ of the spacetime code for \mathcal{L}' as

$$P_L(e) = \bar{P}(\vec{s}(e), \vec{\ell}(e)) \quad (\text{H1})$$

$$= \sum_{g \in \mathcal{G}'} P(eg) \quad (\text{H2})$$

$$= \sum_{e' \in \mathcal{P}_n} P(e') \mathbb{I}_{\mathcal{G}'}(ee') \quad (\text{H3})$$

$$= P * \mathbb{I}_{\mathcal{G}'}(e) \quad (\text{H4})$$

where $\mathbb{I}_{\mathcal{H}}$ is the indicator function of the group \mathcal{H} , taking $\mathbb{I}_{\mathcal{H}}(e) = 1$ if $e \in \mathcal{H}$ and 0 otherwise. The Fourier transform of P_L is therefore:

$$\widehat{P}_L(O) = \widehat{P}(O) \widehat{\mathbb{I}}_{\mathcal{G}'}(O) = |\mathcal{G}'| \Lambda(O) \mathbb{I}_{\mathcal{L}'}(O) \quad (\text{H5})$$

where \mathcal{L}' is the group of "bare" logical operators defined as the group of operators $\mathcal{L} = N(\mathcal{G})$ that commute with the gauge group. As a result, the Fourier transform of the logical error class probability $\widehat{P}_L(O)$ is only non-zero when $O \in \mathcal{L}'$, i.e., it only depends on the Pauli eigenvalue $\Lambda(L')$, $L \in \mathcal{L}'$ of the measured bare logical group.

Similar to Eq. (22), we could write the logarithm of the Pauli eigenvalue of elements in the measured logical group $L \in \mathcal{L}'$ in terms of the transformed eigenvalues $\vec{\mu}$:

$$\log \vec{\Lambda}^{(\mathcal{L}')} = D^{(\mathcal{L}')} \log \vec{\mu}. \quad (\text{H6})$$

where $D^{(\mathcal{L}')}[L, e] = \langle L, e \rangle$. Here, the Pauli eigenvalue of $\Lambda(M)$ for M in the measured stabilizer code \mathcal{M} of the spacetime code can be calculated from the syndrome expectation value of the circuit using the parity check \mathcal{O}^\perp according to Lemma G.3.

Given the fault-tolerant condition (Definition 9) is satisfied, to prove that the logical error rate is determined by the syndrome measurement, i.e., Pauli eigenvalues of operators in \mathcal{M} , one just needs to show all rows of $D^{(\mathcal{L})}$ is linear dependent on rows of the matrix for the syndrome data $D^{(\mathcal{M})}$ in Eq. (18). Consider a circuit with circuit-level Pauli noise defined by \mathcal{N}_Γ that is fault-tolerant to the set of logical operators in the circuit in the sense of Definition 9. This fault-tolerant condition, according to Corollary G.5, is equivalent to following statement when mapped to the spacetime code: For any undetectable error $e \in \mathcal{E}_\Gamma$ in the spacetime code, e commute with all logical operators in \mathcal{L}' , and for any two errors $e_1, e_2 \in \mathcal{E}_\Gamma$ with the same syndrome, then $e_1 e_2$ commute with all logical operators in \mathcal{L}' , i.e., e_1 and e_2 commute/anticommute with the same set of operators in \mathcal{L}' . Therefore, the syndrome class (Definition C.1) $\mathcal{C}^{*(\mathcal{M})}$ and $\mathcal{C}^{*(\mathcal{L}')}$ with respect to the measured stabilizer group \mathcal{M} and the measured logical group \mathcal{L}' respectively, are the same. As a result, according to Lemma C.4 we have

$$\text{rank } D^{(\mathcal{L})} = \text{rank } D^{(\mathcal{M})}. \quad (\text{H7})$$

Since $\mathcal{M} \subseteq \mathcal{L}'$, all rows of $D^{(\mathcal{L})}$ are linearly dependent on rows of $D^{(\mathcal{M})}$ and the Pauli eigenvalue of all logical operators $\Lambda(L), \forall L \in \mathcal{L}$ only depends on the measured syndrome expectations $\{\Lambda(M) | \forall M \in \mathcal{M}\}$. Therefore, using the syndrome data, we can recover the logical error classes probability Eq. (H2) and also the logical error rates according to Eq. (47) and the equivalence of logical error in the circuit and the spacetime code (Lemma G.4).

To prove the other direction, if (case 1) there exists an error $e \in \mathcal{E}_\Gamma$, or (case 2) $e = e_1e_2$ for some $e_1, e_2 \in \mathcal{E}_\Gamma$, such that e is undetectable from the syndrome but anticommutes with some operator in \mathcal{L}' , then the rank of $\mathcal{D}^{(\mathcal{L}')}$ is strictly larger than the rank of $\mathcal{D}^{(\mathcal{M})}$. This is because the new set of non-trivial syndrome error classes (Definition C.1) with respect to \mathcal{L}' can be obtained by either adding some undetectable error e as a new non-trivial class for case 1, or further partitioning the existing non-trivial syndrome classes (case 2). Therefore, according to Lemma C.4 we have

$$\text{rank } \mathcal{D}^{(\mathcal{L}')} > \text{rank } \mathcal{D}^{(\mathcal{M})}. \quad (\text{H8})$$

As a result, for an existing transformed eigenvalues $\vec{\mu}$ satisfying the syndrome constraints and resulting in certain Pauli eigenvalues $\vec{\Lambda}^{(\mathcal{L}')}$, there exists a vector $\vec{e} \in \ker(\mathcal{D}^{(\mathcal{M})})$ such that $\vec{\mu}' = \vec{\mu} + \vec{e}$ is still valid given the Assumption 1 (see Lemma E.1) and $\vec{\mu}'$ produces a different set of Pauli eigenvalues $\vec{\Lambda}^{(\mathcal{L}')}$. Since the logical error class probabilities are related to $\vec{\Lambda}^{(\mathcal{L}')}$ by an invertible Walsh-Hadamard transformation as in Eq. (H5), $\vec{\mu}'$ and $\vec{\mu}$ lead to different sets of logical error class probabilities. Therefore, the logical error class probabilities are not learnable. \square

Note that in the learnable case, the log of syndrome expectation values and the learnable transformed eigenvalues $\log \vec{\nu}$ are related by full column rank matrix $D^{(\mathcal{M})}$ (Lemma C.4), therefore the logical error rates are also determined by $\log \vec{\nu}$.

APPENDIX I: Sample complexity

1. Sample complexity for learning physical error rates

Here, we study the sample complexity of learning syndrome class error rate, where we first consider solving for the learnable transformed eigenvalues $\log \vec{\nu}$ in Eq. (27) and then estimate the syndrome class error rate using the approximation $P_C \approx -\frac{\log \nu_C}{2}$, as explained in Section E. Note that $P_C \approx -\frac{\log \nu_C}{2} \approx \frac{1-\nu_C}{2}$ when error rates are low, and $\frac{1-\nu_C}{2}$ in practice is a slightly more accurate estimator. Moreover, $\frac{1-\nu_C}{2}$ equals the probability of an odd number of errors occurring in C for the detector error model, as shown in Eq. (E15). However, for simplicity in error propagation, we will argue based on the approximation $-\frac{\log \nu_C}{2}$.

We first introduce some notation. Given a set of measured stabilizer generators $\{M_i\}_i^m$ for the measured stabilizer group $\mathcal{M} = \langle M_1, \dots, M_m \rangle$, we denote the indices of the stabilizer generators violated for each syndrome class $C \in \mathcal{C}$ as $J(C) \subseteq [m]$. We define the variables to solve $X_C = \log \nu_C$ as the learnable transformed eigenvalues, and for any $R \subseteq [m]$, let $Y_R = \log \Lambda(\prod_{i \in R} M_i)$ be the logarithm of the Pauli eigenvalues of the stabilizer elements, i.e., syndrome expectation values.

Lemma I.1. *Eq. (35) is the solution of the system of linear equations Eq. (27), where \mathcal{M}' is the subset of measured stabilizer group $\mathcal{M}' = \bigcup_{C \in \mathcal{C}} \{\prod_{i \in J'} M_i \mid J' \subseteq J(C)\}$.*

Proof. We denote $D_{R,C}$ as the matrix element of the syndrome matrix D in the row labeled by the stabilizer element $\prod_{i \in R} M_i$ and column labeled by the syndrome class C and it is given by

$$D_{R,C} = \begin{cases} 1 & , \text{if } R \cap J(C) \text{ is odd,} \\ 0 & , \text{if } R \cap J(C) \text{ is even.} \end{cases} \quad (\text{I1})$$

The system of linear equations Eq. (25) can be rewritten as

$$Y_R = \sum_{C \in \mathcal{C}} D_{R,C} X_C. \quad (\text{I2})$$

where $R \subseteq [m]$. Let us define a linear transformation of Y_R , $\forall R \subseteq [m]$:

$$Z_R = \sum_{S \subseteq R} (-1)^{|S|-|R|} Y_S. \quad (\text{I3})$$

Since the power set of the stabilizer generator indices $[m]$ is a partially ordered set by the inclusion relation, we could order the rows R in the D matrix according to this partial order, and this is essentially row operations on Eq. (I2).

Plugging this into Eq. (I2):

$$Z_R = \sum_{S \subseteq R} (-1)^{|S|} \sum_{C \in \mathcal{C}} D_{S,C} X_C \quad (\text{I4})$$

$$= \sum_{C \in \mathcal{C}} \left(\sum_{S \subseteq R} (-1)^{|S|} D_{S,C} \right) X_C \quad (\text{I5})$$

$$= \sum_{C \in \mathcal{C}} \chi_{R,C} X_C \quad (\text{I6})$$

The matrix χ is "upper triangular" by looking at its elements

$$\chi_{R,C} = \sum_{S \subseteq R} (-1)^{|S|} D_{S,C} = \sum_{\substack{S \subseteq R \\ |S \cap J(C)| \text{ is odd}}} (-1)^{|S|} = \begin{cases} -2^{|R|-1}, & \text{if } R \subseteq J(C), \\ 0, & \text{else.} \end{cases} \quad (\text{I7})$$

In particular, $Z_R = 0$ if R satisfy that for any $C \in \mathcal{C}$, $R \not\subseteq J(C)$. Therefore, only stabilizer elements in $\mathcal{M}' = \bigcup_{C \in \mathcal{C}} \{\prod_{i \in J'} M_i \mid J' \subseteq J(C)\}$ are used.

Combining Eq. (I2) and Eq. (I6) we obtain:

$$-Z_R = 2^{|R|-1} \sum_{\substack{C \in \mathcal{C} \\ J(C) \supseteq R}} X_C = \sum_{S \subseteq R} (-1)^{|S|-1} Y_S \quad (\text{I8})$$

From the second equality, we obtain the solution

$$X_C = - \sum_{\substack{C' \in \mathcal{C} \\ J(C') \supset J(C)}} X_{C'} + \frac{1}{2^{|J(C)|-1}} \sum_{S \subseteq J(C)} (-1)^{(|S|-1)} Y_S. \quad (\text{I9})$$

□

We now show that the sample complexity is constant given a desired precision on the logarithm of the learnable transformed eigenvalues $X_C = \log \nu_C$ for a local sparse qLDPC code and a (r_Γ, c_Γ) -Pauli channel \mathcal{N}_Γ .

Lemma I.2. *Consider a local sparse (r_s, c_s) -Pauli channel on an n -qubit qLDPC code. Choose $\epsilon, \delta > 0$ and any syndrome class $C \in \mathcal{C}^*$, then the sample size N required to estimate the logarithm of the learnable transformed eigenvalues $\log \nu_C$ to additive error within ϵ with confidence $1 - \delta$ using Eq. (35) is independent of n and scales as*

$$N = \mathcal{O} \left(\frac{1}{\epsilon^2} \log \left(\frac{1}{\delta} \right) \right). \quad (\text{I10})$$

Proof. We use the notation in the proof of Lemma I.1. In the local error model setting, we have $|J(C)| \leq r_\Gamma c_s$, and $|\{C' \in \mathcal{C} \mid J(C') \supset J(C)\}| \leq r_s c_\Gamma$ for any syndrome class C since each generator acts on at most r_s qubits and each qubit is affected by at most c_Γ channels. Let $\mathcal{M}' = \bigcup_{C \in \mathcal{C}} \{\prod_{i \in J'} M_i \mid J' \subseteq J(C)\}$ be the subset of stabilizer elements involved in the recursive solution Eq. (35). For any measured stabilizer element M in \mathcal{M}' . Given Assumption 1 of the local channels, the Pauli eigenvalues of any local channels are lower bounded by a constant λ_{\min} , i.e., $\Lambda_\gamma(e) \geq \lambda_{\min} > 0, \forall \gamma \in \Gamma$.

$$\Lambda(M) = \prod_{\substack{\gamma \in \Gamma \\ \text{supp}(M) \subseteq \gamma}} \Lambda_\gamma(M_\gamma) \geq \lambda_{\min}^{r_\Gamma s_\Gamma c_s c_\Gamma} = \Theta(1) \quad (\text{I11})$$

Given the additive error $\epsilon_{\Lambda(M)}$ of syndrome expectation values $\Lambda(M)$ is less than $\Lambda(M)$, the additive error ϵ_{Y_S} of $Y_S = \log \Lambda(M)$ due to shot noise is related to the error $\epsilon_{\Lambda(M)}$ as:

$$\epsilon_{Y_S} \leq \frac{\epsilon_{\Lambda(M)}}{\Lambda(M) - \epsilon_{\Lambda(M)}} \leq \frac{\epsilon_{\Lambda(M)}}{C_\Lambda} \quad (\text{I12})$$

for some constant C_Λ .

For any syndrome class C , $X_C = \log \nu_C$ can be written as linear function of $\{Y_S\}$ using a bounded number of recursions and resulting in a bounded number C_r of terms of Y_S according to Eq. (35). Therefore, it is sufficient that the additive error for each $\epsilon_{\Lambda(M)} \leq \min\left(\frac{C_\Delta}{C_r}\epsilon, \lambda_{\min}^{r_\Gamma s_\Gamma c_s c_\Gamma}\right) = \epsilon_{\Lambda}^{\max}$ with confidence $\leq \frac{\delta}{C_r}$ (union bound). Then we can use Hoeffding's inequality:

$$P\left(\left|\frac{1}{N} \sum_i m_i - \Lambda(M)\right| \geq \epsilon_{\Lambda}^{\max}\right) \leq 2 \exp\left(-\frac{N(\epsilon_{\Lambda}^{\max})^2}{2}\right) \leq \frac{\delta}{C_r}. \quad (\text{I13})$$

to obtain the required sample size

$$N \geq \frac{2}{(\epsilon_{\Lambda}^{\max})^2} \log\left(\frac{2C_r}{\delta}\right) = \mathcal{O}\left(\frac{1}{\epsilon^2} \log\left(\frac{1}{\delta}\right)\right). \quad (\text{I14})$$

□

With the above lemma, we can prove the sample complexity of estimating syndrome class error rates to additive precision for general qLDPC stabilizer codes (qLDPC spacetime subsystem code) under local sparse Pauli channels, when the second-order correction is smaller than the shot noise due to finite sample size.

Theorem 4 (Restated) [Sample complexity for syndrome class learning] Consider a local sparse Pauli channel \mathcal{N}_Γ on an n -qubit qLDPC code. Given $\epsilon > 0, 0 < \delta < 1$, there exists a constant $C_c > 0$ such that if $\|\vec{p}\|_\infty^2 < \frac{\epsilon}{2C_c}$, the sample size N required to estimate the syndrome error class $P_C, \forall C \in \mathcal{C}^*$ to additive error within ϵ with confidence $1 - \delta$ using Eq. (35) is

$$N = \mathcal{O}\left(\frac{1}{\epsilon^2} \log\left(\frac{1}{\delta}\right)\right), \quad (\text{I15})$$

independent of the system size n .

Proof. For any syndrome class $C \in \mathcal{C}^*$, we can approximate the syndrome error class using

$$P_C = -\log \nu_C + \mathcal{O}(\|\vec{p}\|^2) \quad (\text{I16})$$

$$(\text{I17})$$

And we can bound the correction term

$$|P_C + \log \nu_C| \leq C_c p_{\max}^2 \quad (\text{I18})$$

for some $C_c > 0$ due to Taylor's theorem. Moreover, C_c is constant in the context of local sparse Pauli channel on qLDPC codes (see Lemma F.3). If error rates are small enough, i.e. $p_{\max} < \left(\frac{\epsilon}{2C_c}\right)^{\frac{1}{2}}$, then shot noise on $\log \nu_C$ dominates the additive error and the sample size scaling is given by Lemma I.2.

□

2. Sample complexity for learning logical error rates

In this section, we show that for a non-adaptive Clifford circuit that is fault-tolerant to a circuit-level Pauli noise, which corresponds to a local sparse Pauli Channel on the spacetime code of the circuit, then the logical error rate can be learned to the same relative precision as the physical error rate with only an additional overhead in the sample complexity that in the worst case scales quadratically in the spacetime volume. In the low physical error rate regime where the minimum weight fault paths dominate, the overhead is $\Theta(d^2)$.

We prove the sample complexity of learning the logical error to a given relative precision by first proving the sample size required to learn each physical error rate to a certain relative precision and then proving the bounded error propagation to the logical error rate.

Lemma I.3 (Sample complexity for physical error rate estimation). *Consider a non-adaptive logical Clifford circuit with n physical qubits, and of physical depth T that corresponds to a qLDPC spacetime code. Then consider a local sparse Pauli channel \mathcal{N}_Γ with local error rates \vec{p} , mapped from the circuit-level Pauli error model (Definition 4), that acts on the spacetime code. Let \vec{p}' be the error rates that generate the same logical error rate as \vec{p} and satisfy any chosen extra constraints $B\vec{p}' = 0$. Let L_H, K_{G_B} be the two constants in Lemma F.4. For any chosen $\eta > 0, 0 < \delta < 1$,*

if the true error rates satisfy $\|\vec{p}\|_\infty \leq \min\left(\frac{2}{L_H, K_{G_B}}, \left(\frac{\eta P_{C_{\min}}}{2C_c}\right)^{\frac{1}{2}}\right)$, the sample size N required to learn all physical error rate with relative error within η with confidence $1 - \delta$, when compared to \vec{p}' , is given by

$$N = \mathcal{O}\left(\frac{1}{\eta^2 P_{C_{\min}}^2} \log\left(\frac{nT}{\delta}\right)\right). \quad (\text{I19})$$

Proof. We use the circuit-to-code mapping in Section IV A to map the n -qubit non-adaptive Clifford circuit of depth T to an $n(T + 1)$ -qubit spacetime code, which is assumed to be qLDPC. According to Lemma F.4 and Theorem 4, given any extra constraints $B\vec{p} = \vec{0}$ and by setting $\epsilon = P_{C_{\min}}\eta$, when

$$\|\vec{p}\|_\infty \leq \min\left(\frac{2}{L_H, K_{G_B}}, \left(\frac{\eta P_{C_{\min}}}{2C_c}\right)^{\frac{1}{2}}\right), \quad (\text{I20})$$

there exist error rates \vec{p}' satisfying the extra constraints $B\vec{p}' = 0$ and having identical learnable transformed eigenvalues $\log \vec{\nu}(\vec{p}') = \log \vec{\nu}(\vec{p})$ with the ones of the true noise. And we need $N = \frac{\alpha}{\epsilon^2} \log\left(\frac{1}{\delta}\right)$ to reach ϵ additive error in estimating each syndrome class error rate, for some constant α . We further estimate each component of \vec{p}' by applying $B\vec{p}' = 0$ to each estimated syndrome class error rate. To reach relative error η for all syndrome class with confidence $1 - \delta$, for each syndrome class C , it is sufficient that $\epsilon \leq \eta P_{C_{\min}}$ with confidence $1 - \delta_C$ where $\delta_C = \frac{\delta}{|\mathcal{C}^*|}$ (union bound). Moreover, the number of non-trivial syndrome classes $|\mathcal{C}^*| = \Theta(nT)$ since each syndrome class has a constant size. Therefore, plugging in Eq. (I15), we get the scaling as shown in Eq. (I19). Each physical error rate is estimated with relative precision within η compared with \vec{p}' since $B\vec{p}' = 0$ is satisfied. \square

Lemma I.4 (Relative error propagation to logical level). *Consider a logical Clifford circuit with n physical qubits and of physical depth T , and a circuit-level Pauli noise channel that corresponds to a local sparse Pauli channel \mathcal{N}_Γ on the spacetime code. We can achieve learning the probability of any subset of logical Pauli errors that affect logical measurements in the circuit with relative error within η_L if the maximal relative error η_p^{\max} of the learned physical error rates is $\eta_p^{\max} \leq \frac{1}{2|\Gamma|}\eta_L = \Omega(\frac{\eta_L}{nT})$, where $|\Gamma|$ is the number of local channels.*

Proof. We define a fault path f in a spacetime code as a subset of the possible errors \mathcal{E}_Γ (exclusive in each local channel). We call f a failing fault path if it leads to any logical error considered after decoding, and we denote the set of all such failing paths as $\mathcal{F}_{\text{fail}}$. For any local channel \mathcal{N}_γ , $\gamma \in \Gamma$ and a local error e in the channel, we denote the error rate as p_e , and denote $q_\gamma = 1 - \sum_{e \in \mathcal{E}_\gamma} p_e$. We denote the set of local supports not involved in a path f as Γ_f^c . The logical error rate is then given by:

$$P_{\text{fail}} = \sum_{f \in \mathcal{F}_{\text{fail}}} \prod_{e_i \in f} p'_{e_i} \prod_{\gamma \in \Gamma_f^c} q'_\gamma. \quad (\text{I21})$$

We bound the relative error for each term $P^{(f)} = \prod_{e_i \in f} p'_{e_i} \prod_{\gamma \in \Gamma_f^c} q'_\gamma$ as

$$\eta_{P^{(f)}} \leq \frac{|\prod_{e_i \in f} p'_{e_i} (1 + \eta_p^{\max}) \prod_{\gamma \in \Gamma_f^c} q'_\gamma (1 + \eta_q^{\max}) - P^{(f)}|}{P^{(f)}} \quad (\text{I22})$$

$$\leq (1 + \eta_p^{\max})^{|\Gamma|} - 1 \quad (\text{I23})$$

where η_q^{\max} refers to the maximal relative error of q_γ over $\gamma \in \Gamma$, and we used the fact that for small error rates, $\eta_q^{\max} < \eta_p^{\max}$. Since P_{fail} is just a sum of these positive terms, the relative error $\eta_{P_{\text{fail}}}$ of P_{fail} is just bounded by the largest $\eta_{P^{(f)}}$ among all failing paths f :

$$\eta_{P_{\text{fail}}} \leq (1 + \eta_p^{\max})^{|\Gamma|} - 1. \quad (\text{I24})$$

Therefore we have

$$\eta_p^{\max} \geq (1 + \eta_{P_{\text{fail}}})^{\frac{1}{|\Gamma|}} - 1 \geq e^{\frac{1}{|\Gamma|} \ln(1 + \eta_{P_{\text{fail}}})} - 1 \geq \frac{1}{2|\Gamma|} \eta_{P_{\text{fail}}}, \quad \forall 0 \leq \eta_{P_{\text{fail}}} \leq 1, |\Gamma| \geq 1, \quad (\text{I25})$$

where $|\Gamma| = \mathcal{O}(nT)$ is the number of local Pauli channels since we assume \mathcal{N}_Γ is a local sparse Pauli channel, and we used the fact that $e^x - 1 \geq x$. As a result, if $\eta_p^{\max} \leq \frac{1}{2|\Gamma|}\eta_L$, then the relative error $\eta_{P_{\text{fail}}} \leq \eta_L$. \square

Theorem 11 (Restated) Consider a non-adaptive logical Clifford circuit with n physical qubits and of physical depth T that corresponds to a qLDPC spacetime code. We assume the circuit is fault-tolerant to a circuit-level noise that corresponds to a local sparse Pauli channel \mathcal{N}_Γ on the spacetime code, for a set of logical measurements \mathcal{M}_L . Denote by $P_{C\min}$ the minimal syndrome class error rate. We can learn the logical error rates P_{fail} for \mathcal{M}_L with relative error within η_L with confidence $1 - \delta$ using a sample size

$$N = \mathcal{O} \left(\frac{n^2 T^2}{\eta_L^2 P_{C\min}^2} \log \left(\frac{nT}{\delta} \right) \right), \quad (\text{I26})$$

if the true error rates satisfy $\|\vec{p}\|_\infty \leq \min \left(\frac{2}{L_H, K_{G_B}}, \left(\frac{\eta_L P_{C\min}}{4|\Gamma|C_c} \right)^{\frac{1}{2}} \right)$, for constants L_H, K_{G_B}, C_c defined in Eqs. (F27), (F28) and (I18).

Proof. Directly follows from Lemma I.3 and Lemma I.4. \square

For a Clifford circuit encoded in a family of stabilizer codes that have a non-trivial fault-tolerant threshold, when the physical error rates are well below the threshold, then the failing fault path is dominated by the minimum-weight paths. Let d denote the circuit distance (distance of the spacetime code). Then the minimum weight is the minimum number of local channels required to generate a failing path and it is upper bounded by $t = \lfloor \frac{d+1}{2} \rfloor$. In this setting, the sample size needed to reach the same relative precision at the logical level as the physical level has an extra overhead that scales as $\mathcal{O}(d^2)$ instead of $\exp(\frac{d}{2})$ from the logical level fidelity estimation/tomography directly.

However, Theorem 11 does require the upper bound of physical error rate to drop as $\sim \frac{1}{n}$, or $\sim \frac{1}{d}$ when the min-weight fault paths dominate the logical error rate. This is because the correction term in the syndrome class error rate eventually dominates as the physical relative precision required increases with larger n . Therefore, if the scale of physical error rate is independent of the system size, then the quadratic overhead in the theorem holds within a finite-sized system, which is still practically relevant. See numerical results in Fig. 19, where we tested on surface code of various sizes in the simple channel coding setting.

APPENDIX J: Intraclass uniformity constraints

In Section V, we add additional constraints to mitigate the overfitting due to shot noise for learning the experimental data, and we denote the learned result with * . For each randomly selected qubit component, we add a new row to the B matrix in Eq. (29). If the k th error e_k in \mathcal{E}_Γ (corresponds to the k th column of \bar{B}) is randomly selected for an additional row of B (say the i th row), then the matrix elements of row i are:

$$B_{ij} = \begin{cases} 1, & \text{if } i = k, \\ \frac{-r(e_k)}{(|\mathcal{E}_\Gamma| - 2)r(e_j)}, & \text{else.} \end{cases} \quad (\text{J1})$$

Note that the constraints added here can be optimized depending on the strength of the shot noise. We did numerical simulations on the seven-qubit Steane code using single-qubit Pauli channels. Therefore, we have 21 parameters corresponding to the 21 Pauli error components. We see benefits in the large shot noise case, but the extra constraints will have a negative impact on the learning quality when the sample size exceeds a certain threshold. See Fig. 15.

APPENDIX K: Extra plots

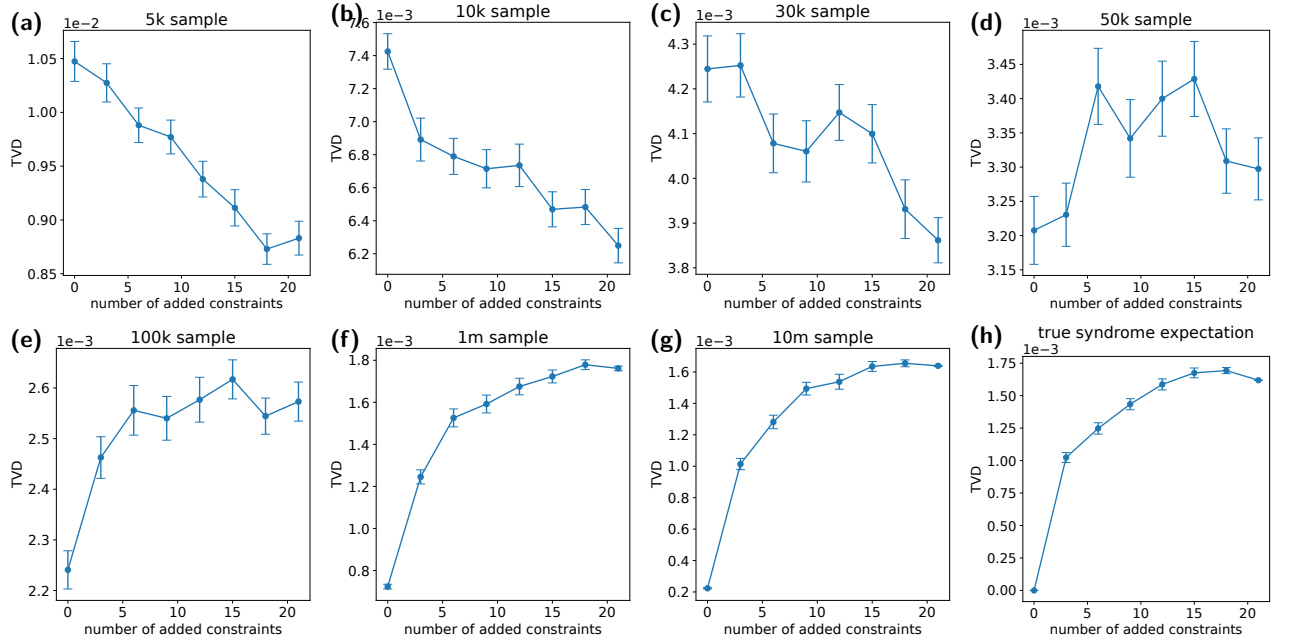


FIG. 15: Numerical simulation of the effect of extra uniformity constraints. The horizontal axis is the number of uniformity constraints acting on random error components. The vertical axis corresponds to the TVD of the learned error rate and the true noise. The uniform constraints benefit small sample sizes and large shot noise samples while degrading the quality of learning in the case of large sample sizes (weak shot noise).

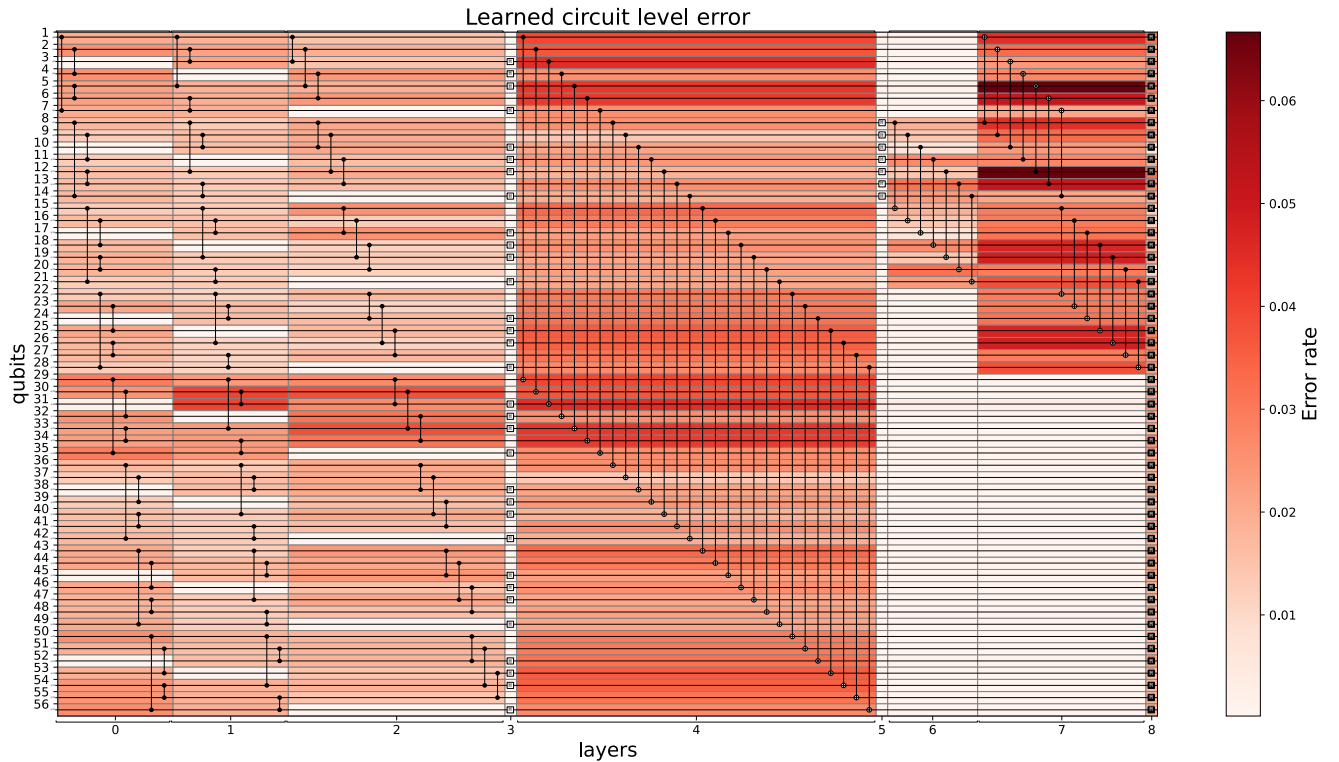


FIG. 16: Physical Pauli error rate learning for the \overline{ZZZZZ} measurement circuits

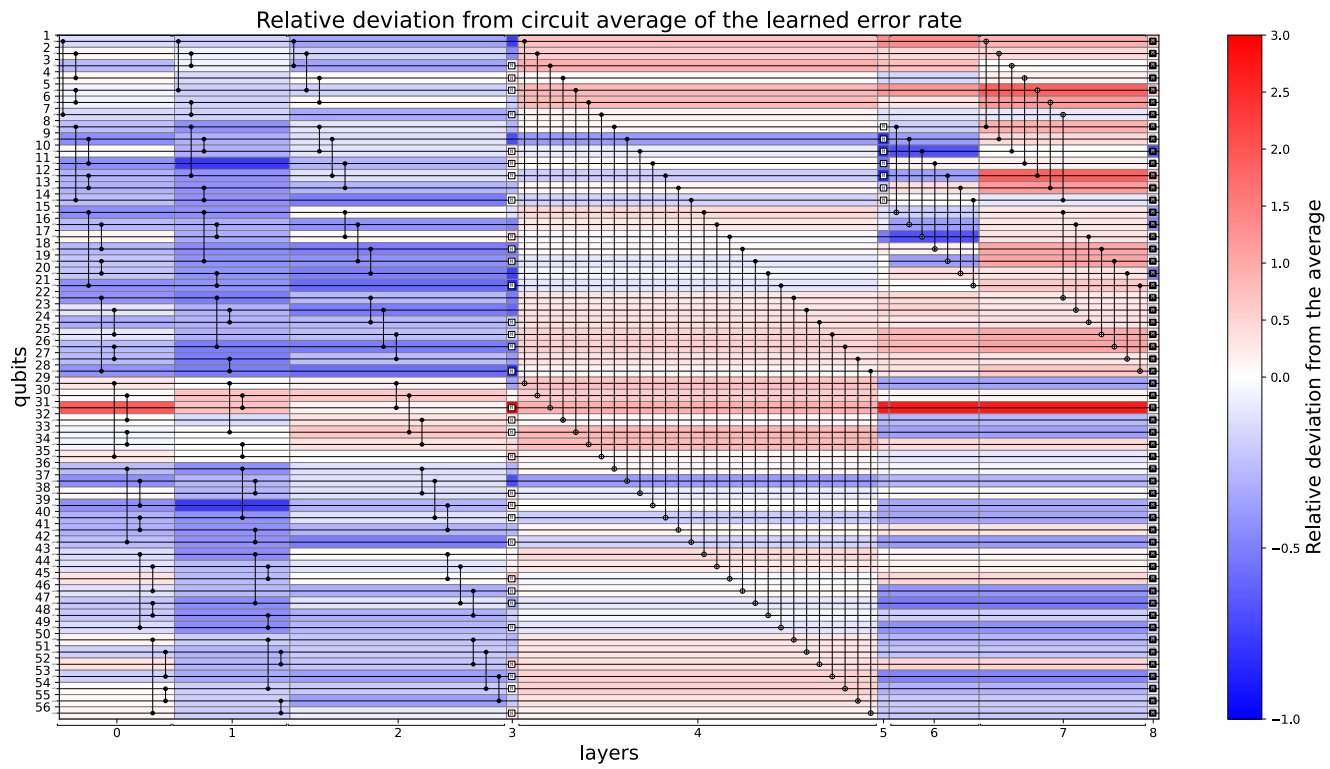


FIG. 17: Relative deviation of gate error rates to the circuit average.

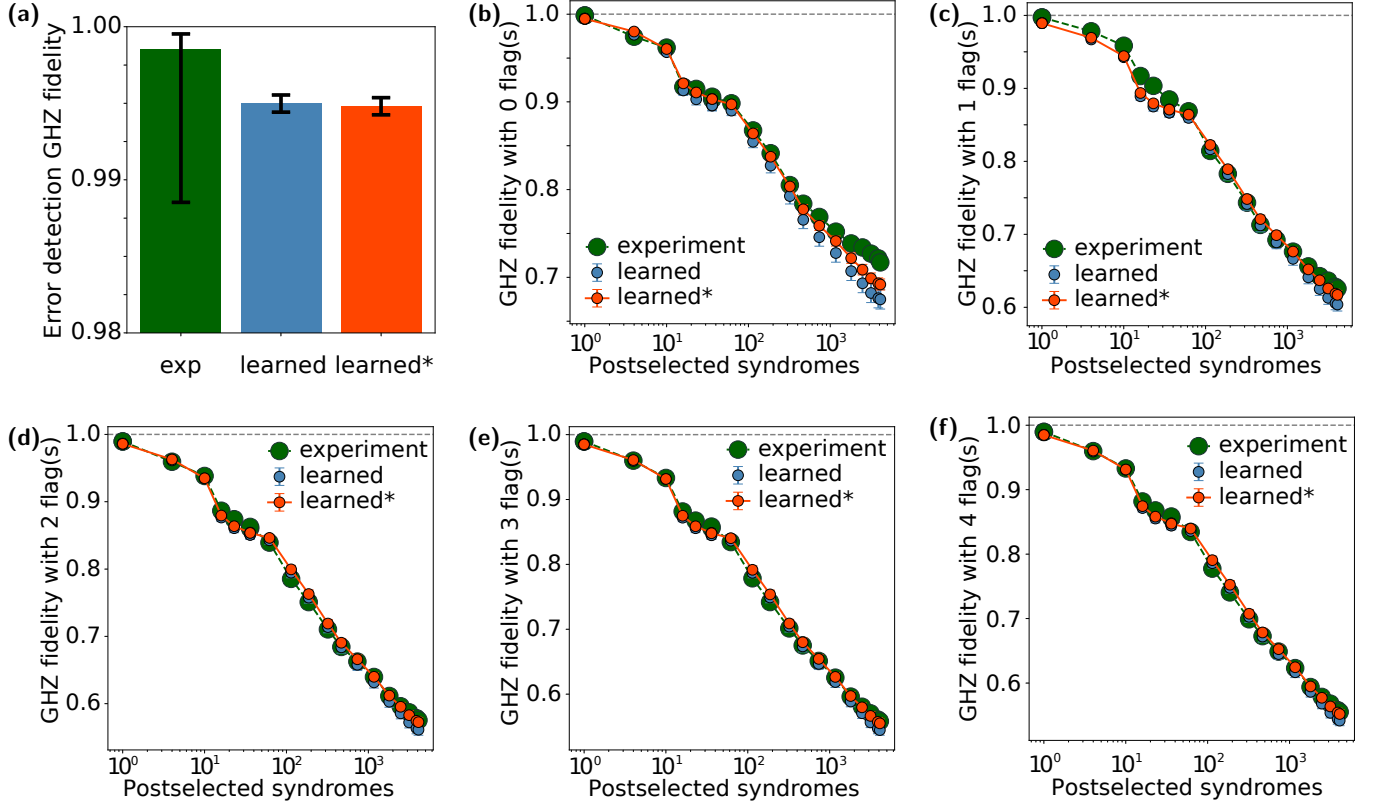


FIG. 18: Full version of Fig. 9. Comparison of logical direct fidelity estimation between experimental results and learned noise models from syndromes. (a) The error detecting results for the logical GHZ fidelity from experimental measurement, learned logical fidelity, and the learned fidelity with extra uniformity constraints, denoted with * (see Section J). (b)-(f) The same comparison of logical fidelity with partial postselection on the syndrome is performed. Each subplot is conditioned on a different number of ancilla blocks that have a non-trivial syndrome (flag).

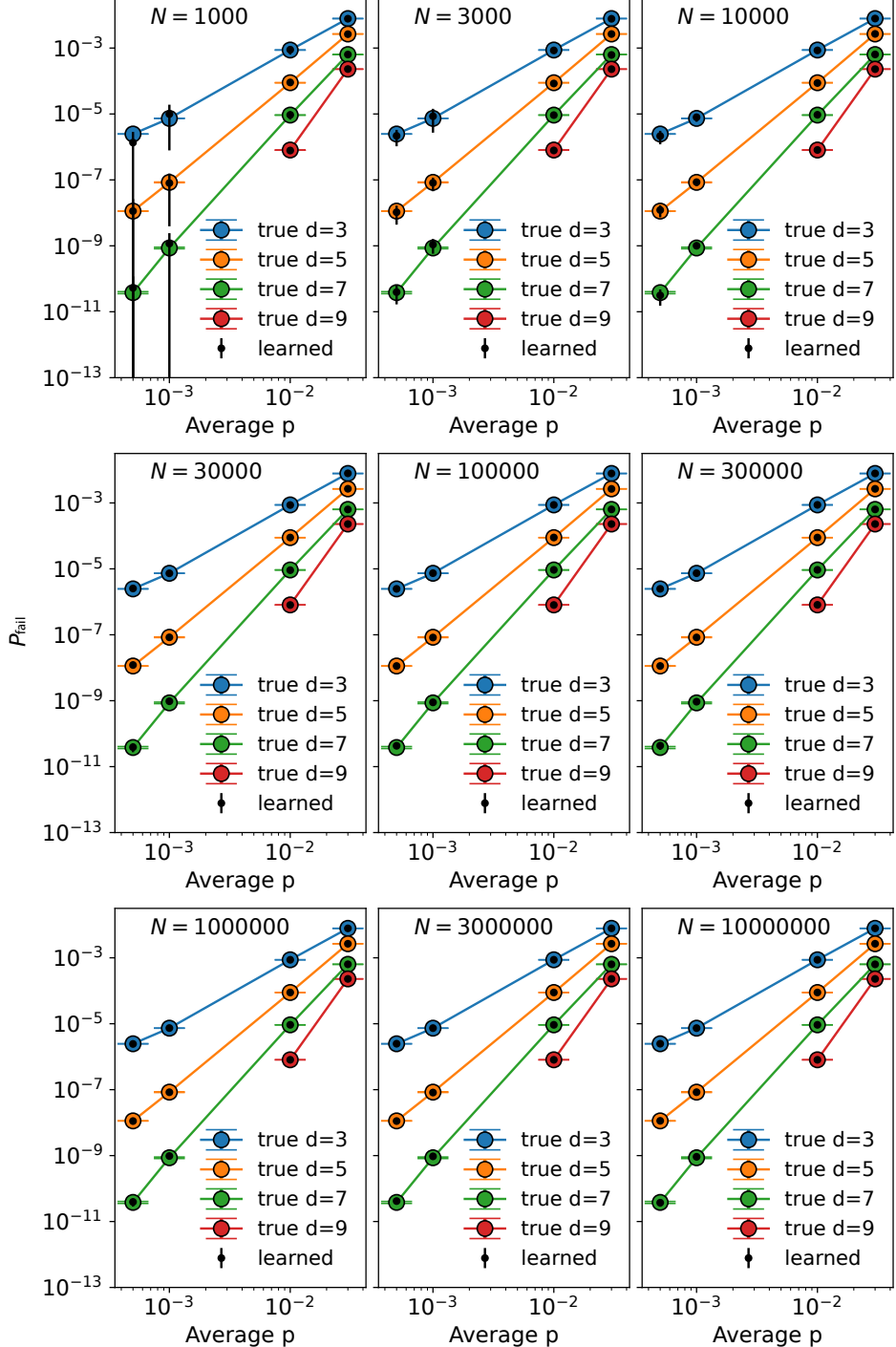


FIG. 19: Surface code logical error rate learning in the code capacity setting for distances $d = 3, 5, 7, 9$. The learning is done by learning the physical error rate with different sample sizes N of syndrome data.